# Protein Dynamics from NMR: The Slowly Relaxing Local Structure Analysis Compared with Model-Free Analysis†

**Eva Meirovitch,*,‡ Yury E. Shapiro,‡ Antonino Polimeno,§ and Jack H. Freed#**

*Faculty of Life Sciences, Bar-Ilan University, Ramat-Gan 52900, Israel, Department of Chemistry, University of Padua, 35131 Padua, Italy, and Baker Laboratory of Chemistry and Chemical Biology, Cornell University, Ithaca, New York 14853-1301*

*Received: December 1, 2005; In Final Form: February 19, 2006*

$^{15}N-^{1}H$ spin relaxation is a powerful method for deriving information on protein dynamics. The traditional method of data analysis is model-free (MF), where the global and local N−H motions are independent and the local geometry is simplified. The common MF analysis consists of fitting single-field data. The results are typically field-dependent, and multifield data cannot be fit with standard fitting schemes. Cases where known functional dynamics has not been detected by MF were identified by us and others. Recently we applied to spin relaxation in proteins the slowly relaxing local structure (SRLS) approach, which accounts rigorously for mode mixing and general features of local geometry. SRLS was shown to yield MF in appropriate asymptotic limits. We found that the experimental spectral density corresponds quite well to the SRLS spectral density. The MF formulas are often used outside of their validity ranges, allowing small data sets to be force-fitted with good statistics but inaccurate best-fit parameters. This paper focuses on the mechanism of force-fitting and its implications. It is shown that MF analysis force-fits the experimental data because mode mixing, the rhombic symmetry of the local ordering and general features of local geometry are not accounted for. Combined multifield multitemperature data analyzed with the MF approach may lead to the detection of incorrect phenomena, and conformational entropy derived from MF order parameters may be highly inaccurate. On the other hand, fitting to more appropriate models can yield consistent physically insightful information. This requires that the complexity of the theoretical spectral densities matches the integrity of the experimental data. As shown herein, the SRLS spectral densities comply with this requirement.

## I. Introduction

NMR is currently the most powerful method for studying protein dynamics at the residue level.[1−3] The commonly used dynamic probe is the $^{15}N-^{1}H$ bond. The relaxation parameters $^{15}N$ $T_1$, $T_2$ and $^{15}N-^{1}\{H\}$ NOE are measured experimentally at one or several magnetic fields. Their expressions are given by the spectral densities, $J(\omega)$, and the relevant magnetic interactions ($^{15}N-^{1}H$ dipolar and the $^{15}N$ CSA).[4,5] The functions $J(\omega)$ are determined by the dynamic model used, and the local geometry at the N−H site.

The traditional method of data analysis is the model-free (MF) approach.[6−8] MF assumes that the global motion of the protein ($R^C = 1/6\tau_m$) and local motion of the N−H bond ($R^L = 1/6\tau^L$) are "independent" or "decoupled", by virtue of the former being much slower than the latter ($\tau_m \gg \tau^L$). The local ordering is measured by a squared generalized order parameter, $S^2$, and the rate of local motion is evaluated by an effective correlation time, $\tau_e$. Both parameters represent mathematical properties of the spectral density. The local geometry is simplified, with the ordering and magnetic tensor frames axial and collinear.

Three point ($^{15}N$ $T_1$, $T_2$ and $^{15}N-\{^{1}H\}$ NOE) data acquired at a single magnetic field, pertaining to structured regions of the protein backbone, can be usually analyzed with optimization (data fitting) methods using the original MF formula.[6,7] Flexible residues residing in loops and mobile domains required the development of the extended MF formula.[8] The latter features a fast effective local motion, $\tau_f$, associated with a generalized squared order parameter, $S_f^2$, and a slow effective local motion, $\tau_s$, associated with a generalized squared order parameter, $S_s^2$. All the modes are assumed to be independent, i.e., $\tau_m \gg \tau_f$, $\tau_m \gg \tau_s$, and $\tau_s \gg \tau_f$.

The MF order parameters, including the global motion correlation time, $\tau_m$, are typically found to be field-dependent. This means that combined multifield data sets cannot be fit with standard fitting schemes unless some data are excluded.[9] Small anisotropies in the global diffusion tensor were found to have a very large effect on the analysis.[10] Nonnormal t-distribution of NOEs was detected.[11] The temperature-dependence of MF order parameters was found to be unduly small.[12,13] The local motion was found to be practically independent of temperature and/or experimentally measured viscosity,[14−16] contrary to expectations based on typical activation energies for motions in flexible molecules. In some cases experimental relaxation parameters exceeded the extreme theoretical values.[13,17] Combined analysis of N−H bond dynamics and $C'-C^{\alpha}$ bond dynamics yielded inconsistent results.[13,18] We found that known functional dynamics in adenylate kinase from *E. coli* is not

† Part of the "Chava Lifshitz Memorial Issue".

* Corresponding authors. E-mail: E.M., eva@nmrsgi5.ls.biu.ac.il; J.H.F., jhf@ccmr.cornell.edu; A.P., antonino.polimeno@unipd.it.

‡ Bar-Ilan University.

§ University of Padua.

# Cornell University.

10.1021/jp056975t CCC: $33.50 
Published on Web 05/16/2006

detected with MF analysis.[19,20] Similar observations were made by other workers in the field.[21]

These shortcomings are usually rationalized by invoking data imperfection. Alternatively, the simplicity of the MF analysis may be the main underlying reason. This option can be tested by analyzing the same data with an improved version of the theory, where the simplifying MF assumptions related to liquid dynamics and local geometry are no longer invoked. This was accomplished by applying to spin relaxation in proteins[22] the slowly relaxing local structure (SRLS) approach of Freed et al.,[23−25] which can be considered a generalized version of the MF approach. Rather than assuming mode independence, the SRLS approach accounts rigorously for mode mixing through a local potential. The latter represents the spatial restrictions on N−H motion, which in the MF approach are expressed by a squared generalized order parameter. Genuine axial and rhombic order parameters are defined in SRLS in terms of the local potential. Unlike the MF approach, the SRLS approach allows for a full range of time scale separations between the local and global motions (e.g., they can be comparable). The magnitude, symmetry and orientation of the ordering, diffusion and magnetic tensors are all allowed to vary. In general, SRLS features pure and mixed local and global dynamic modes. In appropriate asymptotic limits it yields the "mode-independent" MF formulas.

Experimental $^{15}$N relaxation data were subjected in parallel to SRLS (exact solution) and MF (asymptotic solution) analyses.[19,20,22,26,27] Significant improvement on many of the issues mentioned above was obtained with SRLS analysis. The goodness of fit was similar to, but the best-fit parameters significantly different from, the MF counterparts. Given that the more general SRLS approach contains the MF formulas as special cases, this indicates that the experimental data correspond to the general SRLS solution rather than the asymptotic MF solution. It also indicates that it is the simplicity of the MF approach, rather than experimental imperfections, that underlies the inconsistencies mentioned above. That a similar quality of fit can be obtained is related to the fitting process involving specific values of $J(\omega)$, which enter the expressions for $T_1$, $T_2$ and the NOE.[4,5] Different combinations of the required $J(\omega)$ values can yield the same relaxation rates. The process whereby an oversimplified spectral density yields inaccurate best-fit parameters (which depend on the specific $J(\omega)$ values) with good statistics is called "force-fitting".

Let us point out the asymptotic nature of the MF approach. The original MF formula represents the SRLS solution in the Born−Oppenheimer (BO) limit defined by $R^L \gg R^C$, where the local motion, characterized by the rate $R^L$, can be treated for frozen global motion, measured by the rate $R^C$.[27,28] In this limit the total time correlation function, $C(t)$, may be expressed within a good approximation as the product of the time correlation function for global motion, $C^C(t)$, and the time correlation function for local motion, $C^L(t)$. When $C^C(t) = \exp(-t/\tau_m)$ and the local ordering is high, then the $S^2$ from the MF analysis is a good approximation to the squared axial SRLS order parameter $(S_0^2)^2$, and the effective local motion correlation time, $\tau_e$, is given by the "renormalized" local motion correlation time, $\tau_{ren}$.[27] The concept of renormalization was used in early work[29] to characterize significant reduction in $\tau^L = 1/6R^L$ by strong local potentials. It was shown[29] that $\tau_{ren} \cong 2\ \tau^L/c_0^2$, where $c_0^2$ evaluates the strength of the local axial potentials (within the context of a general established potential form—see below). Clearly $\tau_{ren} \ll \tau^L$ when $c_0^2$ is large. Typical values are $c_0^2 = 10-40$ (which is to be multiplied by $k_BT$) corresponding to squared order parameters of 0.8−0.95. Equation A4 of ref 6, based on the wobble-in-a-cone model, is also appropriate for relating $\tau_e$ to $\tau^L$ and $S^2$ provided the ordering is high.[27]

We determined quantitatively over what range the conditions $R^L \gg R^C$ and $(S_0^2)^2 \sim 1$ apply by comparing SRLS and MF results.[27] The original MF formula often yields best-fit parameters that do not fulfill these requirements. These are cases where the experimental spectral density comprises mixed modes, which are incompatible with the simplified MF formula. $S^2$ and $\tau_e$ can no longer be associated with the relevant physical quantities. Instead they just become fitting parameters, which have absorbed the discrepancies between the experimental and oversimplified theoretical spectral densities. Moreover, we found that often the symmetry of the local ordering at the N−H site is rhombic.[26] In these cases the original MF formula is not a good approximation to the experimental spectral density even when $S^2$ is high and $R^C/R^L$ is small, because a single order parameter no longer suffices.

The extended MF formula was obtained in early work as a perturbational expansion of the SRLS solution in rhombic local ordering in the $R^L \gg R^C$ limit,[30] for a 90° tilt between an (axial) magnetic frame and the main local ordering/local diffusion frame (M).[27] This means that the N−H bond experiences fast diffusive local motion in the presence of very small rhombic ordering exerted by the immediate protein environment around, e.g., the $C^\alpha_{i-1}-C^\alpha_i$ axis, or the $N_i-C^\alpha_i$ bond. The components of the diffusion tensor are $R^L_{||} = 1/6\tau^L_{||}$ and $R^L_\perp = 1/6\tau^L_\perp$, and of the ordering tensor, $S_0^2$ and $S_2^2$. The protein surroundings reorient at a rate $R^C = 1/6\tau_m$, much slower than $R^L_{||}$ and $R^L_\perp$. The extended MF formula[8] was offered to represent the scenario where the N−H bond experiences both fast and slow isotropic local motions with eigenvalues and squared order parameters $1/\tau_f + 1/\tau_m$ and $S_f^2$, and $1/\tau_s + 1/\tau_m$ and $S_s^2$, respectively. These motions are assumed to be decoupled from one another, and from the global motion, implying the conditions $\tau_f \ll \tau_s \ll \tau_m$. In practice, the extended MF formula is used when $\tau_s \sim \tau_m$. The coefficients of the local and global motion terms in the extended MF formula are formally expressible in terms of $(S_0^2)^2$ and $(S_2^2)^2$. However, the MF parameters are totally different in implication from the SRLS parameters.

Typical best-fit values obtained with MF fitting of flexible protein residues are $S_s^2 \sim 0.55$, $S_f^2 \sim 0.8$, $\tau_s \sim \tau_m$ and $\tau_f \ll \tau_m$, which are just fitting parameters. This is implied by the presence of mixed modes which dominate the spectral density when $\tau_s$ is on the order of $\tau_m$ (which is typically the case for flexible residues in proteins). It should be pointed out that even if the perturbational conditions would prevail at the N−H site, the MF physical picture would be puzzling, requiring two independent isotropic but restricted local motions associated with different ordering scenarios ($S_s^2$ and $S_f^2$) imposed by the very same protein environment reorienting with correlation time $\tau_m \sim \tau_s$ while being at the same time decoupled from $\tau_s$. On the other hand, an N−H bond may reorient almost independently around $C^\alpha_{i-1}-C^\alpha_i$ (i.e., mixed modes may be ignored) in the limit where $R^L \gg R^C$ when the restricting local potential is very small. In this case the physical properties of axial local diffusion and rhombic local ordering are properly described by the simplified spectral density given by eq 19 below.

The validity ranges of the MF formulas are illustrated in Figure 1a,b. The ordinates represent the logarithm of the time scale separation between the global and local motions and the abscissas represent squared order parameters. The original MF formula is applicable to a good approximation within the solid box on the right-hand side of Figure 1a. This range is often

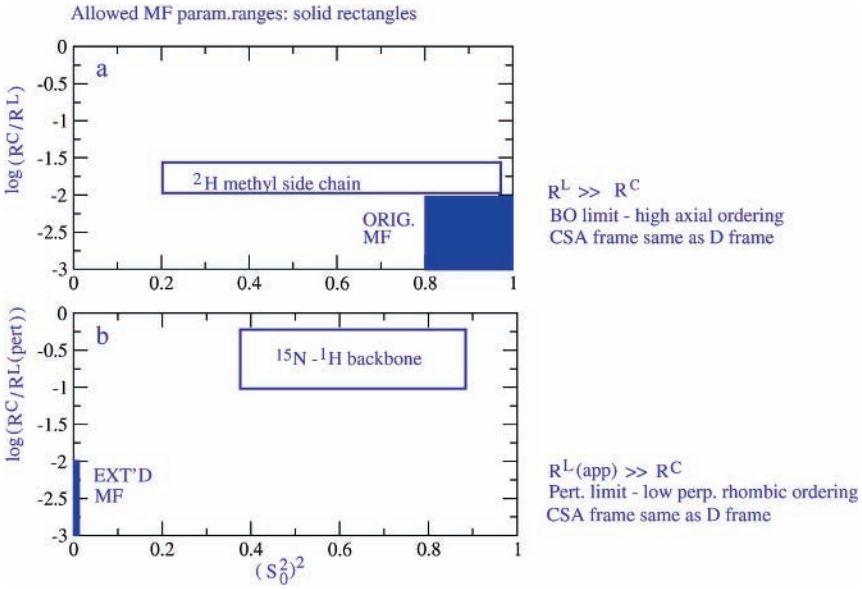


**Figure 1.** Schematic illustration of the range of validity of the original (a) and the extended (b) model-free formulas. $R^C$ ($R^L$) represents the diffusion rate for isotropic global (local) motion. The solid rectangles delineate the valid ranges. The empty rectangles delineate the parameter ranges where these formulas are typically applied in protein dynamics research. The conditions under which the MF formulas are valid are specified on the right-hand side of (a) and (b). $R^L(\text{app}) = 1/3(2R_\perp^L + R_\parallel^L)$.

exceeded in MF studies. We found that typical usage of the original MF formula involves discrepancies on the order of 7−8% between the squared SRLS order parameter, $(S_0^2)^2$, and squared generalized MF order parameter, $S^2$, implied by limited mode mixing effects, and by the simplified MF assumption that the $^{15}N-^{1}H$ dipolar and $^{15}N$ CSA magnetic frames are collinear.[27] If the effective correlation time for local motion, $\tau_e$, is taken to represent the bare correlation time for local motion, $\tau^L$, the latter will be underestimated five-, to 20-fold.[27] The $^2H$ spin relaxation of side chain methyl groups is analyzed mainly with the original MF formula (e.g., refs 31 and 32). The parameter range covered by typical best-fit parameters is shown in Figure 1a by the rectangle labeled "$^2H$ methyl side chain", which clearly digresses from the solid box in this figure. Thus, in this application the original MF formula is mostly used outside of its validity range. The solid box in Figure 1b shows the parameter range in which the extended MF formula is valid. In this case the abscissa represents both the axial, $(S_0^2)^2$, and the rhombic, $(S_2^2)^2$, squared order parameters, which are very small. The rectangle labeled "$^{15}N-^{1}H$ backbone" shows the parameter range in which the extended MF formula is applied in N−H bond dynamics studies. Here the abscissa represents both $S_s^2$ and $S_f^2$. Clearly, in this application, the extended MF formula is used outside of its validity range. We found that the MF parameters $\tau_s$ and $S_s^2$ exceed their formal SRLS analogues, $\tau_\perp^L$ and $(S_0^2)^2$, up to 4-fold and 12-fold, respectively.[19,20,22] Significantly larger disagreements between the SRLS and MF approaches are expected when the SRLS analyses are carried out allowing for rhombic potentials. Illustrative calculations based on a recently developed fitting scheme featuring rhombic potentials are provided below.

Force-fitting will also occur with SRLS versions that are oversimplified as compared to the experimental spectral densities. Therefore, investigating the mechanism of force-fitting with the goal of elucidating the SRLS version, which satisfactorily matches the experimental data as implied by their integrity, is important. This is the subject of the present study. It is shown that the model-free approach force-fits the experimental data because mode mixing, rhombic potentials and general features of local geometry are not accounted for. When possible, the various effects mentioned above are estimated quantitatively. Our general conclusions imply that the dynamic picture yielded by MF analysis is often distorted. We show cases where qualitatively erroneous conclusions were drawn, fictitious phenomena were detected, and known functional dynamics was missed. Conformational entropy and other thermodynamic quantities derived from MF order parameters[33−36] may be inaccurate. Reliable fitting occurs with the SRLS approach when the rhombicity of the local potential is accounted for and the local diffusion is allowed to be axial without limitations on the ratio $N = R_\parallel^L/R_\perp^L$. At this level of complexity the SRLS spectral density matches the integrity of currently available experimental data.

## II. Theoretical Background.

**1. Slowly Relaxing Local Structure (SRLS) Model.** The fundamentals of the stochastic coupled rotator slowly relaxing local structure (SRLS) theory as applied to biomolecular dynamics including protein NMR were outlined recently.[22,25,37] We summarize below key aspects. The various reference frames that define the SRLS model, and their relation to N−H sites in proteins, are shown in Figure 2. A segment of the protein backbone comprising the atoms $C_i^\alpha$, $N_i$, $HN_i$, $C'_{i-1}$, $O_{i-1}$ and $C_{i-1}^\alpha$, the equilibrium positions of which are traditionally taken to lie within the peptide plane defined by $N_i$, $HN_i$, $C'_{i-1}$ and $O_{i-1}$, is illustrated in Figure 2b. The orientation of the N−H bond with respect to the magnetic field is modulated by its local motions and by the global motion of the protein. Thus, in the SRLS model we are dealing with at least two dynamic modes that we can represent by two bodies (N−H bond and protein) whose motions are coupled or mixed.[23,24] For each motion two frames need to be introduced. The first is the local ordering/local diffusion frame, M, which is fixed in body 1 (in this case the N−H bond) and is usually determined by its geometric shape in the context of its motionally restricting environment. The second is the local director frame, C′, whose axes represent the preferred orientation of the N−H bond (Figure 2b) and which is fixed within the protein framework. The motion of body 1 is coupled to, or mixed with, the motion of body 2 (in this case

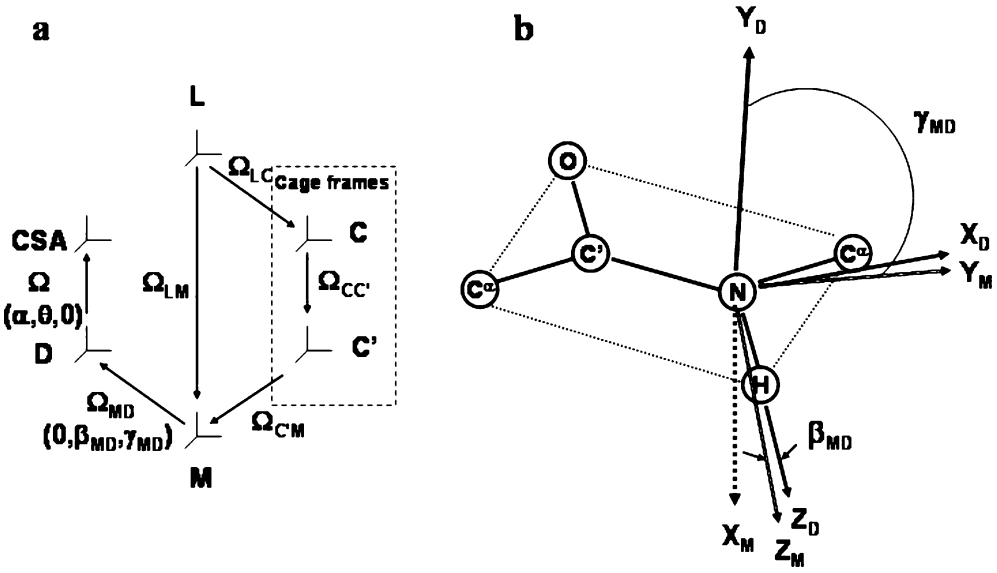


**Figure 2.** (a) Various reference frames which define the slowly relaxing local structure (SRLS) model: L, laboratory frame; C, global diffusion frame associated with protein shape; C′, local director frame associated with the stereochemistry of the local protein structure at the N−H site; M, local ordering/local diffusion frame fixed at the N−H bond; D, magnetic $^{15}N-^{1}H$ dipolar frame; CSA, magnetic $^{15}N$ chemical shift anisotropy frame. (b) $Z_D$, $X_D$, $Z_M$ and $Y_M$ reside within the peptide plane. $Z_D$ lies along the N−H bond and $Y_D$ is perpendicular to the peptide plane.[44] The uniaxial local director (*C*, assuming isotropic global diffusion) is taken to lie along the *equilibrium* $C^{\alpha}_{i-1}-C^{\alpha}_{i}$ axis. The main ordering axis is taken along $C^{\alpha}_{i-1}-C^{\alpha}_{i}$. This implies perpendicular $Y_M$ ordering with $\beta_{MD} = 101.3°$. "Nearly planar $Y_M-X_M$ ordering determined previously[26]", i.e., positive ordering along $X_M$ and almost no ordering along $Z_M$ (for brevity we will denote this ordering symmetry below as "nearly planar $Y_M-X_M$ ordering/symmetry"), implies $\beta_{MD} = 101.3°$ and $\gamma_{MD} = 90°$. For high ordering the $Y_M$ axis is aligned preferentially along *C*. The axes $X_{CSA}$, $Y_{CSA}$ and $Z_{CSA}$ (not shown) are defined to be aligned with the most shielded ($\sigma_{11}$), intermediate ($\sigma_{22}$) and least shielded ($\sigma_{33}$) components of the $^{15}N$ shielding tensor, respectively[44] (information on chemical shielding and local geometry for the $C'-C^{\alpha}$ bond appears in ref 45). The polar angle between $Z_D$ and $Z_{CSA}$ was set equal to 17° in our study.[3] $Y_{CSA}$ is perpendicular to the peptide plane (i.e., parallel to $Y_D$).[44]

the protein) by a local coupling or orienting potential that seeks to bring the N−H bond into alignment with the local director frame. There are no limitations on the relative rates of motion of the two bodies, or the symmetry and strength of the coupling potential.

The reorientation of the $N_i-H_i$ bond is restricted due to limited bond oscillations, conformational reorientations about the adjacent dihedral angles ($\Phi_i$, $\Psi_{i-1}$), the crankshaft motion (anticorrelated rotations about $\Phi_i$ and $\Psi_{i-1}$),[38] nitrogen pyramidalization,[39] peptide-plane motion around $C^{\alpha}_{i-1}-C^{\alpha}_{i}$, etc., and any interactions with the local environment. In general, these processes imply effective Euler angles $\Omega_{MD} = (\alpha_{MD}, \beta_{MD}, \gamma_{MD})$ that define the relative orientation of the local ordering/local diffusion frame, M, and the magnetic $^{15}N-^{1}H$ dipolar frame, D (which lies along the N−H bond). In particular, taking $C^{\alpha}_{i-1}-C^{\alpha}_{i}$ as the local director, C′, and as the main local ordering/local diffusion axis, one has $Y_M$ along the instantaneous orientation of the $C^{\alpha}_{i-1}-C^{\alpha}_{i}$ axis (i.e., "$Y_M$ ordering"), and C′ (i.e., $Z_{C'}$) along the equilibrium orientation of the $C^{\alpha}_{i-1}-C^{\alpha}_{i}$ axis. In this case $\Omega_{MD} = (0°, 101.3°, 90°)$. This geometry is implicit in the 3D Gaussian axial fluctuations (GAF) model[40] (the difference in the $\gamma_{MD}$ values (180° in 3D GAF and 90° in SRLS) is implied by the different definitions of the $X_M$ and $Y_M$ axes). Similar values of $\Omega_{MD}$ are obtained by replacing the $C^{\alpha}_{i-1}-C^{\alpha}_{i}$ axis with the $N_i-C^{\alpha}_{i}$ bond. The N−H bond experiences an increasing orienting potential when $Y_M$ deviates from C′. The global motion of the protein (body 2) is frequently approximated as that of a cylinder, with its long axis taken to be the *z*-axis of the global diffusion (C) frame. For spherical (or globular) proteins the C and C′ frames are the same.

*1a. Geometry.* The various frames of the SRLS model, as applied to amide $^{15}N$ spin relaxation in proteins, are shown in Figure 2a. A formal definition (as compared to the physically descriptive presentation given above) of the various frames follows. The laboratory L frame is space-fixed, both C and C′ are protein-fixed, and the M, D ($^{15}N-^{1}H$ dipolar) and CSA ($^{15}N$ CSA) frames are fixed with respect to the N−H bond. The L frame is considered an inertial frame with respect to which all moving frames are defined. The M frame represents both the local ordering and the local diffusion frame, which for convenience are taken to be the same. The Euler angles $\Omega_{LM}$ are modulated by the local motion and the global motion, whereas the Euler angles $\Omega_{LC}$ are only affected by the latter. These angles are referred to the fixed lab frame to properly describe the diffusion. The local ordering frame M tends to align with respect to a local director C′. The relative orientations of M with respect to C′ and C are defined by $\Omega_{CM}$ and $\Omega_{C'M}$, respectively. The local director C′ is tilted at Euler angles $\Omega_{CC'}$ with respect to the cage (i.e., protein) frame C (tilted with respect to the laboratory frame at Euler angles $\Omega_{LC}$). The Euler angles $\Omega_{CC'}$ are time-independent. It is reasonable to assume that only the polar angle $\beta_{C'C}$ is important. Note that $\Omega_{LM}$ involves the sum of rotations $\Omega_{LC} + \Omega_{CC'} + \Omega_{C'M}$ [here and in the following we shall employ a shorthand notation for indicating sequences of rotations; namely, for a generic rotation $\Omega_{12} = \Omega_2 + \Omega_1$, resulting from first applying $\Omega_1$ and then $\Omega_2$ we can write the explicit relation among Wigner rotation matrices as $D^{j}_{mk}(\Omega_{12}) = \Sigma_{m'} D^{j}_{mm'}(\Omega_1)\, D^{j}_{m'k}(\Omega_2)$]. The time dependence of the Euler angles $\Omega_{C'M}$ is governed by the local orienting potential, which couples the two modes of motion. *Through the time dependence of $\Omega_{C'M}$ the locally reorienting N−H bond follows the slower motion of the protein.*

The magnetic $^{15}N-^{1}H$ dipolar tensor frame, D, and the magnetic $^{15}N$ CSA tensor frame, CSA, are also shown in Figure 2a. The Euler angles specifying the rotation from M to D are $\Omega_{MD}$, and the rotation from D to CSA is given by Ω. The Euler angles $\Omega_{MD}$ and Ω are time independent. The D frame is axially

symmetric. If the M frame is also axially symmetric, then $\Omega_{MD} = (0, \beta_{MD}, 0)$, where $\beta_{MD}$ is known as "diffusion tilt".

The diffusion tensor $R^L$ describing the rotational diffusion properties of the probe (N−H bond in this case) is diagonal in M, whereas the diffusion tensor $R^C$ describing the rotational diffusion properties of the cage (protein in this case) is diagonal in C. We start by assuming Smoluchowski dynamics for the coupled set of orientational coordinates $\Omega_{LM}$ and $\Omega_{LC}$, according to the slowly relaxing local structure approach. Namely, the system consists of two Brownian rotators (or "bodies")—the amide group and the rest of protein—linked by an interaction potential that depends on their relative orientation. Their motions are characterized by slow diffusive changes, controlled by suitable rotational diffusion parameters. Formally, the diffusion equation for the coupled system is given by

$$\frac{\partial}{\partial t}P(X,t) = -\hat{\Gamma}P(X,t) \tag{1}$$

where $X$ is a set of coordinates completely describing the system

$$X = (\Omega_{LM},\Omega_{LC})$$
$$\hat{\Gamma} = \hat{J}(\Omega_{LM})\mathbf{R}^L P_{eq}\hat{J}(\Omega_{LM})P_{eq}^{-1} + \hat{J}(\Omega_{LC})\mathbf{R}^C P_{eq}\hat{J}(\Omega_{LC})P_{eq}^{-1} \tag{2}$$

where $\hat{J}(\Omega_{LM})$ and $\hat{J}(\Omega_{LC})$ are the angular momentum operators for the probe and the cage, respectively.

Changing to different coordinates is straighforward.[28] We select the set defined by $\Omega_{C'M}$ and $\Omega_{LC'}$. *The Euler angles $\Omega_{C'M}$ describe the orientation of the M frame fixed at the N−H bond relative to the protein-fixed C′ frame and the Euler angles $\Omega_{LC'}$ describe the C′ frame orientation with respect to the lab frame*. In the new coordinate frame one has

$$X = (\Omega_{C'M},\Omega_{LC'})$$
$$\hat{\Gamma} = \hat{J}(\Omega_{C'M})\mathbf{R}^L P_{eq}\hat{J}(\Omega_{C'M})P_{eq}^{-1} + [\hat{J}(\Omega_{C'M}) - \hat{J}(\Omega_{LC'})]\mathbf{R}^C P_{eq}[\hat{J}(\Omega_{C'M}) - \hat{J}(\Omega_{LC'})]P_{eq}^{-1} \tag{3}$$

The Boltzmann distribution $P_{eq} = \exp[-U(\Omega_{LM})/k_BT]/\langle\exp[-U(\Omega_{LM})/k_BT]\rangle$ is defined with respect to the probe-cage interaction potential given by

$$u(\Omega_{C'M}) = \frac{U(\Omega_{C'M})}{k_BT} = -c_0^2 D_{0,0}^2(\Omega_{C'M}) - c_2^2[D_{0,2}^2(\Omega_{C'M}) + D_{0,-2}^2(\Omega_{C'M})] \tag{4}$$

This represents the expansion in the full basis set of Wigner rotation matrix elements, $D^L_{KM}(\Omega_{C'M})$, with only lowest order, i.e., $L = 2$, terms being preserved. The coefficient $c_0^2$ is a measure of the orientational ordering of the N−H bond with respect to the local director whereas $c_2^2$ measures the asymmetry of the ordering around the director. Here we follow historical convention by using $L = 2$ terms as the leading terms, rather than $L = 1$. This is sufficient for many purposes, as we have previously shown, because NMR involves second-rank (i.e., $L = 2$) magnetic tensors.[23] However, the SRLS theory can readily be modified to include $L = 1$ terms. The current approach is in the spirit of keeping the number of parameters to a minimum.

The SRLS equation can be solved in terms of the time-dependent distribution $P(\Omega_{C'M},\Omega_{LC'},t)$, which describes the evolution in time and orientational space of the system. Alternatively, it is convenient to directly calculate time correlation functions $C^J_{M,KK'}(t) = \langle D^J_{M,K}{}^*(\Omega_{LM})|\exp(-\hat{\Gamma}t)| \times D^J_{M,K'}(\Omega_{LM})P_{eq}\rangle$, which for proper values of the quantum numbers $J,M,K,K'$ determine the experimental NMR relaxation rates. Actually, the Fourier−Laplace transforms of $C^J_{M,KK'}(t)$ are needed, and they are obtained as the spectral densities at a given frequency $\omega$:

$$j^M_{KK'}(\omega) = \langle D^J_{M,K}{}^*(\Omega_{LM})|(i\omega + \hat{\Gamma})^{-1}|D^2_{M,K'}(\Omega_{LM})P_{eq}\rangle \tag{5}$$

As stated here, the model has eleven parameters: $c_0^2$, $c_2^2$ (potential parameters), $R_i^L$ (probe diffusion $i = 1, 2, 3$ principal values), $R_i^C$ (global diffusion $i = 1, 2, 3$ principal values) and $\Omega_{CC'} = (\alpha_{CC'},\beta_{CC'},\gamma_{CC'})$ (global diffusion tilt angles). For the sake of simplicity we shall limit our analysis to axial probe $R_1^L = R_2^L = R_\perp^L \neq R_3^L = R_\parallel^L$, axial cage $R_1^C = R_2^C = R_\perp^C \neq R_3^C = R_\parallel^C$, and $\alpha_{CC'} = \gamma_{CC'} = 0$. The orientation of the magnetic tensors is specified by $\Omega_{MD}$ and $\Omega$ (defined in Figure 2a). In the past work[19,20,22,26,27] we made use of eq 2 involving $\Omega_{LM}$ and $\Omega_{LC}$. In the present study we have used eq 3 involving $\Omega_{LC'}$ and $\Omega_{C'M}$. The primary reason is that the use of the relative orientation of the N−H bond in the protein specified by the $\Omega_{C'M}$ is the more natural one in terms of conventional intuition. One can simply think of the Euler angles $\Omega_{C'M}$ as just being modulated by the local motion, whereas $\Omega_{LC'}$ is just modulated by the overall tumbling of the protein. Also, as we have already noted, the $\Omega_{C'M}$ are the natural coordinates for expressing the potential energy given by eq 4. (This does, however, render the $\hat{\Gamma}$ operator somewhat more complicated.) Of course, the two forms are mathematically equivalent. In the $C'$ frame, the global diffusion tensor assumes the form

$$\mathbf{R}^C = \begin{pmatrix} R_\perp^C\cos^2\beta_{CC'} + R_\parallel^C\sin^2\beta_{CC'} & 0 & \frac{1}{2}(R_\perp^C - R_\parallel^C)\sin(2\beta_{CC'}) \\ 0 & R_\perp^C & 0 \\ \frac{1}{2}(R_\perp^C - R_\parallel^C)\sin(2\beta_{CC'}) & 0 & R_\perp^C\sin^2\beta_{CC'} + R_\parallel^C\cos^2\beta_{CC'} \end{pmatrix} \tag{6}$$

The probe diffusion tensor is diagonal in the M frame. Note that for $\beta_{CC'} = 0$ or $R_\perp^C = R_\parallel^C$ the global diffusion tensor is diagonal and invariant in both the C and C′ frames.

*1b. Numerically Exact Treatment.* We address here the problem of devising an efficient procedure for evaluating numerically accurate spectral densities. We adopt a variational scheme, based on a matrix vector representation of eq 5, followed by an application of the Lanczos algorithm in its standard form developed for Hermitian matrices. It is convenient to express the generic correlation function as the linear combination of normalized autocorrelation functions. Defining $2A^J_{M,KK'} = D^J_{M,K} + D^J_{M,K'}$, the spectral densities of the normalized autocorrelation functions of interest are

$$j^S_{M,KK'}(\omega) = \langle A^J_{M,KK'}{}^*(\Omega_{LM})P_{eq}{}^{1/2}|(i\omega + \tilde{\Gamma})^{-1}| \times A^J_{M,KK'}(\Omega_{LM})P_{eq}{}^{1/2}\rangle/\langle|A^J_{M,KK'}(\Omega_{LM})|^2P_{eq}\rangle \tag{7}$$

and the generic spectral densities are

$$j_{M,KK'}(\omega) = [2(1 + \delta_{K,K'})j^S_{M,KK'}(\omega) - j^S_{M,KK}(\omega) - j^S_{M,K'K'}(\omega)]/2[J] \tag{7a}$$

where $J = 2$ and $M = 0$ in our case. We use the shorthand notation $[J] = 2J + 1$. A numerical calculation is then performed by choosing a basis set of functions, representing in matrix form

the transformed operator $\tilde{\Gamma} = P_{eq}^{-1/2}\hat{\Gamma}P_{eq}^{1/2}$, and evaluating eq 7 directly by employing a standard Lanczos approach. The latter is reviewed here for completeness in accordance with the standard technique of Moro and Freed.[41,42] Let us suppose that we are interested in calculating the Fourier−Laplace transform of the normalized autocorrelation function of an observable $f(q)$ for a diffusive symmetrized (i.e., Hermitian) operator $\tilde{\Gamma}$ acting on coordinate $q$, in the form $j(\omega) = \langle \delta f^* P_{eq}^{1/2} | (i\omega + \tilde{\Gamma})^{-1} | \delta f P_{eq}^{1/2} \rangle / \langle |f|^2 P_{eq} \rangle$, where $\delta f = f - \langle f P_{eq} \rangle$ is the observable redefined to yield an average value of zero. In the present case we consider only rotational motion in an isotropic fluid, so the relevant $\langle f P_{eq} \rangle = 0$. The Lanczos algorithm is a recursive procedure for generating orthonormal functions that allow a tridiagonal matrix representation of $\tilde{\Gamma}$ in terms of the coefficients $\alpha_n$, $\beta_n$, which form the main and secondary diagonal of the tridiagonal symmetric matrix **T**, and the spectral density can be written in the form of a continued fraction.[41,42] The calculation of the tridiagonal matrix elements can be carried out in finite precision by working in the vector space obtained by projecting all the functions and operators on a suitable set of orthonormal functions $|\lambda\rangle$. One only needs to define the matrix operator, $\Gamma$, and starting vector elements, $\mathbf{v}_1$, given by $\Gamma_{\lambda,\lambda'} = \langle \lambda | \tilde{\Gamma} | \lambda' \rangle$, $v_\lambda = \langle \lambda | 1 \rangle$, respectively.

In the case under study the SRLS diffusion operator is given by eq 3 and the starting vector is given by

$$|1\rangle = A^J_{M,KK'}(\Omega_{LM}) P_{eq}^{1/2} / \langle |A^J_{M,KK'}|^2 P_{eq} \rangle = \sqrt{\frac{2[J]}{1+\delta_{K,K'}}} A^J_{M,KK'}(\Omega_{LM}) P_{eq}^{1/2}$$

A natural choice for a set of orthonormal functions is the direct product of normalized Wigner matrices. What is left is the calculation of the matrix elements $\Gamma_{\lambda,\lambda'}$ and the vector elements $\langle \lambda | 1 \rangle$. The algebraic intermediate steps are relatively straightforward and based on properties of the Wigner rotation matrices, angular momentum operators and spherical tensors; we skip the technical details and list the resulting expressions.[23,24,28]

*1c. Observables.* To interpret $^{15}$N−$^{1}$H dipolar and $^{15}$N CSA autocorrelated relaxation rates, we only need spectral densities with $J = 2$ and $M = 0$. Dependence upon $K,K'$ is slightly more complex and is discussed in detail in the following section.

According to standard analysis for the motional narrowing regime,[43] we can define the observable spectral density for two magnetic interactions $\mu$ and $\nu$ as the real part of the Fourier−Laplace transform of the correlation function of the second-rank Wigner functions for the orientation of the magnetic tensors in the laboratory frame (here $\mu,\nu$ = D or CSA, $\Omega^D = \Omega_{MD}$, and $\Omega^{CSA} = \Omega_{MD} + \Omega$, cf. Figure 2a):

$$J^{\mu\nu}_M(\omega) = \int_0^\infty e^{-i\omega t} \langle D^2_{M,0}{}^*[\Omega^\mu + \Omega_{LM}(t)]\, D^2_{M,0}{}^*[\Omega^\nu + \Omega_{LM}(0)] \rangle \quad (8)$$

and relying on standard properties of the Wigner functions, in the form

$$J^{\mu\mu}_M(\omega) = \int_0^\infty e^{-i\omega t} \sum_{KK'} D^2_{K,0}{}^*(\Omega^\mu)\, D^2_{K',0}(\Omega^\mu) \times \langle D^2_{M,K}{}^*[\Omega_{LM}(t)]\, D^2_{M,K'}{}^*[\Omega_{LM}(0)] \rangle \quad (8a)$$

On the basis of the symmetry relation $j^J_{M,KK'} = j^J_{M,K'K}$ (cf. eq 7a), we obtain

$$\mathcal{R}[J^{\mu\mu}_M(\omega)] = \sum_K |D^2_{K,0}(\Omega^\mu)|^2 \mathcal{R}[j_{M,KK}(\omega)] + 2\sum_{K<K'} \mathcal{R}[D^2_{K,0}{}^*(\Omega^\mu)\, D^2_{K',0}(\Omega^\mu)]\, \mathcal{R}[j_{M,KK'}(\omega)] \quad (9)$$

where $\mathcal{R}$ stands for the real part. Note that for axial potentials ($c_2^2 = 0$) the second term goes to zero and we are left with standard expressions. The coefficients $D^2_{K,0}(\Omega^D)$ are readily evaluated, whereas $D^2_{K,0}(\Omega^{CSA})$ can be calculated in terms of $\Omega_{MD}$ and $\Omega$, as in the expression

$$D^2_{K,0}(\Omega^{CSA}) = \sum_L D^2_{K,L}(\Omega_{MD})\, D^2_{L,0}(\Omega)$$

The spectral densities for $^{15}$N−$^{1}$H dipolar and $^{15}$N CSA autocorrelation are then obtained as $J^{DD}(\omega) = \mathcal{R}[J_0^{D,D}(\omega)]$ and $J^{CC}(\omega) = \mathcal{R}[J_0^{CSA,CSA}(\omega)]$, respectively. The measurable $^{15}N$ relaxation quantities $^{15}$N $T_1$, $T_2$ and $^{15}$N−{$^{1}$H} NOE are calculated as functions of $J^{DD}(\omega_i)$ and $J^{CC}(\omega_i)$, with $\omega_i = 0$, $\omega_H$, $\omega_N$, $\omega_H - \omega_N$ and $\omega_H + \omega_N$, using standard expressions for NMR spin relaxation.[4,5] Note that due to the additional symmetry relation $j_{M,K,K'} = j_{M,-K,-K'}$, only the nine distinct couples $(K,K') = (-2,2), (-1,1), (-1,2), (0,0), (0,1), (0,2), (1,1), (1,2), (2,2)$ need to be considered. For dipolar autocorrelation one has the explicit expression (denoting $j_{KK'} = \mathcal{R}[j^2_{0,KK'}(\omega)]$ for brevity)

$$J^{DD}(\omega) = d^2_{00}(\beta_{MD})^2 j_{00} + 2d^2_{10}(\beta_{MD})^2 j_{11} + 2d^2_{20}(\beta_{MD})^2 j_{22} + 4d^2_{00}(\beta_{MD})\, d^2_{20}(\beta_{MD}) j_{02} + 2d^2_{-10}(\beta_{MD})\, d^2_{10}(\beta_{MD}) j_{-11} + 2d^2_{-20}(\beta_{MD})\, d^2_{20}(\beta_{MD}) j_{-22} \quad (10)$$

with only six couples $(K,K') = (0,0), (1,1), (2,2), (0,2), (-1,1)$ and $(-2,2)$ involved.

A convenient measure of the orientational ordering of the N−H bond is provided by the order parameters, $S_0^2 = \langle D^2_{00}(\Omega_{C'M}) \rangle$ and $S_2^2 = \langle D^2_{02}(\Omega_{C'M}) + D^2_{0-2}(\Omega_{C'M}) \rangle$, which are related to the orienting potential (eq 4), hence $c_0^2$ and $c_2^2$, via the ensemble averages:

$$\langle D^2_{0n}(\Omega_{C'M}) \rangle = \int d\Omega_{C'M}\, D^2_{0n}(\Omega_{C'M}) \times \exp[-u(\Omega_{C'M})] / \int d\Omega_{C'M} \exp[-u(\Omega_{C'M})] \quad (11)$$

One may convert to Cartesian ordering tensor components according to

$$S_{zz} = S_0{}^2 \quad S_{xx} = (\sqrt{3/2} S_2{}^2 - S_0{}^2)/2 \quad S_{yy} = -(\sqrt{3/2} S_2{}^2 + S_0{}^2)/2$$

Note that $S_{xx} + S_{yy} + S_{zz} = 0$.

In case of zero potential, $c_0^2 = c_2^2 = 0$, and axial diffusion, the solution of the diffusion equation associated with the time evolution operator features three distinct eigenvalues:

$$1/\tau_K = 6R^L_\perp + K^2(R^L_\parallel - R^L_\perp) \qquad \text{for} \qquad K = 0, 1, 2 \quad (12)$$

where $R^L_\parallel = 1/(6\tau_\parallel)$ and $R^L_\perp = 1/(6\tau_\perp) = 1/(6\tau_0)$. Only diagonal $j_K(\omega) \equiv j_{KK}(\omega)$ terms are nonzero and they can be calculated analytically as Lorentzian spectral densities, each defined by width $1/\tau_K$. When the ordering potential is axially symmetric, $c_0^2 \neq 0$, $c_2^2 = 0$, again only diagonal terms survive, but they are given by infinite sums of Lorenzian spectral densities, which are defined in terms of eigenvalues $1/\tau_i$ of the diffusion operator, and weighing factors $c_{K,i}$, such that

$$j_K(\omega) = \sum_i \frac{c_{K,i}\tau_i}{1 + \omega^2 {\tau_i}^2} \quad (13)$$

The eigenvalues $1/\tau_i$ represent modes of motion of the system, in accordance with the parameter range considered. Note that although in principle the number of terms in eq 13 is infinite, in practice a finite number of terms is sufficient for numerical convergence of the solution. Finally, when the local ordering potential is rhombic, $c_0^2 \neq 0$, $c_2^2 \neq 0$, both diagonal $j_K(\omega)$ and nondiagonal $j_{KK'}(\omega)$ terms are different from zero and need to be evaluated explicitly according to expressions analogous to eq 13.

Details of the implementation of the SRLS model in a data fitting scheme featuring axial potentials and isotropic global diffusion were outlined previously.[22] For practical reasons this fitting scheme is based on precalculated 2D grids of spectral densities, $j_K(\omega)$. The coordinates of these grids are $c_0^2$ and $R^C$. The structural parameters $\beta_{MD}$ and $\gamma_{MD}$ are used to assemble $J^{DD}(\omega)$ out of $j_K(\omega)$. The set of free variables includes $c_0^2$, $R^C$ and $\beta_{MD}$. The angle $\gamma_{MD}$ was fixed at 90° on the basis of stereochemical considerations, and $R_{||}^L \gg R_\perp^L$ (in analogy with the MF requirement that $\tau_s \gg \tau_f$) was imposed. This scheme is computationally as fast as the commonly used MF fitting schemes.[46,47]

We developed recently a fitting scheme where the functions $j_{KK'}(\omega)$ are calculated on the fly. In this case the set of free variables includes $c_0^2$, $c_2^2$, $R_{||}^L/R_\perp^L$, $R^C$ and $\beta_{MD}$. Clearly the local potential is allowed to be rhombic and the local diffusion, axial. For high rhombic potentials and small $R^C/R^L$ values this scheme is currently rather demanding computationally and efforts to improve its efficiency are underway. A number of conditions can be employed, however, to simplify the analysis. If the local geometry is assumed to be known, as in the 3D GAF model,[40] $\beta_{MD}$ can be fixed (e.g., at 101.3°). If the symmetry of the local ordering is known, $c_2^2/c_0^2$ can be fixed. Note that in the SRLS approach the global diffusion rate, $R^C$, is determined in the same fitting process as the site-specific parameters, as is appropriate when the modes $R^C$ and $R^L$ are "mixed". The next stage will be to allow the global diffusion tensor to be axially symmetric. This requires a complex fitting scheme where the $R^C$ tensor is global whereas all the other parameters are local. Instead of a single variable for global motion, $R^C$, three variables, $R^C(\text{app}) = {}^1/_3(2R_\perp^C + R_{||}^C)$, $R_{||}^C/R_\perp^C$ and $\beta_{CC'}$ will be featured. Note that $R^C$ and $R^C(\text{app})$ define the time scale separation between the global and local motions as rates are given in the SRLS model in units of $R_\perp^L$.

When the local potential is taken to be axially symmetric in the SRLS model, then formal (but not necessarily physical) analogies with the MF formulas can be established. In this case the number of formally analogous free parameters, hence the minimum number of data points required, is the same in the SRLS and MF analyses.[22] Model-free data fitting was carried out in this study with the computer programs Modelfree 4.0[46] and Dynamics.[47]

Thus, the spectral densities $j_K(\omega)$ ($j_{KK'}(\omega)$ for rhombic potentials) are the building blocks for a given dynamic model relative to the local diffusion frame, and the spectral densities $J^x(\omega)$ are the building blocks for a specific geometric implementation of this dynamic model relative to the frames of the magnetic tensors. The measurable quantities are $J^x(0)$, $J^x(\omega_N)$, $J^x(\omega_H)$, $J^x(\omega_H+\omega_N)$ and $J^x(\omega_H-\omega_N)$. Together with the magnetic interactions they determine the experimentally measured relaxation rates according to standard expressions for NMR spin relaxation.[4,5] If the equilibrium orientations of $^{15}N_i-{}^1H_i$ and $^{13}C_{i-1}^\alpha-{}^{13}C'_{i-1}$ are assumed to reside within the peptide plane, then the functions $j_{KK'}(\omega)$ for N−H bond dynamics can also be used to treat $C^\alpha-C'$ bond dynamics. A different local geometry, specific to the $C^\alpha-C'$ bond, determines the $J^x(\omega)$ functions, and different magnetic interactions enter the calculation of the $^{13}C$-related relaxation rates measured experimentally.

**2. Model-Free Approach.** A brief summary of the model-free approach, as formulated by its developers, is outlined below.

*2a. Original MF Spectral Density.*[6,7] The basic premise is that the global motion of the protein is much slower than the local motions of the N−H bond. Consequently, the global and local motions are "independent", and the total time correlation function, $C(t)$, can be expressed as

$$C(t) = C^C(t)\, C^L(t) \quad (14)$$

The global motion is assumed to be isotropic, with $C^C(t) = \exp(-t/\tau_m)$. $C^L(t)$ is given by

$$C^L(t) = S^2 + (1 - S^2)\exp(-t/\tau_e) \quad (15)$$

where $\tau_e$ is the effective correlation time for local motion defined as the area of $C^L(t)$ divided by $(1 - S^2)$, and $\tau_e \ll \tau_m$. The parameter $S^2$, which represents the plateau value of $C^L(t)$ at long times ($t \gg \tau_e$), is taken as the square of a generalized order parameter. This definition of $S^2$ (eqs 14−16 of ref 6) involves the spherical harmonic functions of rank 2, whereas $C^L(t)$ at shorter times is given in terms of the Legendre polynomial of rank 2 (eq 12 of ref 6). All of the equations cited involve the equilibrium probability distribution function, $P_{eq}(\Omega_{CM})$ where C denotes the local director fixed in the protein (called "molecular axis" in ref 6), and M the local diffusion frame (taken in the MF analysis to lie along the N−H bond). Equation 12 of ref 6 features $P_{eq}(0,\beta_{CM},0)$ ($p_{eq}(\theta)$ in the notation of ref 6), whereas eqs 14−16 of ref 6 feature $P_{eq}(0,\beta_{CM},\gamma_{CM})$ ($p_{eq}(\theta,\phi)$ in the notation of ref 6). Thus, there is inconsistency in the symmetry of $C^L(t)$ at short and long times, implied by M considered axial in eq 12 and rhombic in eqs 14−16.

Fourier transformation of eq 14 with eq 15 inserted for $C^L(t)$ yields

$$J(\omega) = S^2\tau_m/(1 + \omega^2{\tau_m}^2) + (1 - S^2)\tau_e'/(1 + \omega^2\,{\tau_e'}^2) \quad (16)$$

where $1/\tau_e' = 1/\tau_e + 1/\tau_m$.

*2b. Original MF Formula as SRLS Asymptote.* It was shown in early work[30] that in the limit where $R^L \gg R^C$ the following equation is valid in the perturbation limit, i.e., *for very small local ordering*:

$$j_K(\omega) = (S_K^2)^2[\tau_m/(1 + \omega^2{\tau_m}^2) + (1 - (S_K^2)^2)\tau_K/(1 + \omega^2{\tau_K}^2)] \quad (17)$$

with $\tau_K$ given by eq 12. $S_K^2$ denotes the principal values of the ordering tensor in irreducible tensor notation (where $S_1^2 = 0$). When the symmetry of the local potential/local ordering is axial, then $S_2^2$ is zero. In this case $j_0(\omega)$ is the same as eq 16 with $S^2 = (S_0^2)^2$ and $\tau_e = \tau_0$, whereas the $j_{K\neq 0}(\omega)$ functions are given by $\tau_K/(1 + \omega^2\tau_K^2)$.[48]

The function $C_0(t)$ corresponding to $j_0(\omega)$ is shown by the dashed curve in Figure 3a, with the plateau value given by $(S_0^2)^2$ and the decay to it by $\tau_0 = 1/6R^L$. The final decay of $C_0(t)$ to zero is given by $\tau_m = 1/6R^C$. However, the local ordering at an N−H bond is never as low as required by the perturbation limit in the local ordering, but rather quite high. Using the full SRLS

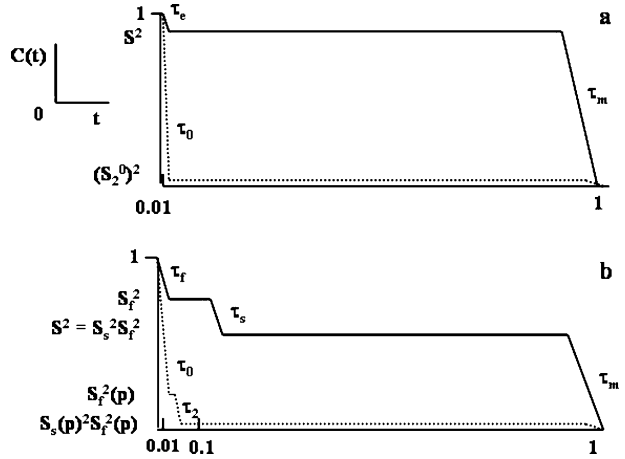


**Figure 3.** (a) Time correlation function, $C(t)$, corresponding to $j_0(\omega)$ of eq 17 (and eq 16 applied in the perturbation limit) with $(S_0^2)^2 \rightarrow 0$ and $\tau_0/\tau_m \ll 1$ (dashed curve). Time correlation function, $C(t)$, corresponding to eq 16 with $(S_0^2)^2 \sim 0.8$ and $\tau_e/\tau_m \ll 1$ (solid curve). (b) Time correlation function, $C(t)$, corresponding to eq 20 (and eq 19 applied in the perturbation limit) with $(S_0^2)^2 \rightarrow 0$ and $(S_2^2)^2 \rightarrow 0$ ($S_f^2 \sim 0.25$ and $S_s^2 \sim 0$) and $\tau_0$, $\tau_2 \ll \tau_m$ ($\tau_f$, $\tau_s \ll \tau_m$) (dashed curve). Time correlation function, $C(t)$, corresponding to eq 19 as applied to treat flexible residues in proteins with $S_f^2 \sim 0.75$, $S^2 \sim 0.55$, $\tau_s/t_f \sim 10$ and $\tau_f/\tau_m \ll 1$ (solid curve). The index "p" stands for "perturbational limit". The abscissas in (a) and (b) are given in units of $\tau^L/\tau_m$. Note that $\tau_e$ and $\tau_f$ are significantly smaller than displayed (for visibility), as they represent renormalized correlation times.

solution we showed in previous work[26] that for high enough $(S_0^2)^2$ and low enough $R^C/R^L$ (see ref 26 for quantitative evaluation of validity ranges) eq 16 is valid with $S^2 \sim (S_0^2)^2$ and the initial decay of $C_0(t)$ given by

$$\tau_{initial} = \tau_e \sim \tau_{ren} = 2\tau_0/c_0^2 \qquad (18)$$

where $\tau_{ren}$ is the renormalized correlation time for local motion.[29] The parameter $1/6\tau_{ren}$ is the rate at which the distribution of orientations is restored to equilibrium when a spin-bearing particle reorients rapidly in the presence of a *strong* orienting potential.[29,49] $\tau_{ren}$ is reduced significantly relative to $\tau_0$, in accordance with the strength, $c_0^2$, and symmetry, of the local potential. The expression given by eq 18 is valid in the SRLS approach in the limit where $R^L \gg R^C$ when the local potential is axial and high.[27] In this case eq 16 is a good approximation of the SRLS solution with $S^2$ representing $(S_0^2)^2$ and $\tau_e$ representing $\tau_{ren}$. The time correlation function corresponding to eq 16 is shown by the solid curve in Figure 3a.

The range of validity of eq 16 depends on $\tau_m$ and the experimental uncertainties. It can be determined by comparing MF results with SRLS results. For example, we showed previously that for $\tau_m = 15$ ns and typical experimental errors, eq 16 may be considered valid when $S^2 \geq 0.8$ and $\tau/\tau_m \leq 0.01$ (ref 27). When these conditions are fulfilled (see below), $S^2$ and $\tau_e$ are physically meaningful. Otherwise they become parametrizing entities.

When $S^2$ is high, the angle $\beta_{CM}$ is restricted to small values; hence the cosine squared potential of the cone model is a good approximation to $U/k_BT = -c_0^2P(\cos\beta_{CM})$, where $P_2$ denotes the Legendre polynomial of rank 2. This represents the first term of eq 4. In this case $\tau_e$ determined with the wobble-in-a-cone model agrees with $\tau_{ren}$, the wobbling rate, $D_w$, of the cone model represents $R_\perp^L$ and $D_{||} = R_{||}^L \rightarrow \infty$. Other models, such as the Woessner model, or jumps between symmetry-related sites,[6] yield $\tau_e$ values, which can disagree with $\tau_{ren}$ (eq 18). The quantity $S^2$, taken as the square of a generalized order parameter, is in actual fact an approximation to $(S_0^2)^2$ when the time scale separation between the global and local motions is large enough, and the ordering high enough for the solution for the local motion to be given solely in terms of the $D_{MK}^L$. When $(S_0^2)^2$ is not very high, additional local motion eigenmodes emerge. Their presence requires a more complex description of how the correlation functions of the $D_{MK}^L$ relate to the eigenmodes of a rotor in a fairly restricted (even static) potential. Quantitative evaluations of validity ranges appear in ref 26.

The order parameter $S_0^2$ is obtained in terms of $U/k_BT = -c_0^2P_2(\cos\beta_{CM})$ on the basis of $P_{eq}(\beta_{CM}) \propto \exp(-U/k_BT)$ (eq 4 with $c_2^2 = 0$, and eq 11). Likewise, conformational entropy (or any other thermodynamic quantity based on $P_{eq}$) is obtained automatically in SRLS analysis. In the MF analysis the form of the axial local potential has to be guessed and its strength derived from $S^2$ to calculate thermodynamic properties, notably residual configurational entropy. This is appropriate only when $S^2$ is a good approximation to $(S_0^2)^2$; i.e., when the conditions specified in the previous paragraph are fulfilled. Because this is often not the case the MF-derived residual configurational entropy is likely to be inaccurate. The form of the potential is clearly ambiguous. As pointed out in the previous paragraph, other forms may not be compatible with the (physical) meaning of $\tau_e$ as given by eq 18, which can complicate their interpretation. In the SRLS approach the potential given by eq 4 represents the leading terms in a complete expansion, and the parameters varied are the potential coefficients. The latter procedure is a general one.

For high rhombic ordering there is no analytical expression for $C(t)$, so the ensuing spectral density, even in the $R^L \gg R^C$ (BO) limit, requires the full SRLS solution. We found that the actual local potential at N−H sites in proteins is rhombic. Note that in SRLS analysis the conformational entropy can still be calculated on the basis of $P_{eq}$ using the rhombic form of the potential (eq 4) with $c_0^2$ and $c_2^2$ determined with data fitting.

For rigid residues, where the fast local fluctuations at the N−H site can be considered harmonic, rhombic local ordering can be treated with the 3D GAF model.[40] The local geometry is predetermined in 3D GAF by selecting $C_{i-1}^\alpha - C_i^\alpha$ as the principal ordering axis ($z$), with $x$ perpendicular to it within the peptide plane. Contrary to the 3D GAF model, the SRLS approach is applicable to arbitrary local geometry and arbitrary rates of local motion.[22−25] Rhombic symmetry of the local ordering is outside the scope of the MF treatment. Taking the D and $^{15}$N CSA frames collinear in the MF approach introduces further inaccuracies (see below).

*2c. Single-Exponential Approximation, $\tau_e$, and the Effect of Additional Local Motion Eigenmodes.* It was shown in early work that a single exponent, with time constant $\tau_e$, is a good approximation for the multiexponential time correlation function of the wobble-in-a-cone model.[50,51] Moreover, an analytical formula which relates $\tau_e$ to $S^2$ and the wobbling rate, $D_w$, was developed.[51] This result is based on the assumption that eq 14 is valid, which implies the neglect of additional local motion eigenmodes. Table 1 shows the SRLS eigenvalues (and corresponding weights) which contribute to $C(t)$ for a time scale separation $\tau^L/\tau_m = 0.01$ and potential strength decreasing from $c_0^2 = 20$ ($(S_0^2)^2 = 0.901$) to $c_0^2 = 4$ ($(S_0^2)^2 = 0.507$). As a benchmark we show the eigenvalues and associated weights when a single local motion eigenmode prevails. These include $1/\tau_m$ (column 3) and $(S_0^2)^2$ (column 1) for the global motion, and $1/\tau_{ren}$ (column 2, calculated with eq 18) and $(1 - (S_0^2)^2)$ (numbers in parentheses in column 6) for the local motion.

**TABLE 1: SRLS Eigenvalues $1/\tau_m$ ($1/\tau^L$) of the Global Motion Mode Term (the Main Local Motion Term, i.e., the Largest $1/\tau(i)$ Value of Eq 13 with Weight Near $(1 - (S_0^2)^2)$), and Associated Weights $wt^C$ ($wt^L$), as a Function of $c_0^2$ in Units of $k_BT$ (and Corresponding $(S_0^2)^2$ Values) Calculated for $\tau^L/\tau_m = 0.01$[a]**

| $c_0^2$ ($(S_0^2)^2$) | $1/\tau_{ren}$ | $1/\tau_m$ | $wt^C$ | $1/\tau^L$ | $wt^L$ [b] | $w^{MM}$, %[c] |
|---|---|---|---|---|---|---|
| 20 (0.901) | 60 | 0.06 | 0.903 | 58.5 | 0.093(0.099) | 0.4 |
| 10 (0.803) | 30 | 0.06 | 0.800 | 27.9 | 0.172 (0.197) | 2.8 |
| 8 (0.754) | 24 | 0.06 | 0.757 | 21.6 | 0.202 (0.246) | 4.1 |
| 6 (0.671) | 18 | 0.06 | 0.676 | 15.4 | 0.239 (0.329) | 8.5 |
| 4 (0.507) | 12 | 0.06 | 0.512 | 10.0 | 0.294 (0.493) | 19.4 |

[a] The eigenvalues are given in units of $R^L$; hence $1/\tau^L = 6$ and $1/\tau_m = (\tau^L/\tau_m \times 6)$. The parameter $1/\tau_{ren}$ represents the renormalized local motion eigenvalue calculated with eq 18. [b] The numbers in parentheses show $(1 - (S_0^2)^2)$. [c] The percent deviation of the correlation function for local motion from its solely $D_{KM}^L$-determined single-local-motion-eigenmode form (see above).

Column 7 shows the percent deviation of the correlation function for local motion from its solely $D_{KM}^L$-determined single-local-motion-eigenmode form (see above). Namely, for each value of $c_0^2$ the numbers in column 7 (in fractional units) have to be added to $wt^L$ (numbers without parenthesis) and $wt^C$ to obtain the total weight of 1.

It can be seen that for $4 \leq c_0^2 \leq 20$ the global motion eigenvalue is given by $1/\tau_m = 0.06$ and its weight, $wt^C$, is given within a good approximation by $(S_0^2)^2$. The main local motion eigenvalue, $1/\tau^L$, decreases relative to $1/\tau_{ren}$ with decreasing $c_0^2$. The difference is 2.5% for $(S_0^2)^2 = 0.901$ ($c_0^2 = 20$), 10% for $(S_0^2)^2 = 0.803$ ($c_0^2 = 10$) and 16.7% for $(S_0^2)^2 = 0.507$ ($c_0^2 = 4$). The deviation of the correlation function for local motion from its solely $D_{KM}^L$-determined single-local-motion-eigenmode form is 0.4% when $(S_0^2)^2 = 0.901$, 2.8% when $(S_0^2)^2 = 0.803$, and 19.4% when $(S_0^2)^2 = 0.507$. A typical $(S_0^2)^2$ value for rigid N−H bonds is 0.8, implying 10% error in $\tau_e$ calculated with the cone model and 2.8% error in assuming that the weight of the local motion term is $(1 - (S_0^2)^2)$. This implies 3.1% error in $S^2$, which should be taken into consideration when the accuracy and precision of $S^2$ are estimated in MF studies.[11,13] The estimates given above are based on direct calculation. When $S^2$ is determined with data fitting, the errors can be larger.

The time scale separation between the global and local motions is evaluated in MF studies on the basis of the $\tau_e/\tau_m$ ratio, which is substantially smaller than the true measure, $\tau^L/\tau_m$, and which is $S^2$-dependent. For example, for $\tau^L/\tau_m = 0.01$ the ratio $\tau_e/\tau_m$ is 0.002 for $(S_0^2)^2 = 0.8$ ($c_0^2 = 10$) and 0.003 for $(S_0^2)^2 = 0.75$ ($c_0^2 = 7.9$). As noted above, for $\tau^L/\tau_m \geq 0.01$ mixed modes (see below) contribute significantly to the spectral density. Tables 2 and 3 show the effect of $\tau^L/\tau_m$ exceeding 0.01 for $(S_0^2)^2$ assuming the values of 0.75 and 0.8. The numbers in parentheses are the values corresponding to an "accurate" MF formula where $S^2 = (S_0^2)^2$ and $\tau_e = \tau_{ren}$. It can be seen that the errors are significant for $\tau_e/\tau_m$ values that might be considered in MF analyses as representing large time scale separations. For example, although the true time scale separation is $\tau^L/\tau_m = 0.01$, the MF analysis would report $\tau_e/\tau_m = 0.02$ (0.025) as the time scale separation for $(S_0^2)^2 = 0.8$ (0.75). A 5.3% (6.8%) contribution of additional local motion eigenmodes implies in this case an increase in $wt^C$ and a decrease in $wt^L$, as shown in Tables 2 and 3. As pointed out above, the error in the compromise value of $S^2$ determined by data fitting may be larger than the estimates of Tables 2 and 3, which are based on direct calculations. Further inaccuracies will be implied by the MF assumption that the dipolar and $^{15}N$ CSA frames are collinear,

**TABLE 2: Eigenvalue ($1/\tau_m$) and Weight ($wt^C$) of the Global Motion, Eigenvalue ($1/\tau^L$) and Weight ($wt^L$) of the Main Local Motion Mode, and Contribution of Additional Local Motion Eigenmodes Modes ($w^{MM}$) to $C(t)$ as a Function of $\tau^L/\tau_m$[a]**

| $\tau^L/\tau_m$ | $1/\tau_m$ | $wt^C$ | $1/\tau^L$ | $wt^L$ | $w^{MM}$, % | $\tau_e/\tau_m$ |
|---|---|---|---|---|---|---|
| 0.01 | 0.06 (0.06) | 0.805 (0.803) | 27.9 (30.0) | 0.172 (0.2) | 2.8 | 0.002 |
| 0.030 | 0.18 (0.18) | 0.813 | 28.5 | 0.167 | 3.3 | 0.006 |
| 0.050 | 0.29 (0.30) | 0.819 | 29.1 | 0.161 | 3.9 | 0.01 |
| 0.100 | 0.55 (0.60) | 0.833 | 30.7 | 0.147 | 5.3 | 0.02 |
| 0.200 | 1.00 (1.20) | 0.858 | 33.8 | 0.119 | 8.1 | 0.04 |

[a] The last column shows $\tau_e/\tau_m$ corresponding to $\tau^L/\tau_m$ in column 1 (eq 18). An axial potential with coefficient $c_0^2 = 10$, corresponding to $(S_0^2)^2 = 0.8$, was used. The terms in parenthesis represent the case in which the local motion is given by the eigenvalue $1/\tau_{ren}$ and the weight $(1 - (S_0^2)^2)$, and the global motion by the eigenvalue $1/\tau_m$ and the weight $(S_0^2)^2$.

**TABLE 3: Same as for Table 2 Except $c_0^2 = 7.9$, Corresponding to $(S_0^2)^2 = 0.75$, Was Used**

| $\tau^L/\tau_m$ | $1/\tau_m$ | $wt^C$ | $1/\tau^L$ | $wt^L$ | $w^{MM}$, % | $\tau_e/\tau_m$ |
|---|---|---|---|---|---|---|
| 0.01 | 0.06 (0.06) | 0.755 (0.75) | 21.30 (23.7) | 0.234 (0.25) | 1.6 | 0.003 |
| 0.030 | 0.18 (0.18) | 0.763 | 21.81 | 0.201 | 4.9 | 0.008 |
| 0.050 | 0.29 (0.30) | 0.770 | 22.32 | 0.196 | 5.4 | 0.013 |
| 0.100 | 0.55 (0.60) | 0.788 | 23.61 | 0.182 | 6.8 | 0.025 |
| 0.200 | 1.00 (1.20) | 0.818 | 26.23 | 0.158 | 9.2 | 0.051 |

and by simultaneously $(S_0^2)^2$ being lower, and $\tau^L/\tau_m$ being higher, than the relevant threshold values.

*2d. Extended MF Formula.*[8] When eq 16 cannot fit the experimental data, the extended MF spectral density, given by

$$J(\omega) = S_f^2 [S_s^2 \tau_m/(1 + \omega^2\tau_m^2) + (1 - S_s^2)\tau_s'/(1 + \omega^2\tau_s'^2)] + (1 - S_f^2)\tau_f'/(1 + \omega^2\tau_f'^2) \quad (19)$$

has been used. The parameter $\tau_f$ is taken as the effective correlation time for the fast local motion, $\tau_s$ as the effective correlation time for the slow local motion, and $S_s^2$ and $S_f^2$ as squared generalized order parameters associated with these motions. $1/\tau_f' = 1/\tau_f + 1/\tau_m$ and $1/\tau_s' = 1/\tau_s + 1/\tau_m$. No effort is made to define any geometric relationships between the axes of fast and slow local motions. Although eq 19 requires that $\tau_f \ll \tau_s \ll \tau_m$, in practice this formula is used when $\tau_s$ is on the order of $\tau_m$.

*2e. Extended MF Formula as a SRLS Asymptote.* As shown previously, an expression similar to eq 19 was obtained in early work as a perturbational expansion of the SRLS solution in rhombic local ordering in the $R^L \gg R^C$ limit for $\beta_{MD} \neq 0°$ (ref 30). Let us reiterate the basics of this derivation. $J^{DD}(\omega)$ is given by eq 10, the functions $j_{K(\omega)}$ are given by eq 13, and setting $\beta_{MD} = 90°$ implies $A = (1.5 \cos^2 \beta_{MD} - 0.5)^2 = 0.25$, $B = 3 \cos^2 \beta_{MD} \sin^2 \beta_{MD} = 0$ and $C = 0.75 \sin^4 \beta_{MD} = 0.75$ ($A$, $B$ and $C$ represent $(d_{00}^2)^2$, $2(d_{01}^2)^2$ and $2(d_{02}^2)^2$, respectively, where "$d$" denotes reduced Wigner rotation matrix elements). The function $J^{DD}(\omega)$ is then given by

$$J^{DD}(\omega) = [0.25(S_0^2)^2 + 0.75 (S_2^2)^2]\tau_m/(1 + \omega^2\tau_m^2) + 0.25[1 - (S_0^2)^2] \tau_0/(1 + \omega^2\tau_0^2) + 0.75[1 - (S_2^2)^2]\tau_2/(1 + \omega^2\tau^2_2) \quad (20)$$

Assuming that $J(\omega) = J^{DD}(\omega) = J^{CC}(\omega)$, eq 20 is formally analogous to the extended MF formula[8] (eq 19) with $\tau_s$ formally equivalent to $\tau_0$, $\tau_f$ to $\tau_2$, and the squared generalized order parameters, $S_s^2$ and $S_f^2$, related to $(S_0^2)^2$ and $(S_2^2)^2$ as

$$S_f^2 = 0.25 + 0.75(S_2^2)^2 \quad (21)$$

and

$$S_s^2 = (S_f^2 - 0.25)/S_f^2 + 0.25(S_0^2)^2/S_f^2 \quad (22)$$

The equivalence outlined above is only formal. Equation 19 is a physically vague mathematical formula whereas eq 20 is a physically precise geometric model based on the SRLS theory. Note also that other SRLS models, such as one featuring an additional mode of internal motion, would yield the form of eq 19 in a perturbational limit.

For $\tau_f$, $\tau_s \ll \tau_m$ (representing the $R^L \gg R^C$ limit) and very low axial local ordering ($(S_0^2)^2 \rightarrow 0$ and $(S_2^2)^2 \rightarrow 0$) one obtains $S_f^2 \sim 0.25$ and $S_s^2 \sim 0$ when eqs 21 and 22 are used. The corresponding time correlation function is shown by the dashed curve in Figure 3b. However, this $C(t)$ function is never used to analyze N−H bond dynamics in proteins because the local ordering at the N−H site is significantly higher than $S_f^2 \sim 0.25$ and $S_s^2 \rightarrow 0$, and $\tau_s$ is on the order of $\tau_m$ rather than being much smaller than $\tau_m$. A typical parameter set obtained with MF analysis for flexible residues in proteins is given by $\tau_f \sim$ 20 ps, $\tau_s \sim 10 \times \tau_f$, $\tau_m \geq 10\tau_s$, $S_f^2 \sim 0.75$ and $S_s^2 \sim 0.55$. The corresponding time correlation function $C(t)$ is shown by the solid curve in Figure 3b. Table 5 of ref 23 (where the SRLS theory has been fully developed) shows quantitatively that mode mixing dominates the time correlation function when $\tau_m \geq 10\tau_s$ and the ordering is $(S_0^2)^2 \sim 0.55$ (corresponding to $c_0^2 \sim 4.4$). In this case the spectral densities given by eq 13 instead of spectral densities given by eq 17 are to be used. For rhombic ordering not only diagonal terms, $j_K(\omega)$, but also cross-terms, $j_{KK'}(\omega)$, need to be considered. $J^x(\omega)$ obtained from $j_K(\omega)$ and $j_{KK'}$ by frame transformations (as determined by the specific local geometry) are therefore intricate functions. In the MF formulation $J(\omega) = J^{DD}(\omega) = J^{CC}(\omega)$ is the Fourier transform of the simple function shown by the solid line in Figure 3b, with the plateau values determined by $S_f^2$ and $S^2 = S_s^2 S_f^2$, and the step between them monitored by $\tau_s$. Therefore, when force-fitting is successful, i.e., the statistical requirements are fulfilled, this can be only accomplished with highly inaccurate best-fit parameters that constitute parametrizing entities. The latter are field-dependent because parametrization by force-fitting depends on which $J(\omega)$ values are to be reproduced. The fitting of larger data sets obtained by combining multifield data is likely to fail when standard fitting schemes are used. The trends in the values of the best-fit parameters upon changing environmental conditions such as temperature and complex formation are devoid of physical meaning and may show abrupt changes, which are not associated with genuine physical phenomena. These features are illustrated below.

The extended MF formula is based on the theory of moments, which is a mathematical approach that ignores physical details for convenience. The physical principles underlying NMR spin relaxation in locally orienting environments have been set forth previously.[52a] The important structural/electronic/charge-related information one can extract when the restrictions on the local motion are properly treated as potentials or ordering tensors have been illustrated amply in the literature (e.g., ref 52b). Within the scope of these established approaches the solution offered by the extended MF formula to N−H bond motion in proteins is physically not reasonable. The very same entity (the cylindrical N−H bond) cannot be involved in two separate motions that are isotropic (as manifested by the scalar quantities $\tau_s$ and $\tau_f$) and at the same time restricted (as manifested by $S_s^2$ and $S_f^2$). The simplification to isotropic local motion is certainly not justified for the restricted slow motion, $\tau_s$, as $\tau_s \sim \tau_m$. It is not reasonable to have no geometric relationship whatsoever between the fast and slow local motions. The very same (internal) protein environment cannot exert multiple different restrictions on the same body. The global motion ($\tau_m$) cannot occur on the same time scale as the slow local motion ($\tau_s$) and at the same time not lead to mixed modes. A restricted motion can be nearly "decoupled" from the slowly relaxing environment, which exerts the spatial restrictions, only when these processes occur on very different time scales ($R_\parallel^L/R_\perp^L \gg 1$) and the ordering ($S_0^2$ and $S_2^2$) is so small that it constitutes a perturbation on the free motion, or so large that the local motion correlation times become renormalized by the strong local potential. Only in these cases can mode mixing be ignored. Accounting for the correct local geometry ($\beta_{MD}$ on the order of 90° in the present case), one may use the analytical function given by eq 20, which is assembled from the simplified functions $j_K(\omega)$ given by eq 17. In this case eq 20 describes properly an axially diffusing N−H bond in the presence of a weak rhombic potential. Note that even in this limit the global and local modes are only nearly "independent" because the terms $(S_K^2)^2(\tau_K^L)/(1 + \omega^2(\tau_K^{L2}))$, $K = 0$ and 2, actually represents statistical interdependence.[48]

A numerical example, which illustrates the distorted picture obtained by using the extended MF formula outside the perturbation limit, is shown in Table 4.

**TABLE 4: Squared Axial ($(S_0^2)^2$) and Rhombic ($(S_2^2)^2$) SRLS Order Parameters in Irreducible Tensor Notation, Formally Equivalent Order Parameters ($S_{xx}$, $S_{yy}$ and $S_{zz}$) in Cartesian Tensor Notation, and Corresponding Squared Generalized MF Order Parameters ($S_f^2$ and $S_s^2$, Based on Eqs 21 and 22)[a]**

| $c_0^2$ | $c_2^2$ | $(S_0^2)^2$ | $(S_2^2)^2$ | $S_s^2$ | $S_f^2$ | $S_{xx}$ | $S_{yy}$ | $S_{zz}$ |
|---|---|---|---|---|---|---|---|---|
| 2 | 3 | 0.008 | 0.327 | 0.50 | 0.50 | 0.306 | −0.394 | 0.088 |

[a] The coefficients $c_0^2$ and $c_2^2$ determine the potential $U/k_BT$ in terms of which $S_0^2$ and $S_2^2$ are defined (eq 11).

The coefficients $c_0^2 = 2$ and $c_2^2 = 3$ represent rhombic $Y_M$ ordering with "nearly planar $Y_M$−$X_M$" symmetry, which we found previously to prevail at the N−H site.[26] This symmetry is reflected clearly in the principal values, $S_{xx}$, $S_{yy}$ and $S_{zz}$, of the Cartesian tensor. In irreducible tensor notation one has $S_0^2 = 0.089$ and $S_2^2 = 0.572$ (Table 4 shows the squared values of $S_0^2$ and $S_2^2$, which appear in eq 20). The corresponding MF parameters are $S_s^2 = 0.50$ and $S_f^2 = 0.50$. The physical picture of two independent isotropic local motions of the N−H bond associated with squared generalized order parameters (incidentally) equal to 0.5 is certainly different from the physical picture associated with an axial N−H bond diffusing in a well-defined rhombic local potential associated with a well-defined ordering tensor with its $Y_M$ axis aligned preferentially along the $C_{i-1}^\alpha$−$C_i^\alpha$ axis (or the $N_i$−$C_i^\alpha$ bond).

In practice a reduced form of eq 19, where $\tau_f'$ is set equal to zero, is used in MF studies. The reason for this simplification is that standard MF fitting schemes can typically only fit three-point single-field data sets, precluding the variation of $\tau_f$ as a free parameter in addition to $S_s^2$, $S_f^2$ and $\tau_s$. Values of $S_f^2$ are typically in the range of 0.8−0.9. The weight of the last term of eq 19 is $(1 - S_f^2)$. Hence a 20−10% contribution is being ignored when the reduced extended MF formula is used, implying further inaccuracies in the best-fit parameters. This can also be realized by noticing that formally the reduced extended MF formula is given by $J(\omega) = S_f^2 j_0(\omega)$, where $j_0(\omega)$

$= S_s^2\tau_m/(1 + \omega^2\tau_m^2) + (1 - S_s^2)\tau_s'/(1 + \omega^2\tau_s'^2)$ has the form of the $K = 0$ perturbational expansion (eq 17) featuring the squared order parameter $S_s^2$ and local motional correlation time $\tau_s'$. This is analogous to $J^{DD}(\omega) = Aj_K(0)$ in the SRLS analysis, with the $K = 1$ and 2 terms set equal to zero in eq 10. We call this form of $J^{DD}(\omega)$ (and ensuing $J^{CC}(\omega)$) "combination 5", in analogy with model 5 in the MF treatment (the term "combination" is used instead of "model" because the hierarchy consists of different parameter combinations within the scope of the same model). Setting $Bj_1(\omega) = Cj_2(\omega) = 0$ in eq 10 was initially considered justified on the basis of the relation $R_{||}^L \gg R_\perp^L$ (implicit in the 2D-grid-based calculations),[22] which is analogous to $\tau_s \gg \tau_f$ in MF analysis.

The fact that the coefficient $A$ is returned by the fitting scheme as 0.8−0.9 instead of unity means that in the presence of significant mode mixing the $Bj_1(\omega)$ term will still contribute to $J^{DD}(\omega)$ even though $R_{||}^L \gg R_\perp^L$. This has been verified by us with relevant calculations.[19] Although SRLS combination 5 is certainly a better spectral density than MF model 5, because SRLS $j_0(\omega)$ accounts for mode mixing whereas MF $j_0(\omega)$ does not, it still misses 10−20% contributions, to be absorbed by the best-fit parameters. As shown below, a consistent physical picture is only obtained with rhombic instead of axial ordering, and arbitrary instead of very high local diffusion anisotropy, $R_{||}^L/R_\perp^L$.

In summary, the mathematical model-free formulas were introduced as parametrizing spectral densities.[6−8] Independently, the stochastic SRLS model has been developed first in the perturbation limit for certain simplified geometries,[30,48] in the BO limit for axial ordering and isotropic local motion,[28] and in its general form.[23,24] It turned out that (1) the original MF formula is given by the SRLS solution in the BO limit and the extended MF formula is given by the perturbational SRLS expansion of ref 30, (2) N−H bond dynamics exceeds the perturbation limits and in most cases the BO limit, (3) mode-coupling and general features of local geometry, ignored in both limits, are important, and (4) MF analysis does not stop at the stage of parametrization but proceeds by interpreting the parametrizing quantities in terms of physical quantities (order parameters, correlation times) inherent to the general SRLS model. This justifies the assessments associated with the detrimental implications of interpreting the MF parameters in terms of physical quantities.

**3. Practical Implementation of the Theoretical Premises of SRLS and MF Analyses.** The basic idea underlying the MF approach is to reproduce the spectral density assuming statistical independence (decoupling) between the mobility of the probe and the mobility of the protein.[6−8] This requires large time scale separation between these motions. On the basis of the theory of moments, analytical expressions for the spectral density were suggested. The price paid for simplicity becomes relevant when the parameters obtained by data fitting[46,47] are interpreted within the scope of specific models. The MF formulas only agree with the high symmetry forms of the various physical SRLS quantities featured, and they accommodate only simplified local geometry, besides requiring mode-decoupling. Hence the usage of the MF approach is prone to overextension.

A different but related idea is to envision the overall system to be composed of two bodies, probe and protein, with mobilities coupled by a phenomenological potential energy function. An established set of dynamic variables is modulated according to an explicit model, typically based on stochastic operators. Contrary to the MF approach there is no pretence for generating a universal tool. Instead, there is an attempt to treat the experimentally relevant situations within the scope of rigorous formal frameworks. The computational burden is greater than that of the analytical model-free formulation.

The SRLS model features such a framework. It is based on a Smoluchowski equation representing the rotational reorientation of two interacting rotors (bodies).[23,24] SRLS analysis was applied earlier to molecular probes in complex fluids and ESR spin relaxation in biomacromolecules.[24,25] Recently, we applied the SRLS approach to NMR spin relaxation in proteins.[19,20,22,26,27] In this application the two rotors are represented by the locally reorienting spin-bearing moiety (e.g., the N−H bond), and the globally reorienting protein. The global and local motions are described at the diffusive level, hence characterized by two distinct diffusion tensors. The coupling potential, which expresses the spatial restrictions imposed by the immediate protein surroundings at the site of the motion of the probe, depends on the mutual orientation of the coupled rotors. The physical tensors may be asymmetric, and features of general local geometry are accommodated. Obviously mode-coupling is accounted for rigorously.

Results of the SRLS analysis were compared with MF results. The SRLS approach is clearly the generalization of the MF approach, yielding the latter in asymptotic limits. We found that the MF formulas are poor approximations of the experimental spectral density. On the other hand, the SRLS solution appears to match the integrity of currently available experimental data.

The practical problem with the SRLS model is computational efficiency, as in some cases the (numerical) calculation of the SRLS spectral densities is significantly more demanding than the instantaneous calculation of the simple analytical MF formulas. Otherwise the SRLS and MF fitting schemes are similar. In our first implementation of the SRLS model in a fitting scheme, we precalculated 2D grids of spectral density values that were then used as look-up tables. This program is comparable in speed with the MF programs and is operated in the same way. The best-fit parameters are formally (but not physically) analogous to the parameters of the extended MF formula. The deficiencies of this scheme are that (1) the global motion is isotropic and determined separately from the local motion (similar to the MF strategy) and (2) the symmetry of the local restrictions is axial, as in MF analysis. We found that these limitations must be eliminated. To this end we developed recently a fitting program for SRLS where the generic spectral densities (eq 13) are calculated on the fly. In terms of operating it the only extra requirement on the part of the user is to determine a truncation parameter that controls the number of terms that need to be taken into account for convergence of the solution (given by eq 13 or similar equations). Several trial and error calculations carried out for typical cases suffice. Some aspects of this program are still under development. It is expected that this effort will be brought to completion shortly, at which time this general fitting scheme will be made available to the community. The 2D-grid-based fitting scheme, as well as and the 2D grids, are available upon request. The "Theoretical Background" section of this paper comprises all the information needed for ab initio programming.

## III. Results and Discussion

**1. SRLS versus MF Analysis in the Asymptotic $\tau^L \rightarrow 0$ Limit.** *1a. Geometric Effects*: *$D \rightarrow$ CSA Frame Transformation.* When $\tau_e$ is very small, the second term in the MF formula (eq 16) can be ignored, yielding the so-called MF "model 1". In this limit the difference between SRLS and MF approaches consists solely of the D-CSA transformation carried out in the

**TABLE 5: Results of Fitting with SRLS Combination 1 and MF Model 1 the Experimental Data of Eight VHHS Residues Fit with Model 1 by Vugymeyster et al.[11] [a]**

| res | SRLS $(S_0^2)^2$ | MF $S^2$ | % diff | SRLS $\chi^2$ | MF $\chi^2$ | NOE % err | NOE % $D_{max}$ |
|---|---|---|---|---|---|---|---|
| 45 | 0.842 | 0.804 (0.803) | −4.5 | 6.44 | 1.7 (1.7) | 2.1 | 1.4 |
| 49 | 0.853 | 0.817 (0.815) | −4.2 | 2.1 | 2.2 (2.2) | 1.9 | 0.0 |
| 57 | 0.887 | 0.847 (0.845) | −4.5 | 6.6 | 1.7 (1.8) | 2.2 | 2.1 |
| 58 | 0.908 | 0.869 (0.860) | −4.3 | 34.0 | 15.5 (20.0) | 2.2 | 7.7 |
| 59 | 0.898 | 0.855 (0.853) | −4.8 | 19.0 | 12.6 (14.2) | 2.4 | 3.5 |
| 60 | 0.849 | 0.810 (0.810) | −4.6 | 27.0 | 18.7 (19.0) | 3.3 | 16.0 |
| 69 | 0.853 | 0.815 (0.814) | −4.5 | 15.6 | 7.7 (7.9) | 2.2 | 4.5 |
| 71 | 0.841 | 0.803 (0.803) | −4.5 | 12.0 | 3.1 (3.3) | 1.9 | 3.1 |

[a] Squared SRLS order parameters, $(S_0^2)^2$, obtained from the best-fit $c_0^2$ values using eq 4 with $c_2^2 = 0$, and eq 11, and best-fit MF $S^2$ values, are shown. The corresponding $\chi^2$ values are also given. The data in parentheses were obtained with the SRLS program where the $^{15}N-^1H$ dipolar and $^{15}N$ CSA tensors were set deliberately collinear. % diff is the percent difference between the MF and SRLS squared order parameters divided by the SRLS value. The last two columns show the experimental NOE error and the percent difference (% $D_{max}$) between the experimental NOE and the maximum NOE obtained for a rigid sphere.

SRLS calculation and omitted implicitly in the MF calculation. The implications of this approximation are illustrated below using the experimental data obtained at 295 K, 11.7 T, by Vugmeyster et al.[11] for eight out of the 35 residues of the villin headpiece helical subdomain (VHHS) that were analyzed with MF model 1. $\tau_m = 2.5$ ns was determined on the basis of $T_1/T_2$ ratios.[53] We subjected these data to MF model 1 analysis using the program Modelfree 4.0,[46] and to SRLS combination 1 analysis using our current fitting scheme operated for axial potentials.[22] From MF $S^2$ we calculated $c_0^2$ using eq 4 with $c_2^2 = 0$, and eq 11. In the SRLS calculations we varied $c_0^2$ and calculated $(S_0^2)^2$ using eq 4 with $c_2^2 = 0$, and eq 11. The results are shown in Table 5.

The data in parentheses, obtained by setting D and CSA deliberately collinear in the fitting program for SRLS, are practically identical with the corresponding MF data. This indicates that the two programs perform identically when the D and CSA frames coincide. Thus, the differences between corresponding data in columns 2 and 3 are due solely to the D-to-CSA frame transformation, which was carried out for a tilt angle $\theta = 17°$ (ref 3) in the SRLS analysis and omitted implicitly in the MF analysis. Underestimation of $(S_0^2)^2$ by the MF calculation on the order of 4.5% is not negligible given that currently reported precision in $S^2$ is, in some cases, on the order of 1% (ref 11) and the precision in the average value of $S^2$, on the order of 0.2% (ref 13). The error in $S^2$ has severe implications for conformational entropy calculations (see below). Recently, $\theta = 21.4°$ was determined with an extensive ubiquitin data set.[54] The larger angle $\theta$ implies even greater inaccuracies than shown in Table 5.

The MF treatment is clearly force-fitting the experimental data yielding $S^2$ and corresponding $c_0^2$ values that are too low. Table 6 illustrates this using the experimental data of residue 49 of VHHS. Back-calculated $^{15}N$ $T_1$, $T_2$ and $^{15}N-\{^1H\}$ NOE relaxation parameters obtained with the best-fit SRLS and MF order parameters of Table 5 are shown in Table 6a aside the experimental data. Table 6b shows the specific $J(\omega)$ values associated with the back-calculated $T_1$, $T_2$ and NOE data of Table 6a. It can be seen that the MF spectral density can fit the experimental data as well as the SRLS spectral density (Table 6a) by compensation of the individual $J(\omega)$ values (Table 6b). In particular, the MF approach yields smaller $J^{DD}(\omega)$ values and larger $J^{CC}(\omega)$ values than their correct SRLS counterparts. Note the significantly different values of $J^{DD}(0)$ and $J^{DD}(\omega_N)$ versus $J^{CC}(0)$ and $J^{CC}(\omega_N)$ in the SRLS analysis, implied by carrying out the D-to-CSA frame transformation. Also note that (with one exception) the experimental NOE exceeds the maximum NOE as shown by % $D_{max} > 0$ (Table 5). This feature will be discussed below in detail.

*1b. Local Motion Effects.* The $^{15}N$ relaxation data of 21 VHHS residues were fit by Vugmeyster et al.[11] with model 2, where the complete original MF formula (eq 16) is used. We subjected 15 out of 21 residues to SRLS analysis using combination 2, and we repeated the calculations of Vugmeyster et al.[11] using the same computer program (Modelfree 4.0). The average results obtained for the squared order parameters and the associated $c_0^2$ values are shown in Table 7 under the heading "model 2". For comparison the average results of Table 5, including $c_0^2$ corresponding to the squared order parameters, are also shown under the heading "model 1".

The differences featured by the "model 1" SRLS and MF results stem solely from the geometric D → CSA frame transformation. The differences featured by the "model 2" SRLS and MF results stem from the D → CSA frame transformation, and from the effect of additional local motion eigenmodes on the form of the local motion correlation function, accounted for in SRLS and ignored in MF. SRLS yielded $\langle \tau^L/\tau_m \rangle = 0.1$ whereas MF yielded $\langle \tau_e/\tau_m \rangle = 0.02$ (data not shown). If $\tau^L$ would be derived from $\tau_e$ according to eq 18, then the MF time scale separation would have been 0.09, which is close to its SRLS counterpart (differing by only 10%).

Table 7 shows that $S^2$ overestimates $(S_0^2)^2$ by nearly 7% in model 2 and underestimates it by approximately 4.5% in model 1. As already mentioned, this has implications for the precision of MF $S^2$. Most importantly, it affects the accuracy of thermodynamic parameters calculated from potentials derived from MF $S^2$.[33−36] The coefficient $c_0^2$ of the general form of the potential (eq 4 with $c_2^2 = 0$) is very sensitive to changes in $(S_0^2)^2$ when $(S_0^2)^2$ is high, as shown in Figure 4 which is the graphical representation of eq 4 with $c_2^2 = 0$. Because of the asymptotic form of the $(S_0^2)^2$ versus $c_0^2$ curve as $(S_0^2)^2 \rightarrow 1$, relatively small uncertainty in $(S_0^2)^2$ implies large uncertainty in $c_0^2$. For example, in Table 5 the $(S_0^2)^2$ errors cover the range between −4.5% and +6.8% whereas the $c_0^2$ errors cover the range between −23% and +20%. Note that these large errors in the strength of the potential, hence in the probability distribution function $P_{eq} = \exp(-U/k_BT)$, stem solely from the geometric effect of omitting the D-to-CSA frame transformation. Significantly larger inaccuracies are implied by also disregarding in the MF treatment the possibility that the correlation function for local motion has a more complex form implied by the presence of additional eigenmodes, and oversimplifying the symmetry of the local ordering.

As discussed above, the effective correlation time, $\tau_e$, typically reported in MF studies as a "correlation time for local motion", is actually a composite, approximately given by $2\tau^L/c_0^2$ (eq 18). For $S^2 = 0.8$, 0.9 and 0.95, corresponding to $c_0^2 = 10$, 20 and 40, respectively, the parameter $\tau_e$ is 5, 10 and 20 times smaller than $\tau^L = 1/6R^L$. The ratio $\tau_e/\tau_m$ grossly overestimates what is considered to represent the time scale separation between the rate of global reorientation ($R^C$) and the rate of local reorientation ($R^L$) (note that $1/\tau_m$ and $1/\tau_e$ are global motion mode and main local motion mode eigenvalues, respectively, whereas $R^C = 1/6\tau_m$ and $R^L = 1/6\tau^L$ are "bare" diffusion constants for global and local motion, respectively). This may lead to inclusion of nonrigid residues into data sets used to determine $\tau_m$ from

**TABLE 6**

(a) Experimental and Back-Calculated SRLS and MF $^{15}N$ $T_1$, $T_2$ and $^{15}N-\{^1H\}$ NOE Values Obtained with the Best-Fit Squared Order Parameters Shown in Table 5 for Residue 49[a]

| | $T_1$, ms | $T_2$, ms | NOE |
|---|---|---|---|
| exp | 381.2 ± 6.1 | 251.5 ± 3.1 | 0.565 ± 0.011 |
| SRLS | 387.8 | 250.9 | 0.5533 |
| MF | 386.7 | 249.5 | 0.5758 |

(b) $J(\omega)$ Values for $\omega = 0$, $\omega_N$, $\omega_H + \omega_N$, $\omega_H$ and $\omega_H - \omega_N$ for Dipolar Autocorrelation and $^{15}N$ CSA Autocorrelation[b]

| | input | | output | | | | | | |
|---|---|---|---|---|---|---|---|---|---|
| | $(S_0^2)^2$ | $c_0^2$ | $J^{DD}(0)$ | $J^{DD}(\omega_N)$ | $J^{DD}(\omega_H+\omega_N)$ | $J^{DD}(\omega_H)$ | $J^{DD}(\omega_H-\omega_N)$ | $J^{CC}(0)$ | $J^{CC}(\omega_N)$ |
| SRLS: | 0.853 | 13.5 | 0.854 | 0.523 | 0.0168 | 0.0130 | 0.0113 | 0.651 | 0.398 |
| MF: | 0.817 | 10.8 | 0.817 | 0.500 | 0.0161 | 0.0130 | 0.0108 | 0.817 | 0.500 |

[a] In this table, and in all of the tables and figures below where $T_1$, $T_2$ and NOE were calculated, we used $^{15}N$ CSA of $\sigma_{||} - \sigma_{\perp} = -170$ ppm, $r_{NH} = 1.02$ Å (e.g., ref 11) and $\theta = 17°$ (ref 3). [b] The $c_0^2$ values (and the corresponding $(S_0^2)^2$ values from Table 5) used in these calculations are given under the heading "input". $\tau_m = 2.5$ ns was used. The units of $J(\omega)$ are ns.

**TABLE 7: Average $c_0^2$ and Corresponding $(S_0^2)^2$ Best-Fit SRLS Parameters and Average $S^2$ and Corresponding $c_0^2$ MF Best-Fit Parameters**

| | model 1 | | | model 2 | | |
|---|---|---|---|---|---|---|
| | SRLS | MF | % diff[a] | SRLS | MF | % diff[a] |
| $(S_0^2)^2$ | 0.87 | 0.83 | −4.5 | 0.73 | 0.78 | +6.8 |
| $c_0^2$ | 15.4 | 11.7 | −23 | 7.5 | 9.0 | +20 |

[a] % diff represents 100 × [Param(MF) − Param(SRLS)]/Param-(SRLS).

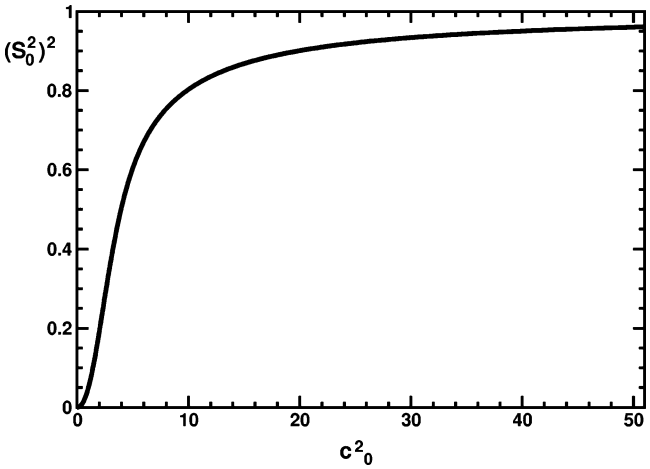


**Figure 4.** Squared order parameter, $(S_0^2)^2$ as a function of the potential coefficient, $c_0^2$ (in units of $k_BT$) determined with eq 4 with $c_2^2 = 0$, and eq 11.

$T_1/T_2$,[53] and improper usage of the reduced spectral density[55−57] and model-independent[58] approaches that are only valid when the local motion correlation time, $\tau^L$, is very fast. It was observed by several authors[14−16] that $\tau_e$ is nearly invariant as a function of temperature. This is not surprising because $\tau_e \propto \tau^L/c_0^2$, with both the numerator and the denominator decreasing with increasing temperature. Though $\tau^L$ may exhibit Arrhenius-type temperature dependence, $\tau_e$ might not.

*1c. General Considerations*. Illustrative simulated SRLS and MF $T_1$, $T_2$ and NOE values are shown in Figures 5−8 for the parameter range where the original MF formula is typically applied. High ordering ($(S_0^2)^2 = 0.85$) and large time scale separation ($\tau_e/\tau_m = 0.015$ when $\tau_m = 5$ ns, and $\tau_e/\tau_m = 0.005$ when $\tau_m = 15$ ns) were used. In Figures 5 and 7 $c_0^2$ is fixed at 13.2, corresponding to $(S_0^2)^2 = 0.85$. In the SRLS calculations the local motion correlation time, $\tau^L = 1/6R^L$, is varied from 0

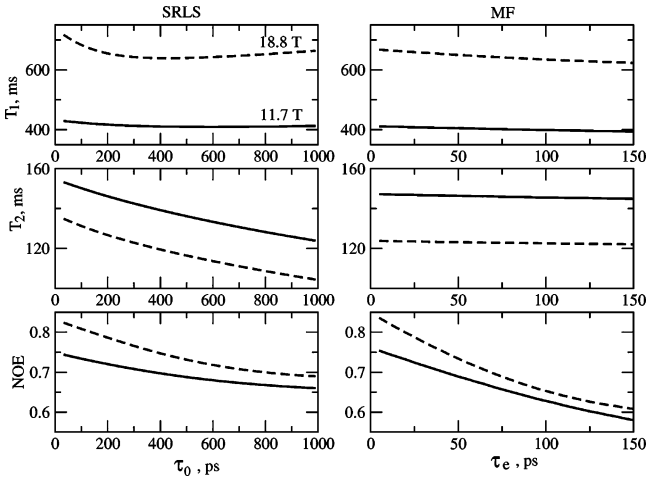


**Figure 5.** $^{15}N$ $T_1$, $T_2$ and NOE calculated with SRLS ($J^{DD}(\omega)$ was calculated according to eq 10, and $J^{CC}(\omega)$ as explained after eq 9) and MF (eq 16) formulas for $\tau_m = 5$ ns, 11.7 and 18.8 T, as a function of $\tau^L = \tau_0 = 1/6R^L$ (left, SRLS) and corresponding $\tau_e = 2\tau_0/c_0^2$ (right, MF). The potential coefficient $c_0^2 = 13.2$, corresponding to $(S_0^2)^2 = 0.85$, was used.

to 1000 ps (curves on the left). The corresponding MF effective local motion correlation time, $\tau_e = 2\tau^L/c_0^2 = \tau^L/6.6$, is varied from 0 to 150 ps (curves on the right). The global motion correlation times are $\tau_m = 5$ and 15 ns, and the magnetic fields are 11.7 and 18.8 T. For fixed $\tau_m$ the parameter $\tau^L$ ($\tau_e$) is in direct proportion to the time scale separation $\tau^L/\tau_m$ ($\tau_e/\tau_m$). The SRLS and MF relaxation parameters in Figures 5 and 7 were calculated using the same physical input (i.e, $\tau^L = 1/6R^L$ in SRLS and $\tau_e = 2\tau^L/c_0^2$ in MF calculations, with all the other parameters the same). It can be seen clearly that all the SRLS relaxation parameters depend significantly on $\tau^L/\tau_m$ in ways that differ for low and high fields and small and large proteins (or high and low temperatures). On the other hand, in the parameter range considered, the MF $T_1$ and $T_2$ values vary to a small extent as a function of $\tau_e/\tau_m$, whereas the MF NOEs vary significantly in ways which differ from the variations in the SRLS NOEs.

Table 8 shows the percent difference between $1/T_1$, $1/T_2$ and NOE shown in Figures 5 and 7 calculated with the SRLS approach for $\tau^L = 495$ ps and the MF approach for $\tau_e = 75$ ps. These data illustrate clearly the field dependence of the best-fit MF parameters. In this example, the features that are likely to yield different results at different fields are the opposite trends in the $1/T_1$ discrepancy between SRLS and MF data at 11.7 and 18.8 T for $\tau_m = 5$ ns, and the very large field-dependence

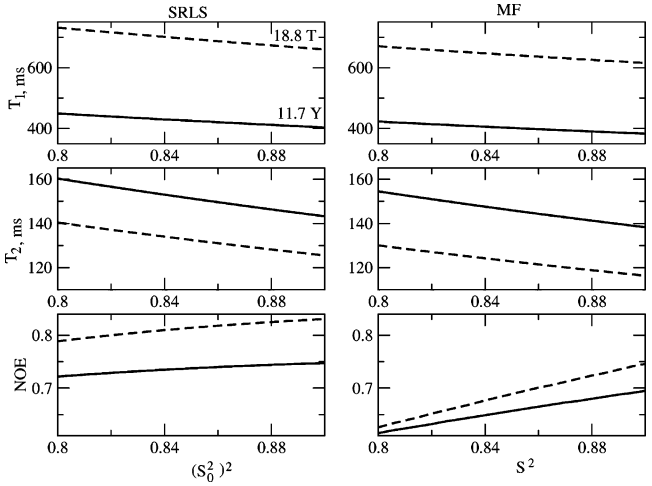


**Figure 6.** $^{15}$N $T_1$, $T_2$ and NOE calculated with SRLS and MF formulas for $\tau_m = 5$ ns, 11.7 and 18.8 T, as a function of the squared order parameter, $(S_0^2)^2$ (left, SRLS) and the generalized squared order, $S^2$ (right, MF). The potential coefficient $c_0^2 = 13.2$, corresponding to $(S_0^2)^2 = 0.85$, was used. $\tau_0 = 75$ ps in the SRLS and $\tau_e = 75$ ps in the MF calculations were used.

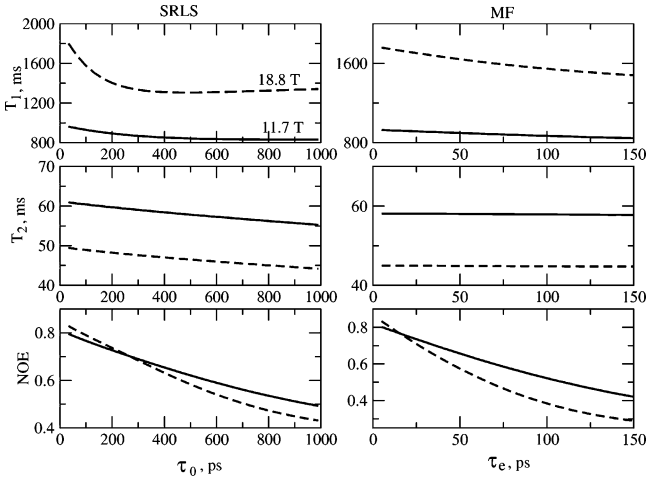


**Figure 7.** $^{15}$N $T_1$, $T_2$ and NOE calculated for $\tau_m = 15$ ns, 11.7 and 18.8 T, as a function of $\tau^L = \tau_0 = 1/6R^L$ (left, SRLS) and corresponding $\tau_e = 2\tau_0/c_0^2$ (right, MF). The potential coefficient $c_0^2 = 13.2$, corresponding to $(S_0^2)^2 = 0.85$, was used.

of the NOE discrepancy for $\tau_m = 15$ ns. Clearly, fitting of combined multifield data is expected to be problematic and in most cases impossible with MF analysis, as often encountered in practice.

Another feature illustrated in Table 8 is the field-dependence of the deviation of the MF $T_1/T_2$ value from the SRLS $T_1/T_2$ value implying field-dependent $\tau_m$ values, as often encountered in MF analyses.

The relaxation parameters shown in Figures 5 and 7 were calculated with the proper analogy between SRLS and MF local motion correlation times; i.e., SRLS $\tau^L$ corresponds to MF $\tau_e = 2\tau^L/c_0^2$. The relaxation parameters shown in Figures 6 and 8 were calculated with the improper analogy, i.e., SRLS $\tau^L$ the same as MF $\tau_e$. This is done to show how misleading it is to consider $\tau_e$ as representing a bare (i.e., $1/6R^L$) local motion correlation time, although Lipari and Szabo[6] indicated that this quantity is a composite. For example, one expects Arrhenius-type temperature dependence of $\tau_e$, and obtains typically near temperature independence. Within the scope of the wobble-in-a-cone model $\tau_e$ depends on $D_w$ and $S^2$ (ref 6). The physical parameter is the wobbling rate, $D_w$. If $\tau_s$ and $S_s^2$, obtained from

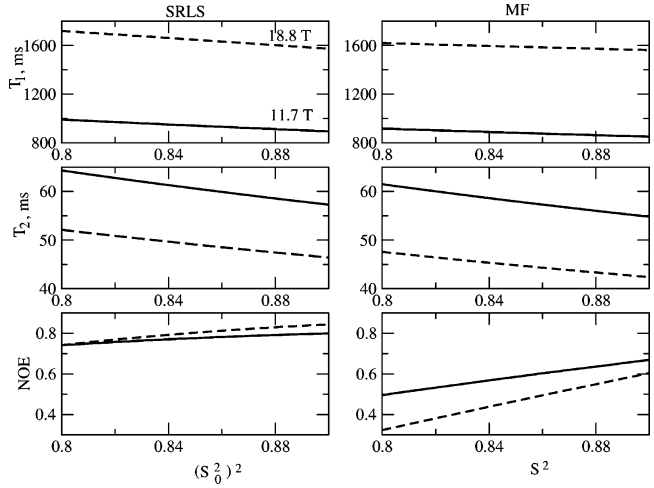


**Figure 8.** $^{15}$N $T_1$, $T_2$ and NOE calculated for $\tau_m = 15$ ns, 11.7 and 18.8 T, as a function of the squared order parameter, $(S_0^2)^2$ (left, SRLS), and the generalized squared order, $S^2$ (right, MF). The potential coefficient $c_0^2 = 13.2$, corresponding to $(S_0^2)^2 = 0.85$, was used. $\tau_0 = 75$ ps in the SRLS and $\tau_e = 75$ ps in the MF calculations were used.

**TABLE 8: Percent Difference ($(\text{var}_{MF} - \text{var}_{SRLS})/\text{var}_{SRLS}$), Where "var" represents $1/T_1$, $1/T_2$ or NOE from Figures 5 and 7 for $\tau^L = 495$ ps and the Corresponding Value of $\tau_e = 75$ ps[a]**

| % diff versus SRLS | $1/T_1$, 1/s | $1/T_2$, 1/s | NOE |
|---|---|---|---|
| 5 ns, 11.7 T | +0.8 | −6.2 | −4.3 |
| 5 ns, 18.8 T | −1.3 | −5.2 | −6.8 |
| 15 ns, 11.7 T | −5.9 | 0.0 | −4.8 |
| 15 ns, 18.8 T | −18.2 | +4.4 | −16.7 |

[a] The potential coefficient $c_0^2 = 13.2$ ($(S_0^2)^2 = 0.8$) was used. The $\tau_m$ values and the magnetic field strengths are given in the table.

data dominated by mode-coupling, are used in this context, the implications can be detrimental, as shown in section 5d.

Figures 5 and 7 show that SRLS relaxation rates calculated with $\tau^L$ agree reasonably with MF relaxation rates calculated with $\tau_e = 2\tau^L/c_0^2$ for $\tau^L < 200$ when $\tau_m = 5$ ns, and for $\tau^L < 100$ ps when $\tau_m = 15$ ns. On the other hand, when $\tau_e = \tau^L$ (Figures 6 and 8) the agreement between the $T_1$ and $T_2$ values is reasonable (because in the MF approach $T_1$ and $T_2$ depend only to a small extent on $\tau_e$; see Figures 5 and 7) but the NOEs differ significantly. This is precisely the empirical observation that motivated the development of the extended MF formula[8] commonly used in its reduced version. In the reduced extended MF formula a slow effective correlation time, $\tau_s$, adjusts the NOE, whereas a scaling factor, $S_f^2$, adjusts $1/T_1$ and $1/T_2$. This is related intimately to the "mode-independent" form of this formula, with $\tau_m$ affecting predominantly the global motion term, $\tau_s$ affecting exclusively the local motion term, and neither affecting the weights of these terms. On the other hand, in the SRLS approach the motional rates and the potential coefficients determine the weights of the various modes contributing to the spectral density, and the eigenvalues of the solution differ from the pure "mode-independent" eigenvalues $1/\tau_m$ and $1/\tau^L$. The MF parametrization of the spectral density impairs statistical properties of genuine fitting. For example, Vugmeyster et al.[11] reported on a nonnormal *t*-distribution in NOE values back-calculated using best-fit MF parameters obtained with models 1 and 2.

*1d. $\tau_m$ Determination.* In MF analysis the determination of the global diffusion tensor[53] is implicitly based on the "Born−Oppenheimer" type approximation inherent in factoring $C(t)$ into $C^L(t)\,C^C(t)$ (eq 14). When $C^C(t) = \exp(-t/\tau_m)$, i.e., when the

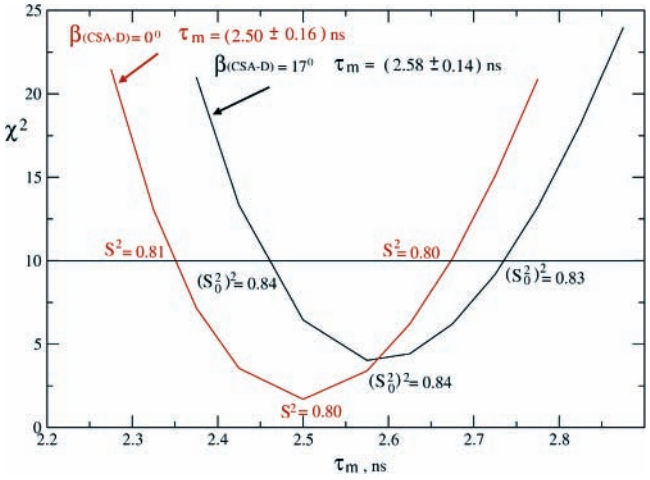


**Figure 9.** $\chi^2$ probability distribution as a function of the global motion correlation time calculated with SRLS combination 1 (blue) and MF model 1 (red) for residue 45 of VHHS. The MF calculations used the same spectral densities as the SRLS calculations, except that the frame transformation D-to-CSA was omitted.

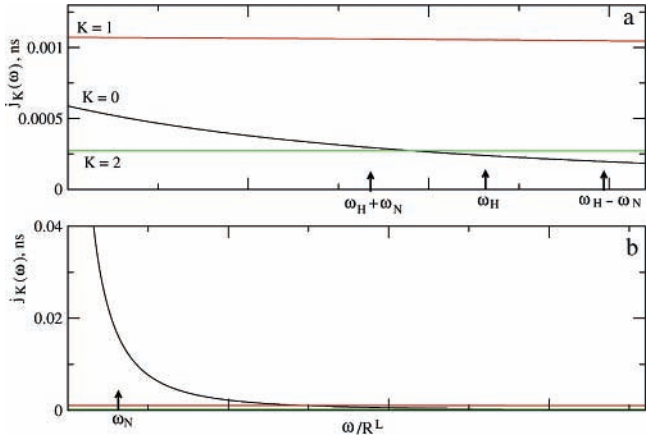


**Figure 10.** $j_K(\omega)$ functions obtained with $c_0^2 = 3.2$ ($(S_0^2)^2 = 0.4$), $\tau_0/\tau_m = 0.45$, $\beta_{MD} = 16.3°$ and $N = R_{||}^L/R_{\perp}^L = 916$. The high-frequency region is shown in panel (a), and the low-frequency region in panel (b).

protein is spherical, and $C^L(t)$ is given by the first term of eq 16 (model 1, where $\tau^L = 0$), then deriving $\tau_m$ from $T_1/T_2$ is appropriate in SRLS studies, but in MF studies it is as inaccurate as implied by the omission of the D-to-CSA frame transformation. The various filtering procedures devised to extract from the complete data set the subset used for $R^C$ determination[53] do not eliminate data that correspond to the original MF formula (eq 16) ("model 2", where $\tau^L \neq 0$). The high sensitivity to $\tau^L$ of $T_1$ and $T_2$ for small proteins (Figure 5), and $T_1$ for large proteins (Figure 7), indicates that significant errors will be introduced by including "model 2" data in the process of $R^C$ determination. When $C^C(t)$ corresponds to axial global diffusion and/or $C^L(t)$ corresponds to eq 19, the full SRLS time correlation function is to be used. Very precise $\tau_m$ values were reported recently by an MF study[15] where $C(t)$ was used in the fitting process, with $C^C(t)$ corresponding to axial global diffusion and $C^L(t)$ given by eq 16 or 19. For the reasons outlined above the accuracy and precision of these results should be re-assessed.

As shown below, when axial potentials are used model 1 is often selected instead of model 2 by force-fitting, yielding unduly high $(S_0^2)^2$ values. This has been documented in the literature by a recent SRLS application to nitroxide-labeled biomacromolecules that showed force-fitting by use of model 1 on a set of synthetic data corresponding to model 2, which generated $(S_0^2)^2$ values that are too high and $\tau_m$ values that are too low.[25] The discrepancies increase with increasing magnetic field.[25] These are precisely the trends observed with MF analyses: higher $S^2$ and lower $\tau_m$ are obtained at higher fields (e.g., see ref 64 cited in section 5d below).

We found that a useful method for estimating the precision of $\tau_m$ is to first determine it from $T_1/T_2$ ratios (desirably acquired at low magnetic fields) of combination 1 fits, where $\tau^L \rightarrow 0$, and then scan the vicinity of this value. Illustrative calculations were carried out for residue 45 of VHHS acquired at 11.7 T, 295 K, fit by Vugmeyster et al.[11] with MF model 1. The $T_1/T_2$-derived $\tau_m$ value is 2.5 ns. $\chi^2$ values obtained as a function of $\tau_m$ within a ±0.5 ns range centered at $\tau_m = 2.5$ ns, using SRLS (black curve) and MF (red curve) approaches are shown in Figure 9. Let us assume that $\chi^2 = 10$ is the threshold (Vugmeyster et al.[11] set $\chi^2 = 25$ as threshold for the site-specific fitting). It can be seen that in both cases practically identical $(S_0^2)^2$ ($S^2$) values are obtained for $\tau_m$ within a range of 5−6% from the 2.58 (2.50) ns minimum. We believe that this is a realistic estimate of the precision with which $\tau_m$ can be currently determined in the BO limit for axial local ordering. Precision estimates of 0.2% (ref 15) are highly overrated. As shown in Figure 9, about 4% accuracy can be gained by using the SRLS instead of the MF approach.

**2. SRLS versus MF Analysis in the Mode Mixing Regime.** One of the greatest benefits of SRLS analysis lies in the treatment of flexible residues where mode mixing dominates the spectral density, as a consequence of local and global motions occurring on similar time scales. Allowing for rhombic local ordering, shown previously to prevail at the N−H bond,[26] and accounting for general features of local geometry,[22−27] constitute an additional significant advantages over MF analysis. As pointed out previously[22,27] and mentioned above, the reduced extended MF formula is formally equivalent to $J^{DD}(\omega) = Aj_0(\omega)$, with SRLS fitting yielding typically $A \sim S_f^2 \sim 0.8-0.9$. This spectral density is inaccurate, among others, because a term that contributes 10−20% has been omitted. Let us illustrate this quantitatively. The value of $A = (1.5 \cos^2 \beta_{MD} - 0.5)^2 = 0.8$ is obtained for $\beta_{MD} = 15.4°$, and $A = 0.9$ is obtained for $\beta_{MD} = 10.7°$. The values of $B = 3 \sin^2 \beta_{MD} \cos^2 \beta_{MD}$ ($C = 0.75 \sin^4 \beta_{MD}$) corresponding to these angles are 0.20 (0.004) and 0.1 (0.0009), respectively. $B$ is clearly not very small, but $Bj_1(\omega)$ could become negligible if $j_1(\omega)$ were much smaller than $j_0(\omega)$, in view of the imposed condition that $R_{||}^L \gg R_{\perp}^L$. This is not borne out by the SRLS analysis of the experiment, because if it were, the fitting scheme would have returned $A = 1$, corresponding to $\beta_{MD} = 0°$. By analogy, the validity of "reducing" the extended MF formula, based on the condition that $\tau_s \gg \tau_f$, is not borne out by the experiment, because if it were, the MF fitting scheme would have returned $S_f^2 = 1$.

The values of $j_1(\omega)$ and $j_2(\omega)$ are, indeed, much smaller than $j_0(\omega)$ values for all $\omega$ values when $R_{||}^L \gg R_{\perp}^L$, *in the absence of mode mixing*. The presence of mode mixing invalidates the relations $j_1(\omega) \ll j_0(\omega)$ and $j_2(\omega) \ll j_0(\omega)$ in the high $\omega$ regime. This is illustrated in Figure 10, where we show the SRLS functions $j_K(\omega)$ calculated using as input the best-fit parameters obtained by fitting with the SRLS theory the $^{15}N$ relaxation data of residue 124 of RNase H, acquired at 11.7 T, 300 K. This residue pertains to the flexible loop $\alpha_D/\beta_5$ and was fit previously with model 5 by Mandel et al.[12] It can be seen that in the low-frequency region $j_0(\omega) \gg j_1(\omega)$ and $j_2(\omega)$. However, in the frequency range comprising the $\omega$ values relevant for the NOE ($\omega_H + \omega_N$ and $\omega_H - \omega_N$) the $j_1(\omega)$ values exceed the corresponding $j_0(\omega)$ and $j_2(\omega)$ values. Clearly even when $R_{||}^L \gg$

**TABLE 9**

(a) Best-Fit $T_1$, $T_2$ and NOE Values Corresponding to the Best-Fit Parameters Shown in Table 9b under the Heading "input"[a]

| | $T_1$, ms | $T_2$, ms | NOE |
|---|---|---|---|
| exp | 633.8 ± 10.1 | 112.3 ± 3.1 | 0.5343 ± 0.031 |
| SRLS | 633.8 | 112.3 | 0.5344 |
| MF | 633.8 | 112.3 | 0.5343 |

(b) Best-Fit $J(\omega)$ Values Corresponding to the Best-Fit Parameters Listed under the Heading "input", Used To Calculate the Data of Table 9a[b]

| | input | | | | output | | | | | | |
|---|---|---|---|---|---|---|---|---|---|---|---|
| | $c_0^2$ | $(S_0^2)^2$ | $\beta_{MD}$ | $R^C$ | $J^{DD}(0)$ | $J^{DD}(\omega_N)$ | $J^{DD}(\omega_H+\omega_N)$ | $J^{DD}(\omega_H)$ | $J^{DD}(\omega_H-\omega_N)$ | $J^{CC}(0)$ | $J^{CC}(\omega_N)$ |
| SRLS | 3.01 | 0.368 | 16.6 | 0.470 | 2.61 | 0.318 | 1.09 | 0.0093 | 0.0081 | 1.96 | 0.241 |
| MF | 10.2 | 0.806 | 15.0 | 0.114 | 2.48 | 0.303 | 1.08 | 0.0087 | 0.0074 | 2.48 | 0.303 |

(c) Significantly Contributing SRLS Eigenvalues and Associated Weights, and Corresponding "Independent" MF Eigenvalues and Associated Weights[c]

| | SRLS | | | | MF | |
|---|---|---|---|---|---|---|
| eigenvalue | 2.13 | 10.12 | 24.52 | 14.13 | 0.678 | 6 |
| weight | 0.61 | 0.325 | 0.042 | 0.019 | 0.652 | 0.157 |

[a] The $\chi^2$ values were practically zero for both SRLS and MF calculations. [b] The SRLS input set includes $R^C = 0.47$ ($\tau_\perp^L = 4.36$ ns, $\tau_m = 9.28$ ns)), $c_0^2 = 3.04$ ($(S_0^2)^2 = 0.37$) and $\beta_{MD} = 16.6°$ (formally $S_f^2 = 0.770$). $N = R_\parallel^L/R_\perp^L$ was fixed at the value of 1000. The MF input set includes $\tau_s/\tau_m = 0.114$, $c_0^2 = 10.2$ derived from $S_s^2 = 0.806$ (eqs 4 and 11), $S_f^2 = 0.809$ and $\tau_f = 0$. The formally[22,27] analogous SRLS parameters are $R^C$, $c_0^2$, $A = (P_2(\cos(\beta_{MD})))^2$ and $R_\parallel^L \gg R_\perp^L$, respectively. The units of $J(\omega)$ are ns. [c] The eigenvalues are given in units of $R^L$; hence the "independent" local motion eigenvalue is 6.

$R_\perp^L$ (or $\tau_s \gg \tau_f$ in MF studies) the term $Bj_1(\omega)$ cannot be ignored in eq 10 when mode mixing is important. For the very same reason eq 19 is further impaired when its last term is omitted.

In principle, setting $Bj_1(\omega)$ and $Cj_2(\omega)$ equal to zero implies the $\beta_{MD} = 0°$ geometry, which corresponds to $A = 1$. In practice, the fitting schemes returns $A \neq 1$, indicating that force-fitting has occurred. The $\beta_{MD} = 90°$ geometry (which is approximately correct as the angle between N−H and $C_{i-1}^\alpha$−$C_i^\alpha$ is 101.3°) corresponds to $A = 0.25$, $B = 0$ and $C = 0.75$. As shown below, this materializes by fitting when the potential is allowed to be rhombic and $R_\parallel^L/R_\perp^L$ is allowed to be arbitrary instead of being forced to be very high.

In the perturbation limit the ordering is very small. Motion about $Z_M$ is prohibited physically as the N−H bond is attached to the protein backbone. The highly plausible local diffusion/local ordering axes $C_{i-1}^\alpha$−$C_i^\alpha$ and $N_i$−$C_i^\alpha$ are tilted at approximately 90° from the N−H bond. Therefore, the $\beta_{MD} = 90°$ geometry is actually implied in this limit. Outside the perturbation limit, $Z_M$ *may be* tilted with respect to the N−H bond. To assign physical meaning to the tensor $R^L$, we will assume, on the basis of stereochemical considerations, that the $\beta_{MD} = 90°$ is preserved in the general case.

The experimental data of residue 124 of RNase H are further used for illustrative purposes as follows. They are shown in Table 9a along with the NMR relaxation data back-calculated with MF and SRLS formulas using the best-fit parameters (given in Table 9b) obtained with the respective fitting processes. Clearly both SRLS and MF approaches reproduce the experimental data. The specific $J(\omega)$ values entering the expressions for $T_1$, $T_2$ and NOE are shown in Table 9b. It can be seen that the MF approach can fit the experimental data as well as the SRLS approach, but this requires that the relevant $J^{DD}(\omega)$ values be underestimated, and the relevant $J^{CC}(\omega)$ values overestimated. This is a clear example of force-fitting. The different best-fit parameters can be further rationalized by examining Table 9c, where we show the dominant eigenvalues and their weights, which are clearly different in the SRLS and MF analyses. Thus, a fictitious physical situation characterized by MF eigenvalues and weights of $C(t)$ and best-fit parameters of $J(\omega)$ obtained with force-fitting can reproduce technically very well the experimental data.

Note that the weights of the local and global motion terms in Table 9c, yielded by the reduced extended MF formula (eq 19 with the last term set equal to zero), do not sum up to unity. There is no requirement in the MF fitting schemes for normalization in the so-called "model 5", which uses this formula. This is yet another aspect of the MF treatment that implies force-fitting of the experimental data. Additional confusion with regard to what the parameter $\tau_s$ represents is implied by the phenomenon of renormalization, which is important when the local potential is high. Because some $S_s^2$ values are low and others are high, this complicates further the comparison among the $\tau_s$ values of different N−H sites. Finally, conformational entropy is often calculated from $S^2$ instead of $S_s^2$. The parameter $S_s^2$ is formally equivalent to $(S_0^2)^2$, whereas $S^2$ taken as $S_f^2 S_s^2$ includes the parameter $S_f^2$, which is formally analogous to a geometric factor, $(P_2(\cos\beta_{MD}))^2$.[22] $S_s^2$ is highly inaccurate;[19,20,22] $S^2$ is qualitatively problematic.

We conclude this section by discussing the limit $N = R_\parallel^L/R_\perp^L \gg 1$, which is the analogue of the MF restriction $\tau_s \gg \tau_f$. The $j_K(\omega)$ functions in Figure 10 were obtained with $N \sim 1000$. We show in Figure 11 SRLS $j_K(\omega)$ functions obtained with $N = 1$. Except for the value of $N$, the parameters used to calculate the Figure 11 functions ($R^C = \tau_\perp^L/\tau_m = 0.57$, $c_0^2 = 4.04$ ($(S_0^2)^2 = 0.51$), $\beta_{MD} = 20°$ and $R_\parallel^L \gg R_\perp^L$) are quite similar to those used to calculate the Figure 10 functions. It can be seen that for a small time scale separation ($\tau_\perp^L/\tau_m = 0.57$), moderate ordering ($(S_0^2)^2 = 0.51$) and the $\beta_{MD} = 20°$ geometry, the functions $j_1(\omega)$ and $j_2(\omega)$ are comparable in magnitude to $j_0(\omega)$ over the entire range of $\omega$ values when $N = 1$ (Figure 11). On the other hand, $j_0(\omega) \gg j_1(\omega)$, $j_2(\omega)$ in the low-frequency regime, whereas $j_1(\omega) > j_0(\omega)$, $j_2(\omega)$ in the high-frequency regime when $N \gg 1$ (Figure 10). Thus, the parameter $N$ affects the analysis significantly.

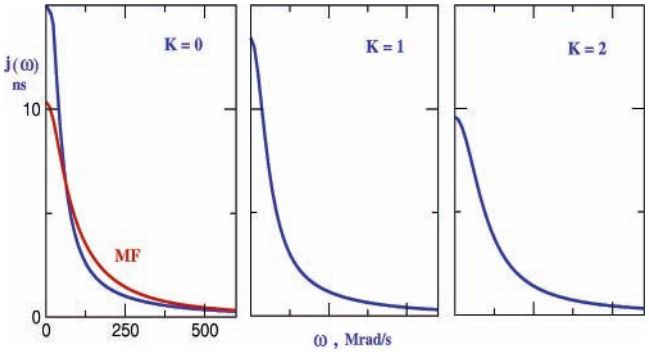


**Figure 11.** SRLS spectral densities $j_K(\omega)$ obtained with $c_0^2 = 4.04$ ($(S_0^2)^2 = 0.51$), $\tau_\perp^L/\tau_m = 0.57$, $\beta_{MD} = 20°$ and $R_{||}^L/R_\perp^L \gg 1$ (blue curves). Reduced extended MF spectral density calculated with $S_s^2 = 0.51$, $S_f^2 = 0.68$ and $\tau_s'/\tau_m = 0.57$ (red curve). The coefficients of the SRLS $j_K(\omega)$ functions shown in the expression of $J^{DD}(\omega)$ are 0.68, 0.31 and 0.01 for $K = 0$, 1, 2, respectively.

The restriction to high $N = R_{||}^L/R_\perp^L$ was imposed in our first fitting scheme for SRLS (ref 22) for practical reasons. $R_{||}^L$ and $R_\perp^L$ represent the principal values of the diffusion tensor of "body 1", i.e., the N−H bond. The inequality $R_{||}^L/R_\perp^L \gg 1$ is clearly a simplifying approximation. As shown below, only by removing this restriction, and allowing for rhombic potentials, is a consistent physical picture obtained with data fitting. In the SRLS approach the principal values of the local diffusion tensor comprise information on physically meaningful variations among the various N−H sites (examples of such variations among nitroxide-labeled sites in proteins appear in ref 37). This information is lost when the restriction that $N \gg 1$, whereby $R_{||}^L$ is forced to be in the extreme motional narrowing limit, is imposed.

Within the scope of the *formal* (definitely not physical) analogy between SRLS and MF, $R_{||}^L/R_\perp^L \gg 1$ in the SRLS model corresponds to $\tau_s/\tau_f \gg 1$ in the MF model. Based on the results presented below, which indicate that $R_{||}^L/R_\perp^L \gg 1$ is not to be imposed, the mathematical MF inequality $\tau_s/\tau_f \gg 1$ constitutes an inappropriate oversimplification.

For comparison we also show in Figure 11 the reduced extended MF spectral density obtained with the analogous parameters: $\tau_s'/\tau_m = 0.57$, $S_s^2 = 0.51$, $S_f^2 = 0.68$ ($S_f^2 = A = 1.5\cos^2(20°) - 0.5$) and $\tau_f' = 0$ (red curve). This function is clearly a poor approximation of $J^{DD}(\omega)$ assembled according to eq 10 from the $j_K(\omega)$ functions of Figure 11, with the coefficients $A = 0.68$, $B = 0.31$ and $C = 0.01$, corresponding to the $\beta_{MD} = 20°$ geometry. This illustrates clearly the limited capabilities of the MF approach, which cannot reproduce physical situations where $R_{||}^L/R_\perp^L \sim 1$.

**3. Conformational Entropy Derived in MF Analysis from $S^2$.** In recent years squared generalized MF order parameters have been used extensively to derive thermodynamic quantities, notably configurational entropy.[33−36] The logic behind this approach is as follows. $S^2$ is determined with data fitting. Subsequently, it is assumed that $P_{eq}$ is axially symmetric. Thereby the squared generalized order parameter becomes the square of an axial order parameter. This enables the derivation of the strength of an axial potential—the form of which must be guessed—based on equations similar to our eq 11. Because the MF approach is an SRLS asymptote, the potential form given by eq 4 (with $c_2^2$ set equal to zero) is appropriate. Employing other potential forms[33−36] may increase the inaccuracy in the configurational entropy derived from the already inaccurate $S^2$ value.

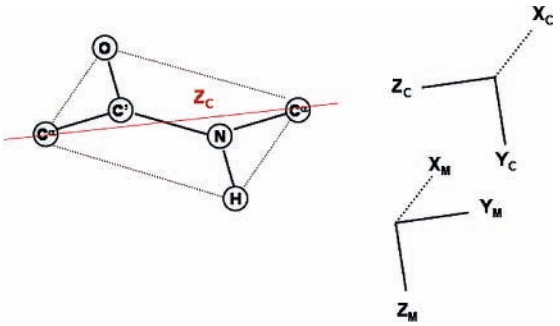


**Figure 12.** Schematic illustration of high "nearly planar $Y_M-X_M$ ordering" prevailing at the N−H site, with $Y_M$ as main ordering axis. The M frame denotes the rhombic local ordering/local diffusion frame. $Y_M$ lies along the instantaneous orientation of the $C_{i-1}^\alpha-C_i^\alpha$ axis (or the $N_i-C_i^\alpha$ bond). $X_M$ lies along the symmetry axis of the lone pair of the nitrogen. The *C* frame denotes the uniaxial local director frame with $Z_C$ along the equilibrium orientation of the $C_{i-1}^\alpha-C_i^\alpha$ axis (or the $N_i-C_i^\alpha$ bond). Within the scope of high ordering $Y_M$ is aligned preferentially along the *C* axis.

Large errors in the strength of the potential $U/k_BT = -c_0^2P_2(\cos\beta_{MD})$ are illustrated in Table 7 in the best-case scenario where $S^2$ is determined with models 1 or 2. As pointed out above, the errors in $c_0^2$ are significantly larger than the errors in $S^2$ due to the functional form of the $(S_0^2)^2$ versus $c_0^2$ dependence for high $(S_0^2)^2$ values (Figure 4). Table 7 shows that within the context of model 1 (or combination 1) the potential coefficient ($c_0^2$) derived from $S^2$ MF analysis *underestimates* the SRLS potential coefficient on average by 23%, whereas in the context of model 2 (or combination 2) the potential coefficient derived from $S^2$ MF analysis *overestimates* the SRLS potential coefficient on average by 20%. Much larger inaccuracies in the potential underlying the calculation of configurational entropy are expected in the extended MF regime, where MF $S_s^2$ and SRLS $(S_0^2)^2$ differ by factors of 3−4 (refs 19, 20, and 22). When the local potential is rhombic, as it turns out to be at the N−H site,[26] MF studies cannot provide the equilibrium probability distribution function, $P_{eq} = \exp(-U/k_BT)$, because only one parameter is available whereas a rhombic potential is defined by at least two coefficients, implying two order parameters.

Contrary to MF studies, in the SRLS approach the general rhombic form of the potential is implicit in the theory and its coefficients ($c_0^2$ and $c_2^2$) can be obtained directly with data fitting. The SRLS theory also emphasizes the relevance of the Euler angles $\Omega_{C'M}$. $P_{eq}$, and therefore the thermodynamic quantities, are obtained straightforwardly in SRLS. Order parameters are thus not required to infer the potential to derive conformational entropy. They can be calculated independently, if so desired, using eqs 4 and 11.

**4. Rhombic Symmetry of the Local Potential/Local Ordering.** *4a. Rhombicity of the Local Ordering and the Axiality of the Global Diffusion.* A very large effect on the analysis not accounted for in MF analysis is the rhombicity of the potential $U(\Omega_{CM})/k_BT$. This is illustrated below in quantitative terms. The form of the potential depends on the symmetry of local diffusion/local ordering frame, M, and the symmetry of the local director frame, C. In the SRLS approach the local director is taken to be uniaxial for simplicity but the M frame is in general allowed to be rhombic. We found previously that the particular rhombic symmetry of the M frame is of the "nearly planar $Y_M-X_M$" type.[26] Figure 12 illustrates these frames in the context of the stereochemistry of the peptide plane. The *C* axis is considered to lie along the equilibrium $C_{i-1}^\alpha-C_i^\alpha$ axis. The main ordering

**TABLE 10: Percent Difference [var(axial) − var(rhombic)]/var(axial) × 100 between $^{15}$N $T_1$, $T_2$ and NOE Calculated with $\tau_m = 15$ ns, $R^C = 0.01$, and an Axial ($c_0^2 = 8$ and $c_2^2 = 0$) or a Rhombic ($c_0^2 = 8$ and $c_2^2 = 4$) Potential[a]**

| | 11.7 T | 14.1 T | 18.8 T |
|---|---|---|---|
| $T_1$ | −2.4 | −1.0 | +1.5 |
| $T_2$ | −7.6 | −7.5 | −7.6 |
| NOE | +31.6 | +39.3 | +46.3 |

[a] Calculations are shown for magnetic fields of 11.7, 14.1 and 18.8 T.

**TABLE 11: Percent Difference [var($\beta_{CC'}$=0°) − var($\beta_{CC'}$=90°)]/var($\beta_{CC'}$=0°) × 100 between $^{15}$N $T_1$, $T_2$ and NOE Calculated with $\tau_m$(app) = 15 ns, $R^C$(app) = 0.01, an Axial Potential Given by $c_0^2 = 8$, $\beta_{CC'} = 0°$ and a Global Diffusion Anisotropy of $R_{||}^C/R_{\perp}^C = 1$ or 1.2[a]**

| | 11.7 T | 14.1 T | 18.8 T |
|---|---|---|---|
| $T_1$ | +7.4 | +7.1 | +6.1 |
| $T_2$ | −9.0 | −9.0 | −9.2 |
| NOE | −2.7 | −3.5 | −4.0 |

[a] Calculations are shown for magnetic fields of 11.7, 14.1 and 18.8 T.

axis, $Y_M$, is parallel to the instantaneous orientation of the $C_{i-1}^{\alpha}-C_i^{\alpha}$ axis. $Z_M$ is perpendicular to $Y_M$ within the peptide plane and $X_M$ is perpendicular to both $Y_M$ and $Z_M$, i.e., perpendicular to the peptide plane. The axis $X_M$ lies along the symmetry axis of the lone electron pair of the nitrogen, assigning clear meaning to the "nearly planar $Y_M-X_M$ ordering" symmetry, where $|S_{xx}|$, $|S_{yy}| \gg |S_{zz}|$, $S_{yy} > 0$ and $|S_{yy}|$ is slightly larger than $|S_{xx}|$. In the original MF formula, and in the extended MF formula as presented by its developers, C lies implicitly along the equilibrium N−H orientation. In a high ordering scenario the implied motion around N−H is not viable. On the other hand, motion around $C_{i-1}^{\alpha}-C_i^{\alpha}$, is definitely viable. Note that taking the local director to lie along the $C_{i-1}^{\alpha}-C_i^{\alpha}$ axis within a presumed rigid peptide plane sets the angle $\beta_{MD}$ close to 90° for the N−H bond and close to 0° for the $C'-C^{\alpha}$ bond.

The rhombicity of the local ordering tensor, **S**, is outside the scope of MF analysis. Because the potential rhombicity was shown with SRLS to affect the analysis significantly,[26] it must be absorbed by the best-fit MF parameters. We showed previously[26] that the conformational exchange parameter, $R_{ex}$, can absorb **S** rhombicity in the data fitting process. Another likely candidate, in particular in the BO limit where mode mixing is limited, is $R^C$ axiality, as explored below.

The large effect of the symmetry of the local potential on the analysis is illustrated in Table 10 which shows NMR relaxation rates calculated for $R^C = 0.01$, $\beta_{MD} = 0°$, $\tau_m = 15$ ns and axial or rhombic potentials on the order of 10 $k_BT$. In the axial case we utilized $c_0^2 = 8$ ($(S_0^2)^2 = 0.754$), whereas in the rhombic case we utilized $c_0^2 = 8$ and $c_2^2 = 4$. These latter values represent moderate rhombicity, corresponding to $(S_{xx} - S_{yy})/S_{zz} = 8.6\%$, where $S_{xx} = -0.382$, $S_{yy} = -0.454$ and $S_{zz} = 0.836$ are the principal values of the corresponding Cartesian ordering tensor. As shown in Table 10, potential (or ordering) rhombicity affects the NOE to a very large extent, amounting to 31.6% (46.3%) difference from the axial case at 11.7 T (18.8 T). The parameters used in Table 10 for the axial potential case are also used in Table 11 to illustrate the effect of global diffusion axiality with $R_{||}^C/R_{\perp}^C = 1.2$, which is a typical value for globular proteins.[10] "%diff" denotes the percent difference between corresponding variables calculated with $\beta_{CC'} = 0°$ and $\beta_{CC'} = 90°$, where $\beta_{CC'}$ denotes the angle between the (uniaxial) local director frame, C′, and the (axial) global diffusion frame, C. The effect illustrated in Table 11 is small relative to the large effect of moderate potential rhombicity on the NOE illustrated in Table 10. It is very likely that in many cases the rhombicity of the ordering tensor, **S**, was absorbed in the MF analyses by introducing $\mathbf{R}^C$ axiality, in particular when the total time correlation function, $C(t)$, rather than the time correlation function for global motion, $C^C(t)$, was used to determine $\mathbf{R}^C$. In the former case $^{15}$N $T_1$, $T_2$ and $^{15}$N−{$^1$H} NOE enter the analysis, whereas in the latter case only $^{15}$N $T_1$ and $T_2$ enter the analysis.

**TABLE 12: Potential Coefficients $c_0^2$ and $c_2^2$ (Eq 4) and Corresponding Principal Values of the Ordering Tensor in Spherical Tensor Notation, $S_0^2$ and $S_2^2$ (Eq 11), and in Cartesian Notation, According to $S_{xx} = (1/2)\sqrt{3/2}S_2^2 - 0.5S_0^2$; $S_{yy} = -(1/2)\sqrt{3/2}S_2^2 - 0.5S_0^2$; $S_{zz} = S_0^2$ [a]**

| $c_0^2$ | $c_2^2$ | $S_0^2$ | $S_2^2$ | $S_{xx}$ | $S_{yy}$ | $S_{zz}$ |
|---|---|---|---|---|---|---|
| 2 | 0 | +0.440 | 0.000 | −0.220 | −0.220 | +0.440 |
| 2 | 2 | +0.265 | +0.368 | +0.093 | −0.358 | +0.265 |
| 2 | 2.45 | +0.188 | +0.460 | +0.188 | −0.376 | +0.188 |
| 2 | 3 | +0.088 | +0.572 | +0.306 | −0.394 | +0.088 |
| 2 | 4 | −0.082 | +0.750 | +0.500 | −0.418 | −0.082 |
| 2 | 6 | −0.183 | +0.878 | +0.739 | −0.446 | −0.293 |

[a] Note that reversing the sign of $c_2^2$ will cause the values of $S_{xx}$ and $S_{yy}$ to be exchanged.

The data shown in Table 11 were obtained for a time scale separation of 0.01, which is quite large, and a potential strength of $c_0^2 = 8$, which corresponds to the relatively high ordering of $(S_0^2)^2 = 0.754$. In this parameter range the effect of additional local motion eigenmodes on the correlation function is not very large.[27] However, not accounting for it, and oversimplifying the local geometry, render the MF-based $T_1$ and $T_2$ values inaccurate by 7% and 9%, respectively. Interestingly, the field dependence of these discrepancies is small. This indicates that in those cases where MF analysis yields significantly field-dependent $\tau_m$ values either mode mixing is pervasive in the experimental data or the data feature rhombic potentials.

It should be noted that in general all the parameters entering the $J^x(\omega)$ functions, including the global diffusion tensor, are to be determined in the same fitting process. The separate determination of $\mathbf{R}^C$ in the MF approach is implied by the mode-independence concept, the applicability of which to N−H bond dynamics we challenge herein.

*4b. "Nearly Planar $Y_M-X_M$" Rhombic Ordering.* As pointed out above, the "nearly planar $Y_M-X_M$" ordering symmetry with $Y_M$ as the main ordering axis represents realistic stereochemical and electronic properties of the N−H site in proteins. Let us investigate this symmetry in further detail. For convenience we use $c_0^2 = 2$, and allow $c_2^2$ to increase from 0 to 6, scanning thereby over a range of symmetries.

Table 12 shows potential coefficients and corresponding ordering tensor components in spherical tensor notation, $S_0^2$ and $S_2^2$, and in Cartesian tensor notation, $S_{xx}$, $S_{yy}$ and $S_{zz}$. The numerical values of the Cartesian tensor components indicate clearly that the entry with $c_2^2 = 0$ represents positive axial $Z_M$ ordering; the entry with $c_2^2 = 2.45$ represents negative axial $Y_M$ ordering; the entry with $c_2^2 = 3$ represents rhombic negative $Y_M$ ordering with "nearly planar $Y_M-X_M$ symmetry"; the entry with $c_2^2 = 4$ represents positive rhombic $X_M$ ordering with "nearly planar $X_M-Y_M$ symmetry"; the entry $c_2^2 = 6$ represents positive $X_M$ ordering and substantial negative $Y_M$ ordering. The angle $\gamma_{MD}$ was fixed in the calculations of this study, and all our

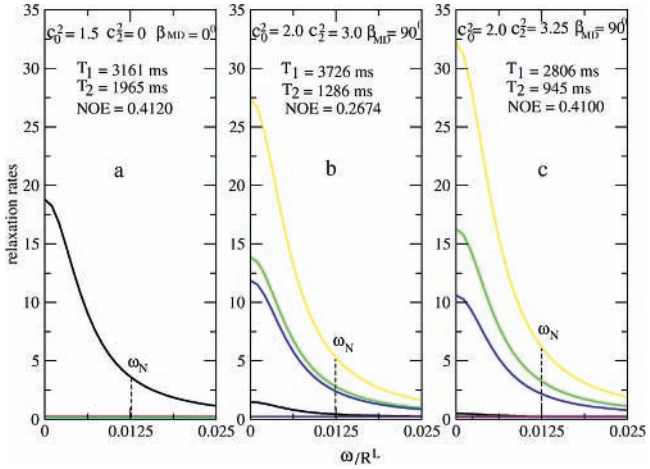


**Figure 13.** Functions $j_K(\omega) = j_{KK}(\omega)$ (a) and $j_K(\omega) = j_{KK'}(\omega)$ and $j_{KK'}(\omega)$ (b, c) calculated for $R^C = 0.001$, and $c_0^2$ and $c_2^2$ as depicted in (a)−(c). The potential coefficients correspond to axial symmetry with $c_0^2 = 1.5$ (a), and "nearly planar $Y_M$−$X_M$ symmetry" with $c_0^2 = 2$ and $c_2^2 = 3$ (b) and $c_0^2 = 2$ and $c_2^2 = 3.25$ (c). The black, red and green curves represent the functions $j_K(\omega)$ with $K = 0$, 1, 2, respectively. The blue, yellow and indigo curves in (b) and (c) represent the functions $j_{KK'}(\omega)$ with $KK' = (2,0) = (0,2)$, $KK' = (2,-2) = (-2,2)$ and $KK' = (1,-1) = (-1,1)$, respectively. The NMR relaxation rates were calculated for $\beta_{MD}$ equal to 0° (a) or 90° (b, c), $\tau_m = 5.5$ ns and a magnetic field of 11.7 T. Note that for $\beta_{MD} = 90°$ the contributing cross-terms include $j_{20}(\omega) = j_{02}(\omega)$ and $j_{2-2}(\omega) = j_{-22}(\omega)$).

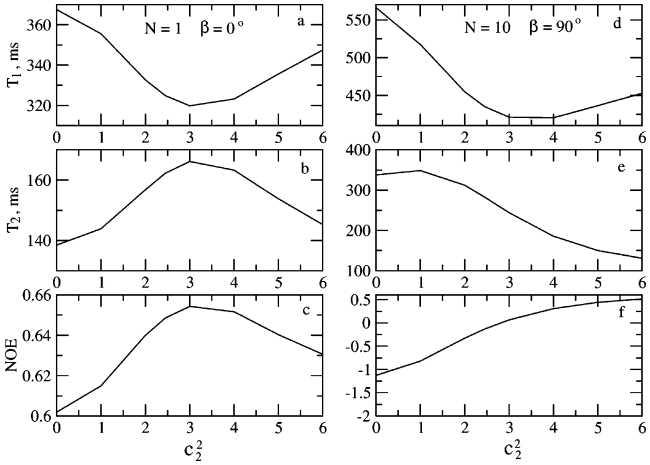


**Figure 14.** $^{15}T_1$, $T_2$ and $^{15}$N−{$^1$H} NOE calculated with $\tau_m = 6.1$ ns, $R^C = 0.5$ and a magnetic field of 11.7 T. Isotropic $R^L$ and $\beta_{MD} = 0°$ were used in (a)−(c), and axial $R^L$ with $N = R_\parallel^L/R_\perp^L = 10$ and $\beta_{MD} = 90°$ were used in (d)−(f). The potential used was given by $c_0^2 = 2$, with the rhombic coefficient, $c_2^2$, varied from 0 to 6.

previous studies, at 90°, in agreement with stereochemical considerations (Figure 2b).

The high sensitivity of the analysis to the symmetry of the local ordering (local potential) is illustrated in Figure 13. We show the functions $j_{KK'}(\omega)$ for all the relevant combinations of quantum numbers $K$ and $K'$, as determined by the symmetry of the local potential. The potential is axial in Figure 13a, with $c_0^2 = 1.5$, and of the "nearly planar $Y_M$−$X_M$ ordering" type in Figures 13b ($c_0^2 = 2$ and $c_2^2 = 3$) and 13c ($c_0^2 = 2$ and $c_2^2 = 3.25$). To calculate the $j_{KK'}(\omega)$ functions, we used $R^C = 0.001$, and to further calculate $T_1$, $T_2$ and NOE, we used $\beta_{MD} = 0°$ in Figure 13a and $\beta_{MD} = 90°$ in Figure 13b,c, and the value of $\tau_m = 5.5$ ns.

There are significant differences between the axial and rhombic potential scenarios. First of all, rhombic symmetry requires the cross terms $j_{2-2}(\omega) = j_{-22}(\omega)$, $j_{20}(\omega) = j_{02}(\omega)$ and $j_{1-1}(\omega) = j_{-11}(\omega)$ in addition to the diagonal terms $j_0(\omega)$, $j_1(\omega)$ and $j_2(\omega)$ required for axial symmetry. The corresponding relaxation rates of Figure 13a,b differ significantly, illustrating the importance of the symmetry of the potential and the local geometry. The NOE generated with the rhombic potential given by $c_0^2 = 2$ and $c_2^2 = 3.25$ (Figure 13c) can also be reproduced with an axial potential given by $c_0^2 = 1.5$ (Figure 13a) (with all the other input parameters being the same). However, $T_1$ and $T_2$ differ substantially indicating that a completely different set of input parameters featuring an axial potential would be required to reproduce satisfactorily the $T_1$, $T_2$ and NOE of Figure 13c. This illustrates force-fitting, with Figure 13c representing "model" experimental data. Parts b and c of Figure 13 show that the NMR relaxation rates are altered substantially when the rhombicity of the potential changes moderately. Thus, an 8% increase in $c_2^2/c_0^2$ implies a 53% increase in the NOE, pointing out the very high sensitivity of the analysis to the precise form of the local potential.

The examples shown in Figure 13 pertain to the large time scale separation regime where mode mixing is limited. The effect of potential symmetry on the experimental variables for $R^C = 0.5$, where mode mixing is important, is illustrated in Figure 14. The other parameters used include $\tau_m = 6.1$ ns and $c_0^2 = 2$. Isotropic $R^L$ ($N = 1$) and $\beta_{MD} = 0°$ were used in Figure 14a−c, and axial $R^L$ (with $N = 10$) and $\beta_{MD} = 90°$ were used in Figure 14d−f. The rhombic potential coefficient, $c_2^2$, was varied from 0 to 6. Positive axial $Z_M$ ordering corresponds to $c_2^2 = 0$ ($S_{zz} = 0.440$, $S_{xx} = S_{yy} = -0.220$), negative $Y_M$ corresponds to $c_2^2 = 2.45$ ($S_{yy} = -0.376$, $S_{xx} = S_{yy} = 0.188$), "nearly planar $Y_M$−$X_M$ ordering" with $Y_M$ as main (negative) ordering axis corresponds to $c_2^2 = 3$ ($S_{xx} = 0.306$, $S_{yy} = -0.394$ and $S_{zz} = 0.088$), and rhombic $X_M$ ordering corresponds to $c_2^2 = 6$ ($S_{xx} = 0.629$, $S_{yy} = -0.446$ and $S_{zz} = -0.184$).

The "nearly planar $Y_M$−$X_M$" ordering symmetry with $Y_M$ as the main (but negative) ordering axis, which corresponds to $c_0^2 = 2$ and $c_2^2 = 3$, has unique features. For $\beta_{MD} = 0°$ the NOE and $T_2$ assume their maximum values, whereas $T_1$ assumes its minimum value for this symmetry. For $\beta_{MD} = 90°$, $T_1$ goes through a shallow minimum, whereas $T_2$ and the NOE exhibit maximum slope for this symmetry in the $c_2^2$ range shown. Particularly noteworthy is the fact that the NOE is significantly higher when the symmetry of the local potential is rhombic instead of axial. *By analogy with Figure 14, the maximum NOE corresponding to rhombic "nearly planar $Y_M$−$X_M$ ordering" is expected to be higher than the maximum NOE corresponding to axial ordering of similar magnitude.* This turns out to be an important issue, discussed below in detail.

**5. Examples of Misleading Force-Fitting with MF Analysis.** *5a. "Missing" Contribution to $^{15}N$ $1/T_2$.* Lee and Wand,[9] who carried out a comprehensive MF analysis of multifield ubiquitin data acquired at 300 K, reported on an apparently missing contribution to $1/T_2$ that led to large $\tau_m$ values despite having allowed for variations in the $^{15}$N CSA interaction. Only when $T_2$ was excluded from the analysis was the expected value of $\tau_m = 4.1$ ns recovered. As shown in Figure 5, for $\tau_m = 5$ ns mixed modes contribute to $1/T_2$ significantly already for $\tau_e$ on the order of 20 ps for $S^2 = 0.85$. Quantitative estimates given in Table 8 show that even when the contribution of mixed modes is relatively small, the $1/T_2$'s obtained with MF analysis are 5−6% lower than the $1/T_2$'s obtained with SRLS analysis. Smaller time scale separation and lower ordering, which imply larger effects of additional eigenmodes for local motion on the

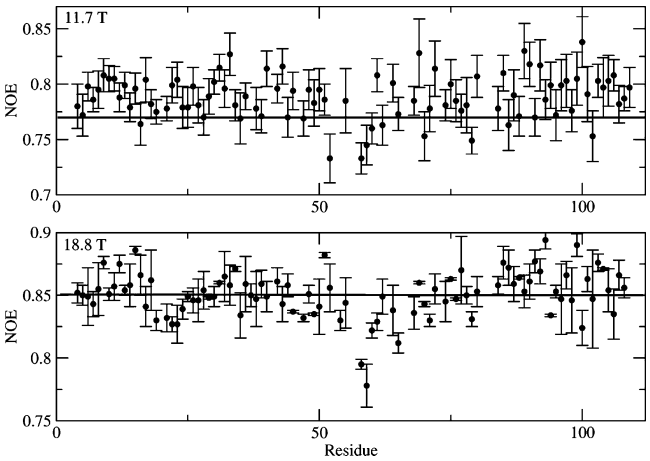


**Figure 15.** Experimental NOEs of the ribonuclease binase acquired at 11.7 and 18.8 T, 303 K.[21] The horizontal lines show the maximum NOE for 6.1 ns (11.7 T) and 5.5 ns (18.8 T), with the global motion correlation times determined on the basis of $T_1/T_2$ ratios.

correlation functions, will increase further the difference between $1/T_2$ obtained with SRLS and $1/T_2$ obtained with the MF approach. The data shown in Table 8 were obtained with axial potentials. For rhombic potentials the $1/T_2$ differences will be significantly larger because the SRLS and MF approaches differ, in general, to a larger extent when the potential is rhombic in SRLS and axial in MF (e.g., see Table 10).

Because MF analysis does not account for either mode mixing or potential rhombicity, the only way to render the fitting feasible is to exclude $T_2$ from the analysis.[9] SRLS-based data fitting with rhombic potentials and arbitrary $R_{\parallel}^{L}/R_{\perp}^{L}$ is expected to provide insightful fitting of complete multifield data from ubiquitin and other proteins.

*5b. Low Performance of the N−H Bond as Dynamic Probe.* The commonly used probe for studying protein backbone dynamics is the N−H bond. The experimental autocorrelated relaxation rates $^{15}$N $T_1$, $T_2$ and $^{15}$N−{$^1$H} NOE are analyzed with data fitting. Recently the $^{13}$C′−$^{13}$C$^{\alpha}$ bond has been suggested as a complementary dynamic probe (ref 13 and papers cited therein). In this application the $^{13}$C′−$^{13}$C$^{\alpha}$ dipolar-$^{13}$C′ CSA cross-correlated relaxation rate, $\Gamma$, is measured. Because only a single relaxation rate is measured only model 1 cases, which feature $\tau_m$ and $S^2$(C′−C$^{\alpha}$) as free variables, can be treated. In such cases one can calculate $S^2$(C′−C$^{\alpha}$) from the expression of $\Gamma$ using $\tau_m$ determined with $^{15}$N spin relaxation. Hence within the scope of the MF approach, combined N−H and C′−C$^{\alpha}$ analysis is relevant for rigid proteins where model 1 applies, assuming that the peptide plane is rigid.

The ribonuclease binase was studied earlier with $^{15}$N spin relaxation at 11.7 and 18.8 T,[21] and recently with combined $^{15}$N−$^1$H and C′−C$^{\alpha}$ spin relaxation at 11.7 T.[13] In the earlier study the 18.8 T data could not be fit with MF formulas, and the 11.7 T data yielded an altogether rigid backbone although other methods (X-ray crystallography, molecular dynamics and $^{13}$C′−$^{13}$C$^{\alpha}$ cross-relaxation) indicated that the catalytic loops L2 and L5 are flexible.[21] In ref 13 it was found that at 278 K $S^2$(N−H) and $S^2$(C′−C$^{\alpha}$) are practically the same, in agreement with nearly rigid N−H and C′−C$^{\alpha}$ bonds. However, when the temperature was increased to 303 K, $S^2$(C′−C$^{\alpha}$) decreased by 10%, whereas $S^2$(N−H) decreased by only 2%. This was considered contrary to the expectation that at the higher temperature the N−H bond should be more sensitive than the C′−C$^{\alpha}$ bond to the crankshaft motion[38] occurring about an axis close to the $N_i$−$C_i^{\alpha}$ bond, because N−H is perpendicular to this axis whereas C′−C$^{\alpha}$ is parallel to it. Similar results were obtained for ubiquitin.

**TABLE 13: Maximum NOE (Obtained with Model 1) and Minimum $T_1$ and $T_2$ (Obtained with Model 1 and $S^2 = 1$) Values Corresponding to 11.7 T and 13.44 (5.5) ns at 278 (303 K) (Row 1); Average Experimental $T_1$ and $T_2$ and NOE Values from Ref 13 (Row 2); and Percent Difference between Corresponding Data in Rows 1 and 2 (Row 3)**

| | $T_1$, ms | $T_2$, ms | NOE |
|---|---|---|---|
| | 303 K | | |
| 1 | 368.5 | 117.2 | 0.771 |
| 2 | 408.2 ± 6.5 (1.6%) | 129.4 ± 2.5 (1.9%) | 0.771 |
| 3 | 10.8% | 10.4% | 0 |
| | 278 K | | |
| 1 | 720.4 | 55.0 | 0.816 |
| 2 | 781.3 ± 18 (2.3%) | 59.2 ± 2.1 (3.6%) | 0.816 |
| 3 | 8.5% | 7.7% | 0 |

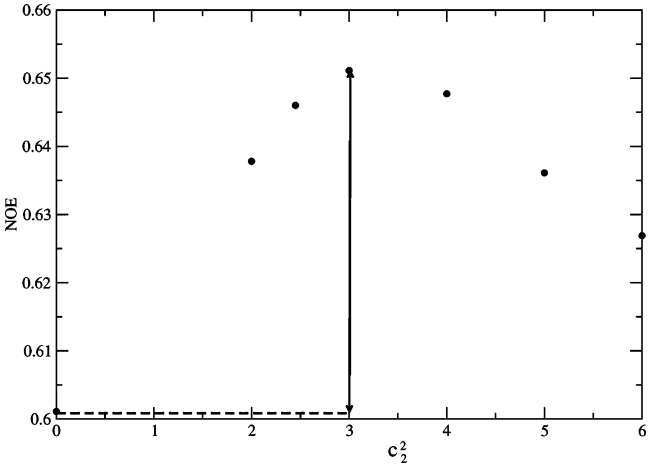


**Figure 16.** $^{15}$N−{$^1$H} NOE calculated with $\tau_m = 6.1$ ns, $R^C = 0.5$, $R_{\parallel}^{L}/R_{\perp}^{L} = 0.5$ and $c_0^2 = 2$. The rhombic potential coefficient, $c_2^2$, was varied from 0 to 6.

The unexpected temperature-independence of $S^2$(N−H) is actually imprinted in the raw data. Figure 15 shows the experimental NOEs obtained at 303 K, 11.7 and 18.8 T. The horizontal lines show the maximum "rigid sphere" NOEs corresponding to $\tau_m$ values determined with $T_1/T_2$ analysis. It can be seen that most NOEs exceed the "rigid sphere" value. This feature necessarily imposes on the fitting scheme model 1, where the "rigid sphere" NOE value is obtained. The latter is independent of $S^2$. $T_1$ and $T_2$ assume minimum values for $S^2 = 1$. As shown in Table 13, the difference between the average experimental and minimum $T_1$ and $T_2$ values is approximately 8% at 278 K and 10% at 303 K. The $S^2$ values yielded by the MF analysis are 0.903 at 278 K and 0.884 at 303 K, which differ from 1 by 10 and 12%, respectively. Hence, the unexpectedly small temperature-dependence of $S^2$(N−H) is to be assigned to issues related to the analysis, rather than issues related to the sensitivity of the experimental data. A plausible interpretation is outlined below.

The maximum theoretical NOE value has been determined for axial local potentials. However, we found previously that "nearly planar $Y_M$−$X_M$ ordering" prevails at the N−H bond. Figure 16 shows the effect of potential symmetry on the NOE. Calculations were performed for $\tau_m = 6.1$ ns, $\tau_{\perp}^{L}/\tau_m = 0.5$, $R_{\parallel}^{L}/R_{\perp}^{L} = 0.5$, $c_0^2 = 2$ and $\beta_{MD} = 0°$. The rhombic potential coefficient, $c_2^2$, was varied from 0 to 6, scanning thereby over the various symmetries of the coupling potential and the corresponding ordering tensor. As pointed out earlier, $c_2^2 = 0$ corresponds to axial $Z_M$ ordering; $c_2^2 = 2$ corresponds to

**TABLE 14: Order Parameters $S_0^2$ and $S_2^2$, and $(S_0^2)_{axial}^2 = 0.25\ (S_0^2)^2 + 0.75\ (S_2^2)^2$, for $c_0^2$ and $c_2^2$ As Given in the Table**

| $c_0^2$ | $c_2^2$ | $S_0^2$ | $S_2^2$ | $(S_0^2)_{axial}^2$ | $c_{0(axial)}^2$ | $c_2^2/c_0^2$ |
|---|---|---|---|---|---|---|
| 10 | 16 | −0.305 | 1.034 | 0.825 | 11.3 | 1.6 |
| 10 | 18 | −0.381 | 1.100 | 0.943 | 34.9 | 1.8 |
| 10 | 20 | −0.412 | 1.130 | 0.971 | >50 | 2.0 |
| 10 | 22 | −0.432 | 1.147 | 1.005 | very high | 2.2 |

rhombic $Z_M$ ordering; $c_2^2 = 2.45$ corresponds to axial perpendicular $Y_M$ ordering; $c_2^2 = 3$ corresponds to rhombic "nearly planar $Y_M-X_M$ ordering" with $Y_M$ as the main ordering axis; $c_2^2 \sim 5$ corresponds to rhombic $X_M$ ordering. It can be seen that the largest NOE value is obtained for $c_2^2 = 2$ and $c_2^2 = 3$, i.e., rhombic "nearly planar $Y_M-X_M$ ordering", with $Y_M$ as main ordering axis.

Figure 16 shows clearly that rhombic potentials can yield higher NOEs than axial potentials. Therefore, if the theoretical spectral density used in the fitting scheme yields *maximum NOE*s corresponding to "nearly planar $Y_M-X_M$ ordering", the experimental NOEs may not exceed the maximum NOE, and model 1 may not be imposed on the fitting scheme. Instead model 2, which yields significantly lower $S^2$ values than model 1 (Table 7), may be selected at 303 K.

Yet another illustrative example is presented in Table 14 which shows high $c_0^2$ and $c_2^2$ values, corresponding to high order parameters, $S_0^2$ and $S_2^2$, as appropriate for model 1. For the expected $\beta_{MD} = 90°$ geometry corresponding to the "nearly planar $Y_M-X_M$ ordering", the term $\tau_m/(1 + \omega^2\tau_m^2)$ in the combination 1 spectral density is multiplied by the coefficient $[0.25\ (S_0^2)^2 + 0.75\ (S_2^2)^2]$, because $(d_{00}^2)^2 = 0.25$ and $2[d_{20}^2)^2] = 0.75$ (eq 20). Let us assume that this expression is mimicked by $(S_0^2)_{axial}^2$ in an axial potential scenario. We calculated $S_0^2$ and $S_2^2$ in terms of the potential of eq 4 with $c_0^2 = 10$ and $c_2^2$ varied from 16 to 22. These potentials correspond to "nearly planar $Y_M-X_M$ ordering". Table 14 also shows $c_{0(axial)}^2$, corresponding to $(S_0^2)_{axial}^2$. It can be seen that for $c_2^2/c_0^2 \geq 1.6$ the axial mimic $(S_0^2)_{axial}^2$ corresponds to very high potentials. This agrees with the high $S^2$(N−H) values obtained in ref 13 at the higher temperatures for binase and ubiquitin.

Combined analysis of N−H and C′−C$^\alpha$ bond dynamics can be carried out when the peptide plane is assumed to be rigid. The local ordering tensor (diagonal in the M frame) is then a common property. Because the magnetic frames of $^{15}$N−$^1$H and $^{13}$C′−$^{13}$C$^\alpha$ differ, the local geometry ($\Omega_{MD}$) differs. However, for high local ordering corresponding to model 1 (combination 1) $S^2$ ($(S_0^2)^2$) represents the mean square fluctuation amplitude of all the local motions.[25] In this limiting case the angle $\beta_{MD}$ does not enter the analysis any longer. For that, a rhombic M frame is required (eq 20). Hence one cannot expect differential sensitivity of the N−H and C′−C$^\alpha$ bonds to the crankshaft motion unless the local ordering is allowed to be rhombic in the theoretical spectral density. As pointed out previously,[26] this ordering symmetry actually prevails at the N−H site. As shown herein, it can be treated with the SRLS model.

Unlike $S^2$(N−H), which is determined with combined fitting of the relaxation quantities $^{15}$N $T_1$, $T_2$ and $^{15}$N−{$^1$H} NOE, $S^2$(C′−C$^\alpha$) is calculated directly from the expression for the cross-correlated relaxation rate, Γ. This can be accomplished by assuming that model 1 is valid, i.e., the spectral density is given by the first term of eq 16. With $\tau_m$ determined with N−H bond dynamics analysis, $S^2$(C′−C$^\alpha$) is the only unknown parameter. The maximum Γ value for 11.7 T is −2.395 (−1.194) for $\tau_m = 13.44$ ns (5.5 ns) whereas the corresponding experimental value is −1.992 (−0.885). Hence limitations implied by the experimental values exceeding maximum values implied by axial potentials, as in the N−H case, do not exist in this case. For rigid residues the $^{13}$C′−$^{13}$C$^\alpha$ dipolar-$^{13}$C′ CSA cross-correlated relaxation rate depends to a large extent on $J^{DD}(0)$ and $J^{CC}(0)$. Therefore, local motion effects are small, justifying the use of model 1. Because $\beta_{MD}$ is approximately 0° for C′−C$^\alpha$, $(S_0^2)_{axial}^2$ is approximately equal to $(S_0^2)^2$. For this reason at the higher temperatures the relatively accurate $S^2$(C′−C$^\alpha$) MF value is smaller than the force-fitted $S^2$(N−H) MF value.

**TABLE 15: Best-Fit Parameters for N−H Site Dynamics Obtained with Rhombic Potentials for the Average Experimental Data of Binase at 11.7 T, 303 K (Ref 21[a]) and for the Combined 11.7 and 18.8 T Data of Binase Residue 16 at 303 K (Ref 21[a]) ($\tau_m = 5.5$ ns)**

| | $c_0^2$ | $c_2^2$ | $R^C$ | $\beta_{MD}$, deg | $R_\parallel^L/R_\perp^L$ | $S_{xx}$ | $S_{yy}$ | $S_{zz}$ |
|---|---|---|---|---|---|---|---|---|
| av | 5.5 | 9.7 | 0.97 | 90_fixed | 1000_fixed | −0.470 | 0.761 | −0.291 |
| res 16 | 5.0 | 10.0 | 1.0 | 90.0 | 30.0 | −0.65 | 0.75 | −0.10 |

[a] Kindly provided by Prof. E. R. P. Zuiderweg of the University of Michigan, Ann Arbor, MI.

The 3D Gaussian axial fluctuations (GAF) model[40] accounts quantitatively for the different geometric features at the N−H and C′−C$^\alpha$ sites. In this approach the MF $S^2$ is expressed in terms of harmonic fluctuations around the $C_{i-1}^\alpha-C_i^\alpha$ axis ($\sigma_\gamma^2$) and perpendicular to it ($\sigma_{\alpha\beta}^2$). The 3D GAF model was applied to ubiquitin at 300 K.[40] Molecular dynamics simulations showed that $\sigma_\gamma^2 > \sigma_{\alpha\beta}^2$. MF fitting of the $^{15}$N relaxation data showed the same trend with even larger absolute magnitudes of $\sigma_\gamma^2$ and $\sigma_{\alpha\beta}^2$. The $S^2$(N−H) values obtained with the usual MF analysis were reproduced by the $S^2$(N−H) values calculated with the 3D GAF model when (relatively small) contributions, which are usually ignored in $^{15}$N spin relaxation of $^{15}$N,$^{13}$C-labeled proteins, were taken into account. $S^2$(C′−C$^\alpha$) values calculated with the 3D GAF model were found to be *higher* than $S^2$(N−H) as N−H senses the $\sigma_\gamma^2$ fluctuations, which can be considered to represent the crankshaft motion, whereas C′−C$^\alpha$ senses the $\sigma_{\alpha\beta}^2$ fluctuations. *Thus, accounting for the asymmetry of the local ordering with the 3D GAF model yields $S^2$(N−H) < $S^2$(C′−C$^\alpha$), as expected.*

Instead of harmonic fluctuations $\sigma_\gamma^2$ and $\sigma_{\alpha\beta}^2$ (suitable for "rigid" residues only) and a predetermined geometry, which is implicit in the 3D GAF model, the SRLS approach allows for a rhombic ordering tensor with principal values $S_0^2$ and $S_2^2$ (eq 11) defined in terms of a rhombic potential (eq 4). Furthermore, the SRLS treatment is not limited to "rigid" residues, and the orientation of the M frame is not fixed. The perpendicular (to the $C_{i-1}^\alpha-C_i^\alpha$ axis) orientations are not considered equivalent and the magnitude of the local asymmetry is quantified through $c_0^2$ and $c_2^2$, or $S_0^2$ and $S_2^2$. The local motion is treated as diffusive, which is reasonable (although improved modeling can be introduced to account for any inertial effects).[23]

Calculations using our fitting scheme for SRLS, which allows for rhombic ordering, were carried out for the average values of $^{15}$N $T_1$, $T_2$ and NOE acquired at 303 K and 11.7 T, and for combined 11.7 and 18.8 T data of residue 16 of binase acquired at 303 K. In the former case we fixed the ratio $R_\parallel^L/R_\perp^L$ at 1000 and the angle $\beta_{MD}$ at 90°, allowing $c_0^2$, $c_2^2$ and $R^C$ to vary. In the latter case we allowed $c_0^2$, $c_2^2$, $R^C$, $R_\parallel^L/R_\perp^L$ and $\beta_{MD}$ to vary. The results are shown in Table 15. $S^2$(C′−C$^\alpha$) = 0.806 was derived in ref 13 from the experimental cross-correlated relaxation rate, Γ, measured at 11.7 T and 303 K, as outlined above. On the basis of eq 11, $S^2$(C′−C$^\alpha$) = 0.806 corresponds to $c_0^2 = 10.2$. The components of the Cartesian ordering tensor are $S_{xx} = S_{yy} = -0.449$, $S_{zz} = 0.898$. It can be seen that the magnitudes of

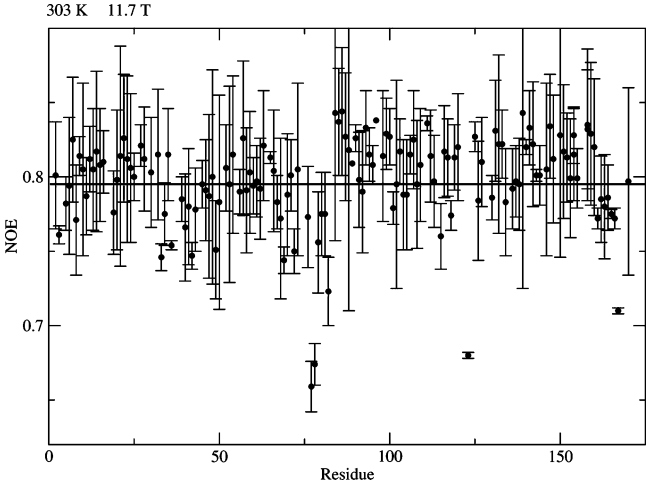


**Figure 17.** Experimental NOEs of oxidized flavodoxin acquired at 11.7, 303 K (ref 17). The horizontal line shows the maximum NOE for 7.6 ns, with the global motion correlation time determined on the basis of $T_1/T_2$ ratios.

the local potentials at N−H and C′−C$^\alpha$ sites are similar ($c_0^2$ associated with $^{13}C'_{i-1}-^{13}C^\alpha_{i-1}$ motion is comparable in magnitude with $c_2^2$ associated with $^{15}N_i-^1H_i$ motion). The local geometry is different with $\beta_{MD} = 90°$ for the N−H bond and $\beta_{MD} = 0°$ for the C′−C$^\alpha$ bond. Because $R_\parallel^L/R_\perp^L$ and $\beta_{MD}$ were fixed in the fitting of the average $^{15}$N relaxation data (as only 3 data points are available), and rhombic potentials could not be used to treat C′−C$^\alpha$ bond dynamics (as only one data point is available), we regard the data in Table 15 as interim results. However, they can be used for illustrative purposes. If the peptide plane is rigid, it is expected to determine the same tensor components permuted from $Z_M$ ordering for C′−C$^\alpha$ to $Y_M$ ordering for N−H. Thus, $S_{zz} = 0.898$ is to be compared with $S_{yy} = 0.761$ (results for the average data). If $(S_{yy})^2$ is considered to represent the crankshaft fluctuations, then 0.58 for N−H is to be compared with 0.20 for C′−C$^\alpha$. Clearly proper analysis bears out the higher sensitivity of N−H bond dynamics as compared to C′−C$^\alpha$ bond dynamics to the crankshaft fluctuations.

It is concluded that the effects of potential rhombicity, mixed modes and the D-to-CSA tilt must be accounted for in the theoretical spectral density to obtain physically insightful information. This is outside the scope of the model-free approach and can only be accomplished with the SRLS model. As shown above, combined $^{15}$N and $^{13}$C spin relaxation analysis is expected to be useful within the scope of SRLS analysis. As shown below, binase is not a singular case but a representative case.

Figure 17 shows the experimental NOEs of oxidized flavodoxin acquired at 11.7 T, 300 K.[17] Similar to the case for binase, most NOEs exceed the maximum NOE calculated for axial potentials, depicted by the horizontal line. $^{15}$N spin relaxation data of oxidized flavodoxin data could not be fit with the standard MF fitting scheme. Fitting became possible only after reducing the experimental NOEs globally by 10%, rendering them smaller than the maximum NOE. Even then model 1 was used predominantly, the $S^2$ values were very high, and $\tau_m$ was 7.6 ns, which is about 2 ns shorter than expected for a bare sphere with a molecular weight of nearly 20 kDa, corresponding to oxidized flavodoxin. Clearly, the experimental data were force-fitted, similar to the binase case. SRLS-based fitting with axial potentials gave similar results, in support of the assessment that rhombic potentials are to be used.

The enzyme ribonuclease H (RNase H) was studied with $^{15}$N spin relaxation at 285, 300 and 310 K, 11.7 T.[12] The experimental NOEs are shown in Figure 18. It can be seen that quite a few NOEs exceed the maximum NOE values depicted by horizontal lines. The average slope $d(1 - S)/dT$ determined with MF analysis was $5.9 \times 10^{-4}$ K$^{-1}$, to be compared to $8 \times 10^{-4}$ K$^{-1}$ for binase, considered to be low. SRLS analysis, using the equivalents of MF models 1−5 (ref 46) as implemented in our 2D grid-based fitting scheme for SRLS featuring axial potentials,[22] yielded $6.4 \times 10^{-4}$ K$^{-1}$ for the $\beta_2$ strand of RNase H. Thus, the detrimental features of model 1 analysis with axial potentials outlined for binase recur with RNase H.

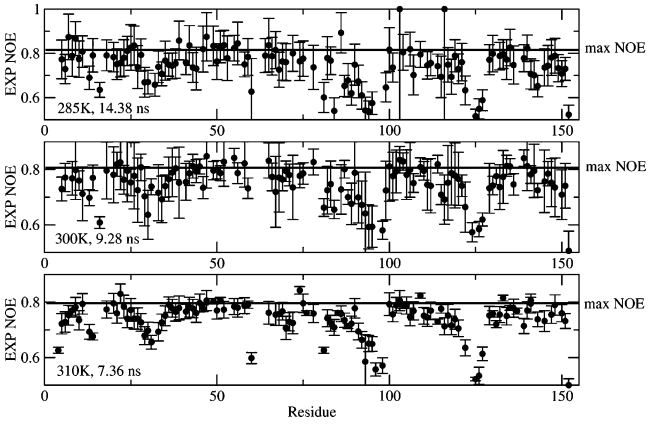


**Figure 18.** Experimental NOEs of RNase acquired at 285, 300 and 310 K, 11.7 T.[12] The horizontal lines show the maximum NOE for the $\tau_m$ values shown, which were determined on the basis of $T_1/T_2$ ratios.

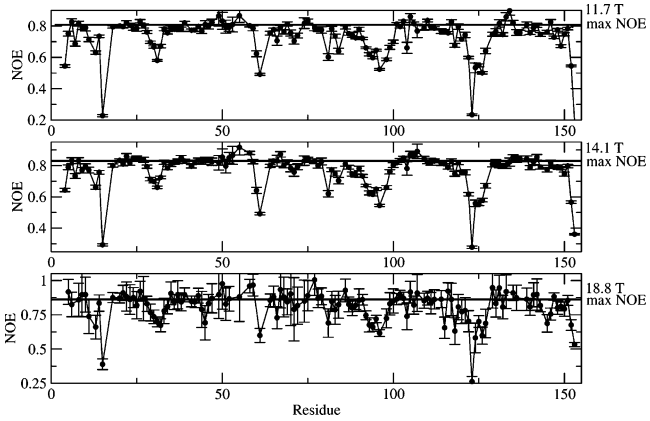


**Figure 19.** Experimental NOEs of RNase H acquired at 11.7, 14.1 and 18.8 T, 300 K.[59] The horizontal lines show the maximum NOE for the $\tau_m = 9.28$ ns determined on the basis of $T_1/T_2$ ratios.

$^{15}$N relaxation data of RNase H were also acquired at 11.7, 14.1 and 18.8 T, 300 K (ref 57). The NOEs obtained for the rigid part of the protein backbone are shown in Figure 19. NOEs exceeding the maximum NOE are pervasive at 18.8 T, where the local motion contributes significantly to the spectral density. Hence valuable information will be lost with force-fitted MF analysis.

A small value of $d(1 - S)/dT$ was also reported for ubiquitin. The experimental NOEs acquired for ubiquitin by Lee and Wand[9] are shown in Figure 20. It can be seen that similar to the cases for binase and RNase H, many NOEs exceed the maximum NOE.

Figures 15−20, as well as the last column of Table 5, indicate that in many cases MF fitting schemes select model 1 by force-fitting, yielding inaccurate $S^2$ values. When the main effect is the omission of the D-to-CSA frame transformation, as for the villin headpiece (Table 5), $(S_0^2)^2$ is underestimated by $S^2$. When the main effect is oversimplified symmetry of the local ordering,

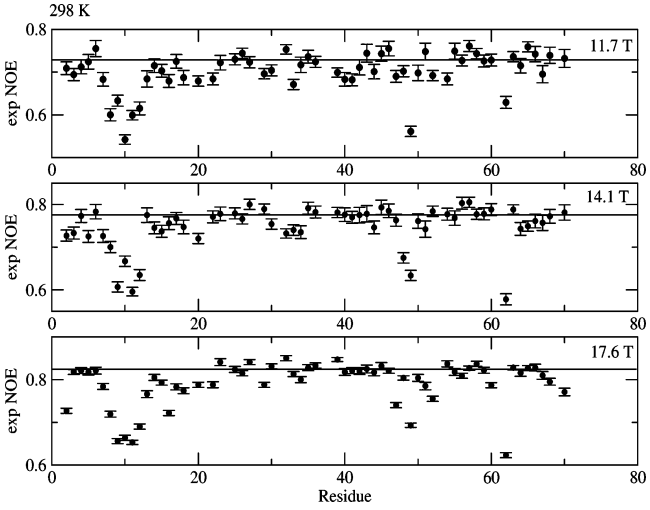


**Figure 20.** Experimental NOEs of ubiquitin acquired at 11.7, 14.1 and 18.8 T, 298 K.[9] The horizontal line shows the maximum NOEs for 4.1 ns.

$(S_0^2)^2$ is overestimated by $S^2$ (Table 14). Thus, the $S^2$ profile over the protein backbone may become qualitatively inaccurate.

*5c. Limited Information on Main-Chain Conformational Entropy from N−H Bond Dynamics*. Similar to its low sensitivity to temperature variations, $S^2$(N−H) was also found to exhibit low sensitivity to ligand binding. The parameters $S^2$(N−H) and $S^2$(C′−C$^\alpha$) of ligand-free and ligand-bound $Ca^{2+}$−calmodulin (CaM) were derived in ref 18. The experimental data were acquired at 11.7 T, 308 K, and the MF analysis used predominantly model 1. Except for the central linker and several loops, $S^2$(N−H) changed very little whereas $S^2$(C′−C$^\alpha$) changed significantly upon ligand binding. As in the temperature-dependent study, it was concluded that the N−H bond does not sense (in this case ligand-binding-dependent) backbone fluctuations sensed by the C′−C$^\alpha$ bond. This is important for conformational entropy derivation from MF $S^2$ in the context of complex formation.

Similar to the apparently low sensitivity of $S^2$(N−H) of binase, RNase H and ubiquitin to temperature changes, the apparently low sensitivity of $S^2$(N−H) to ligand binding to CaM stems from force-fitting the experimental data with axial potentials, instead of using physically sounder rhombic potentials. Routine interpretation requires a very efficient SRLS fitting scheme featuring rhombic potentials, which is currently being developed. Therefore, we illustrate below the need for model generality using our SRLS fitting scheme featuring axial potentials. Table 16 features results obtained for the residues 30, 100 and 135 of CaM (associated with high experimental NOEs) and for the central linker residues 77 and 80 (associated with low experimental NOEs). $\tau_m = 7.5$ ns for the free form and $\tau_m = 8.3$ ns for the bound form were used.[35,60] SRLS combinations 1 and 2, which correspond to MF models 1 and 2, did not yield acceptable results. SRLS combination 5, with $N$ fixed at the value of 1, gave the results shown in Table 16. This combination differs from MF model 2 in allowing the orientation of the ordering tensor, $\beta_{MD}$, to vary (recall that $(1.5 \cos^2 \beta_{MD} - 0.5)^2$ is formally equivalent to $S_f^2$ in MF analysis). For all the residues examined the local potential and the local ordering are high for both calmodulin forms, as found in ref 60, whereas $\beta_{MD}$ is small for the free form and on the order of 25° for the bound form. Thus, ligand binding changes the *orientation* of the ordering tensor preserving the *magnitude* of its principal value. This could not be determined with the MF approach because in models 1 and 2 the angle $\beta_{MD}$ is implicitly zero.

**TABLE 16: Best-Fit Parameters Obtained by Subjecting the Domain Residues 30, 100 and 135, Which Feature High Experimental NOEs, and Residues 77 and 80 of the Central Linker Region, Which Feature Low Experimental NOEs, to SRLS Analysis Using Combination 5 ($(S_0^2)^2$, $R^C$ and $\beta_{MD}$ Varied) with $N = R_{||}^L/R_\perp^L = 1$[a]**

| | $c_0^2$ | $(S_0^2)^2$ | $R^C$ | $\beta_{MD}$, deg | $\chi^2$ [b] |
|---|---|---|---|---|---|
| 30_f | 19.3 | 0.897 | 0.05 | 0.01 | 4.9 |
| 30_b | 18.3 | 0.892 | 0.06 | 20.0 | 5.0 |
| 100_f | 16.4 | 0.879 | 0.07 | 2.6 | 0.016 |
| 100_b | 15.7 | 0.874 | 0.05 | 22.5 | 25.2 |
| 135_f | 21.4 | 0.907 | 0.01 | 0.03 | 0.3 |
| 135_b | 16.4 | 0.879 | 0.06 | 22.2 | 13.1 |
| 77_f | 8.6 | 0.771 | 0.06 | 8.0 | 0.0 |
| 77_b | 8.4 | 0.765 | 0.03 | 24.8 | 7.9 |
| 80_f | 8.7 | 0.773 | 0.06 | 0.0 | 18.2 |
| 80_b | 8.2 | 0.760 | 0.03 | 28.0 | 21.6 |

[a] The symbols "f" and "b" denote the ligand-free and ligand-bound forms, respectively. [b] Note that a threshold value of $\chi^2 = 25$ was also used by Vugmeyster et al.[11]

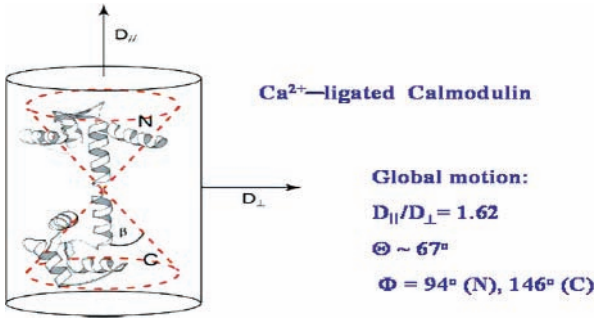


**Figure 21.** Ribbon diagram of $Ca^{2+}$-ligated calmodulin reproduced from ref 64. The coordinates of the crystal structure of Babu et al.[61] (PDB accession number 3CLN) were used. The data depicted define the global diffusion tensor as determined in ref 64. "N" and "C" denote the N- and C-terminal domains of $Ca^{2+}$-ligated calmodulin.

As shown in Figure 11, MF analysis does not have the capability to fit flexible N−H sites where $N \sim 1$ because it does not know of the spectral density components $j_1(\omega)$ and $j_2(\omega)$. The fact that the MF scheme converged to models 1 and 2 instead of model 5 is a consequence of force-fitting. With SRLS analysis we found that residues 77 and 80 of the central linker are associated with an average $c_0^2$ value of 8.5 (corresponding to an average $(S_0^2)^2$ value of 0.77), whereas residues 30, 100 and 135 are associated with $c_0^2 \sim 17.9$ ($(S_0^2)^2 \sim 0.9$). Hence axial-potential-based SRLS fitting differentiates between the central linker and the N- and C-domains of CaM. The results will change when the potential will be allowed to be rhombic and $N$ will be allowed to vary. However, Table 16 illustrates clearly the fact that sensitivity to ligand binding can be borne out by properties of the ordering tensor other than $S^2$, which is the only ordering-related parameter determined with MF models 1 and 2. The local ordering is characterized by a tensor, not merely a parametrizing scalar quantity, $S^2$.

*5d. Calmodulin: Detection of an Incorrect Phenomenon*. $Ca^{2+}$-ligated calmodulin is made of an N-terminal domain and a C-terminal domain connected by a helical linker, which is flexible in the middle. In the crystal CaM adopts an elongated dumb-bell structure[61] with the N- and C-terminal regions of the helical linker parallel to one another (Figures 21 and 22). Because the middle linker region is flexible the N- and C-domains may adopt various relative orientations in solution.

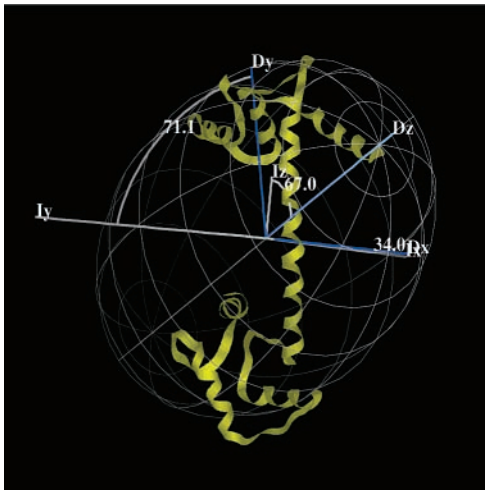


**Figure 22.** Ribbon diagram of the crystal structure of Babu et al.[61] (PDB accession number 3CLN) and corresponding inertia frame, I. The global diffusion frame, D, shown in Figure 21 is also depicted.

The helical target peptide, essential for CaM recognition and regulation, binds between the domains. Hence molecular shape, linker flexibility, and domain mobility are related to function, and deriving a reliable dynamic picture is important.

Several experimental and theoretical methods, including NMR spin relaxation, have been used to study CaM flexibility. The NMR-based dynamic picture changed as data were acquired at an increasing number of magnetic fields and temperatures. The first $^{15}$N spin relaxation study of $Ca^{2+}$-saturated Drosophila CaM data acquired at 11.7 T, 35°, was carried out in 1992.[62] These data were analyzed with the original MF formula. The assumption that $Ca^{2+}-$CaM is nearly spherical in solution (also found in refs 18 and 60) was corroborated by comparing N−H orientations in solution and in the crystal structure,[61] and by the nearly flat $T_1/T_2$ profile. Somewhat different isotropic correlation times on the order of 6−8 ns were assigned to the N- and C-domains. Except for the flexible residues 78−81 of the central linker and two loops, the CaM backbone was found to be quite rigid, with $S^2 \sim 0.85$ and $\tau_e < 100$ ps.

At low magnetic fields the local motion makes a relatively small contribution to the spectral density. If the spectral density used to calculate the NMR variables is appropriate, the addition of higher field data will merely increase accuracy and precision. If it is not, then inconsistencies will arise because local motion effects will be parametrized in different ways at different magnetic fields. The $Ca^{2+}$-free Xenopus CaM study of Tjandra et al.[63] identified such inconsistencies when 11.7 and 14.1 T data were analyzed in concert. The inconsistencies detected could be reconciled by using the reduced extended MF formula (eq 19 with $\tau_f'$ set equal to zero) instead of the original MF formula (eq 16). With $S_f^2$ fixed at 0.85 and uniform parameters within each domain, the fitting yielded $\tau_m = 12$ ns, $S_s^2 \sim 0.7$ and $\tau_s \sim 3$ ns. The parameters $S_s^2$ and $\tau_s$ were interpreted within the scope of wobble-in-a-cone motions of the two domains. The vertex angle of the cones was approximately 30°, which is incompatible with isotropic $\tau_m$. Semiquantitative arguments in support of an elongated solution structure with $N = R_{||}^C/R_\perp^C \sim 1.6$ were invoked.

$^{15}$N spin relaxation data of $Ca^{2+}$-saturated Xenopus CaM were acquired by Baber et al.[64] at 8.5 (except for NOEs), 14.1 and 18.8 T, 308 K. The analysis was similar to that of Tjandra et al.[63] The larger data set available made possible determination of the global diffusion tensor, $\mathbf{R}^C$, and removal of the restrictions that $\tau_f = 0$ and $S_f^2 = 0.85$. Chang et al.[65] extended the

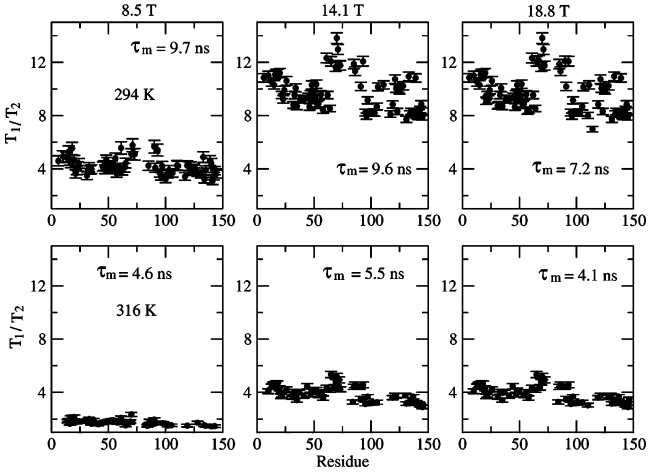


**Figure 23.** Experimental $T_1/T_2$ ratios at 8.5, 14.1 and 18.8 T, 294 and 316 K, from ref 65. The isotropic global diffusion correlation times, $\tau_m$, determined with the program QUADRIC,[66] are also shown.

experimental data set of Baber et al.[64] so that $^{15}$N $T_1$, $T_2$ and NOEs became available at 8.5, 14.1 and 18.8 T, at 294, 300, 308 and 316 K. These data were analyzed in concert assuming that (1) $S_f^2$, $\tau_f$ and $N = R_{||}^C/R_\perp^C$ are the same for all the residues within a given domain and are independent of temperature, and (2) the temperature dependence of $\tau_m$(app) (with $\tau_m$(app) = 1/6$D$(app), $D$(app) = 1/3(2$D_\perp$ + $D_{||}$)) is controlled by the Stokes−Einstein formula. A sudden decrease (increase) in $S_s^2$ ($\tau_s$) was observed when the temperature was increased from 308 to 316 K, interpreted as "melting" of residues 74−77 of the central linker, considered important from a biological point of view.

Because data acquired at several magnetic fields and several temperatures are analyzed in concert, the analysis is particularly prone to force-fitting. It will be shown below that qualitatively erroneous results were obtained in the case of $Ca^{2+}-$calmodulin.

*5d-i. Global Diffusion.* The axial global diffusion tensor, $\mathbf{R}^C$, was determined together with the site-specific parameters using the total time correlation function, $C(t)$ (eq 14), with $C^L(t)$ given by the extended MF formula, and using the coordinates of the elongated dumb-bell shaped crystal structure.[61] In most MF studies $\mathbf{R}^C$ is determined separately on the basis of $C^C(t)$. The $C(t)$-based fitting of the combined multifield multitemperature data yielded $\Theta = 68°$, as shown in Figure 21, with the global diffusion axis, $C$, along the symmetry axis of the molecule. Accordingly, the principal axis of the inertia tensor, $\mathbf{I}$, must be tilted at 68° from C. This disagrees with the orientation of the inertia tensor in the crystal structure, shown in Figure 22. Clearly the latter orientation of the inertia tensor is correct, hence the orientation of the global diffusion tensor is likely in error.

Figure 23 shows the experimental $T_1/T_2$ data acquired at 8.5, 14.1 and 18.8 T, and 294 and 316 K and filtered according to traditional criteria.[64,65] The width of the distribution divided by the average error is 6 (4), 8.5 (9.0) and 13.0 (14.0) for 8.5, 14.1 and 18.8 T at 294 K (316 K). It is obvious that the distribution in $T_1/T_2$ is significantly smaller at 8.5 T, in agreement with the 11.7 T data of Barbato et al.[62] and Wand and co-workers.[18,60] Isotropic global diffusion analysis with the program QUADRIC[66] yielded the $\tau_m$ values depicted in Figure 23. The shape of the distribution in $T_1/T_2$ values is both field- and temperature-dependent, although it has been assumed that $\mathbf{R}^C$ is temperature-independent except for $\tau_m$(app), which does not affect the shape of the $T_1/T_2$ distribution. It is very likely that the structured $T_1/T_2$ profiles at the higher fields represent mixed-mode contributions and unaccounted for geometric

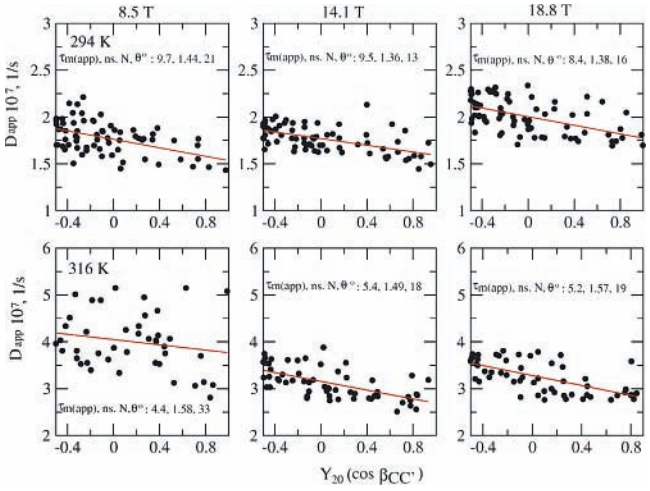


**Figure 24.** Analysis of the experimental data shown in Figure 23 with the program QUADRIC[66] assuming axial global diffusion ($R^C$). The resulting parameters, which define the $\mathbf{R}^C$ tensor, are also shown.

effects. If this is not the case, then analyses based on single-field data and the concerted analysis should yield the same results. This test is carried out below.

Using the filtered $T_1/T_2$ data of Chang et al.[65] we determined the axial global diffusion tensor $\mathbf{R}^C$ at each magnetic field and temperature separately with the program QUADRIC.[66] This corresponds to using $C^C(t)$ instead of $C(t)$. In Figure 24 we show $D(\text{app}) = 1/3(D_\parallel + 2D_\perp)$ ($R^C(\text{app})$ in our notation) as a function of $P_2(\cos(\beta_{CC'}))$ at 8.5, 14.1 and 18.8 T, and at the temperatures of 294 and 316 K.

The spread of points about the theoretical straight lines (obtained with linear regression) in Figure 24 is invariably large, indicating that theory and data are incompatible. There are relatively few points corresponding to $\beta_{CC'} = 0$, in disagreement with the purported solution structure (Figure 21). The largest spread of points is obtained for 8.5 T, 316 K, although $\chi^2$ assumes the smallest value ($\chi^2 = 2$) in this case. This is certainly not expected for models matching the data to which they are applied, but it can occur when force-fitting sets in. All four parameters defining the global diffusion tensor are field-dependent. In all the cases except for 8.5 T, 316 K, the angle $\Theta$ of the individual analyses is much closer to 0° (coincident inertia and diffusion frames) than to the nonphysical angle of 68° yielded by the concerted multifield multitemperature MF analysis. The contradictions between the raw data, the single-field analysis and the concerted MF analysis are substantial. For example, the raw $T_1/T_2$ profile at 8.5 T, 316 K is nearly flat (Figure 23), whereas the $\mathbf{R}^C$ tensor illustrated in Figure 24 is closest to the axial tensor yielded by the concerted analysis. As shown in Figure 23, isotropic $\mathbf{R}^C$ analysis also yielded inconsistent $\tau_m$ values. Inaccuracies in $C^L(t)$ must have been clearly absorbed by $C^C(t)$. Therefore, the local motion parameters must be highly inaccurate, as demonstrated below.

*5d-ii. Local Motion.* Figure 25 reproduces the $S_s^2$ and $\tau_s$ temperature-dependent profiles obtained by Chang et al.[65] The squared generalized order parameter $S_s^2$ shows very limited temperature dependence between 294 and 308 K and decreases abruptly upon increasing the temperature to 316 K. The slow local motion correlation time, $\tau_s$, is temperature-independent between 294 and 308 K and *increases* abruptly upon increasing the temperature to 316 K. Within the scope of the cone model used by Chang et al.[65] the correlation time for slow local motion, $\tau_s$, depends analytically on $S_s^2$ and $D_w$. The respective expression is used to show that the abrupt increase in $\tau_s$ is due to the abrupt

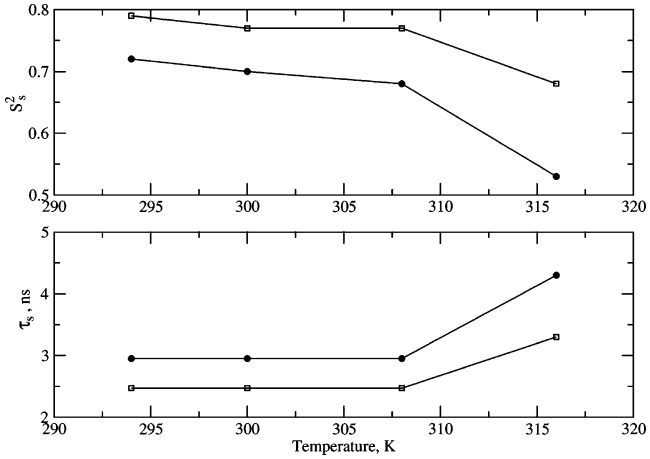


**Figure 25.** Best-fit $S_s^2$ and $\tau_s$ values obtained with the extended MF formula as outlined in ref 65 for the N-domain (open squares) and C-domain (solid circles) for $Ca^{2+}$-saturated Xenopus CaM. Additional best-fit parameters are $S_f^2 \sim 0.86$, $\tau_f \sim 15$ ps and global diffusion parameters $D_\parallel/D_\perp = 1.62$, $\Theta \sim 68°$, $\Phi \sim 94°$ for the N-domain and 146° for the C-domain. The $\tau_m(\text{app})$ values are 11.55, 9.87, 8.12 and 6.88 ns at 294, 300, 308 and 316 K.

decrease in $S_s^2$, whereas $D_w$ increases with temperature. However, inspection of the absolute values of $D_w$ shows that $1/6D_w$ is equal to 8.3 (6.8) ns for the N-domain (C-domain), whereas the apparent global motion correlation time is 6.88 ns. That $\tau_s$ is larger than $\tau_m$ is not tenable physically, nor consistent with the basic MF mode-independence assumption of time scale separation between the global and local motions.

The discontinuities in $S_s^2$ and $\tau_s$ between 308 and 316 K in Figure 25 results from the force-fitting process veering into a different region of the parameter space at 8.5 T and 316 K. Inspection of the experimental data presented in Figures 26−28 shows that the $T_2$'s at 8.5 T, 316 K, are outliers. Figure 24 shows that the graph obtained for 8.5 T, 316 K is an outlier. Inspection of Figures 5−8, where SRLS and MF analyses are compared for corresponding parameter values near the BO limit, shows that for $\tau_m = 15$ ns the corresponding NMR variables are comparable in magnitude. On the other hand, for $\tau_m = 5$ ns $T_2$ obtained with the MF approach is significantly higher than $T_2$ obtained with the SRLS approach. This supports the assertion that artificial results can be obtained by force-fitting large data sets covering extensive parameter ranges. In the case under consideration the experimental data acquired at low fields and high temperatures do not accommodate the force-fitted parameters, which fit all the other data. Therefore, discontinuities in $S_s^2$ and $\tau_s$, which are merely technical in nature, ensue.

*5d-iii. SRLS Analysis.* The calmodulin data were analyzed separately for each temperature and magnetic field using our SRLS fitting scheme based on axial potentials. We assumed that in view of large-amplitude domain motion $\mathbf{R}^C$ is on average isotropic, and used the $\tau_m(\text{app})$ values of Chang et al.[65] Isotropic $\mathbf{R}^C$ is consistent with the calmodulin studies of Barbato et al.[62] and Wand and co-workers,[18,60] and with other $^{15}N$ spin relaxation studies of proteins exhibiting large-amplitude domain motion.[19,21] As mentioned above, this SRLS fitting scheme assumes implicitly that $R_\parallel^L \gg R_\perp^L$, in analogy with $\tau_s \gg \tau_f$ in the MF approach. The SRLS fitting scheme selected primarily combination 5, which corresponds to MF model 5. The average $(S_0^2)^2$ (the formal analogue of MF $S_s^2$) and $\tau_\perp^L$ (the formal analogue of MF $\tau_s$) values for each magnetic field are shown as a function of temperature in Figure 29.

It can be seen that SRLS $\tau_\perp^L$ differs in magnitude from MF $\tau_s$ (cf. Figure 25). $\tau_s$ shows the nonphysical temperature depen-

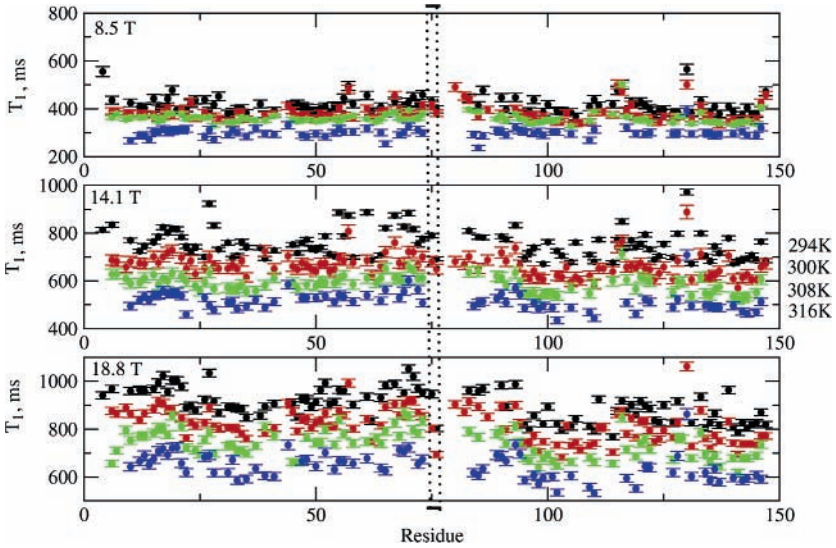


**Figure 26.** Longitudinal $^{15}$N $T_1$ relaxation times of $Ca^{2+}$−calmodulin at 294 K (black), 300 K (red), 308 K (green) and 316 K (blue), and 8.5, 14.1 and 18.8 T.[65] The vertical dashed lines depict the central linker (residues 74−78).

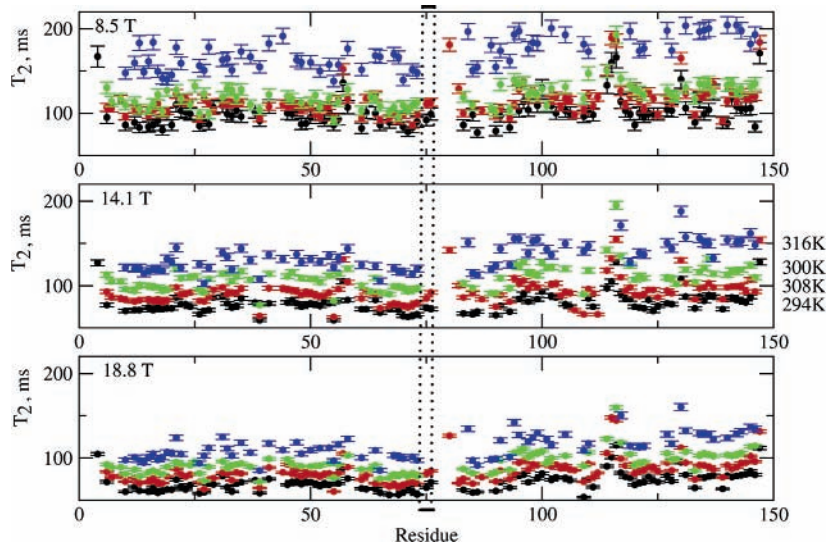


**Figure 27.** Transverse $^{15}$N $T_2$ relaxation times of $Ca^{2+}$−calmodulin at 294 K (black), 300 K (red), 308 K (green) and 316 K (blue), and 8.5, 14.1 and 18.8 T.[65] The vertical dashed lines depict the central linker (residues 74−78).

dence illustrated in Figure 25, whereas $\tau_\perp^L$ shows physically reasonable temperature dependence illustrated in Figure 29. SRLS $(S_0^2)^2$ is approximately half of MF $S_s^2$ and decreases monotonically with increasing temperature. No sudden change is observed between 308 and 316 K in either parameter. The inconsistencies among $(S_0^2)^2$ and $\tau_\perp^L$ values obtained at different magnetic fields are expected to be eliminated in future work, where rhombic potentials will be used.

*5d-iv. Dynamic Picture According to MF Analysis.*[65] CaM is an elongated dumb-bell shaped molecule. The N- and C-terminal domains wobble within cones with vertex angles increasing suddenly from 22.5° (27°) to 27° (37°) for the N-domain (C-domain) when the temperature is increased from 308 to 316 K. This corresponds to a squared generalized order parameter, $S_s^2$, decreasing from 0.77 (0.68) to 0.68 (0.53) for the N-domain (C-domain). The average wobbling rate, $D_w$, is $1.7 \times 10^7$ ($2.0 \times 10^7$) $s^{-1}$ at 295 (316 K) for the N-domain, which translates into correlation times, $1/6D_w$, of 9.8 (8.3) ns. The value of $D_w$ is $2.0 \times 10^7$ ($2.45 \times 10^7$) $s^{-1}$ at 295 (316 K) for the C-domain, which translates into correlation times of 8.3 (6.8 ns). The correlation time for global motion is 11.55 (6.88) ns at 295 (316 K). Hence, at 316 K the correlation time for local motion, $1/6D_w$, is larger than the correlation time for global motion, $\tau_m$, for the N-domain, and equal to $\tau_m$ for the C-domain. Motion about the N−H bond is on the order of 20 ps and $S_f^2$ is on the order of 0.85 throughout the temperature range investigated.

The abrupt change in best-fit parameters values upon increasing the temperature from 308 to 316 K is interpreted as "melting" of residues 74−77. This process is purported to have biological implications for target peptide binding by prolonging the flexible part of the central linker by 50%. Note that the experimental data of residues 74−77 (as well as many other CaM residues) are not observed experimentally at 316 K (Figures 26−28, residues demarcated by the dashed vertical lines).

*5d-v. Dynamic Picture According to the Current SRLS Analysis.* CaM is on average spherical in solution due to large-amplitude nanosecond segmental motions of its N- and C-terminal domains. This is physically plausible, consistent with the $T_1/T_2$ profiles at 11.7 T that are determined predominantly by the global motion, and the quantitative analysis by Barbato at al.[62] and Wand and co-workers.[18,60] Average spherical shapes in solution were also determined with $^{15}$N spin relaxation for

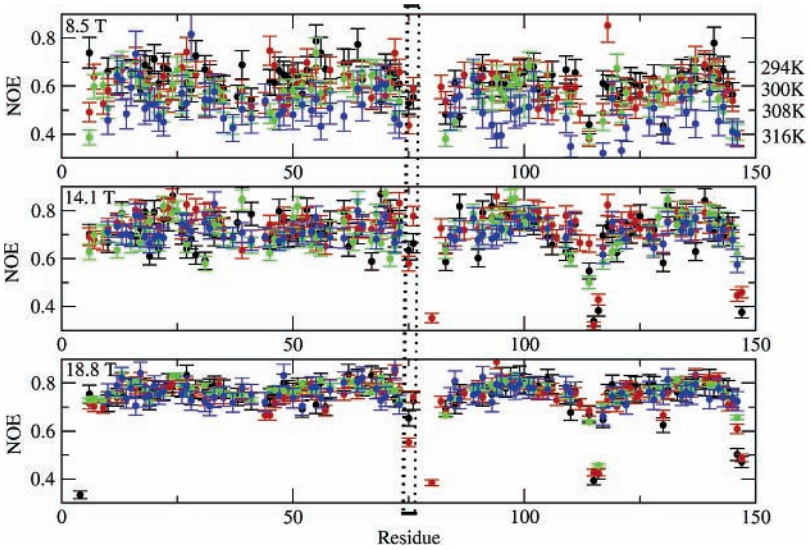


**Figure 28.** Steady-state $^{15}N-\{^1H\}$ NOEs of $Ca^{2+}$−calmodulin at 294 K (black), 300 K (red), 308 K (green) and 316 K (blue), and 8.5, 14.1 and 18.8 T.[65] The vertical dashed lines depict the central linker (residues 74−78).

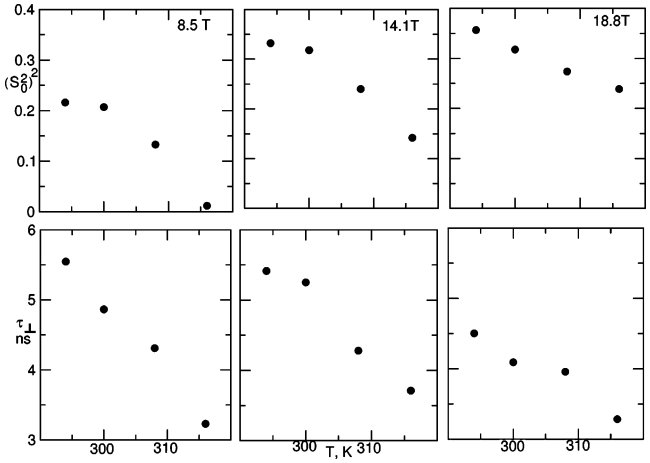


**Figure 29.** Best-fit $(S_0^2)^2$ and $\tau_\perp^L$ values obtained with SRLS combination 5 by averaging over the results obtained for the individual residues using $\tau_m$ values of 11.55, 9.87, 8.12 and 6.88 ns at 294, 300, 308 and 316 K. $\beta_{MD}$ was on average 15°. Experimental data from ref 65 were used.

AKeco[19] and binase,[21] which, being similar to CaM, feature large-amplitude domain or loop motions in solution. Both AKeco and binase have elongated shapes in the crystalline state, similar to the crystal structure of CaM.

Domain motion is expected to occur on the same time scale as the global motion, implying mode mixing. This is accounted for by the SRLS analysis, which yields $\tau_\perp^L$ on the order of 3−6 ns in the temperature range of 294−316 K. As expected, $\tau_\perp^L$ decreases monotonically with increasing temperature. $(S_0^2)^2$ is on the order of 0.2−0.35 in this temperature range and decreases monotonically with increasing temperature. No discontinuity is exhibited by either the $\tau_\perp^L$ or the $(S_0^2)^2$ temperature profiles.

The results shown in Figure 29 are interim results because the analysis used oversimplified axial symmetry for the local orienting potential/local ordering, and assumed implicitly that $R_\parallel^L/R_\perp^L \gg 1$. The implications of removing these restrictions are illustrated and discussed in the next section.

**6. Reliable Fitting; Mixed Mode Concept.** In our current fitting scheme the local and global diffusion tensors are allowed to be axially symmetric, and the local ordering tensor (or local coupling/mixing/orienting potential) is allowed to be rhombic.

**TABLE 17: Best-Fit Parameters Obtained with the SRLS Combination 5 (SRLS_5) and SRLS Combination 6 (SRLS_6) Using the Axial-Potential 2D Grid-Based Fitting Scheme[a]**

| | $R^C$ | $c_0^2$ | $c_2^2$ | $S_{xx}$ | $S_{yy}$ | $S_{zz}$ | $\beta_{MD}$, deg | $N$ |
|---|---|---|---|---|---|---|---|---|
| SRLS_5 | 0.44 | 3.2 | 0.0 | −0.315 | −0.315 | 0.63 | 16.1 | 1000 (fixed) ($\chi^2 = 15.9$) |
| SRLS_6 | 0.45 | 3.2 | 0.0 | −0.315 | −0.315 | 0.63 | 16.3 | 916 ($\chi^2 = 15.8$) |
| SRLS_rh | 0.23 | 4.8 | 10.1 | −0.469 | 0.799 | −0.330 | 99.5 | 40.0 ($\chi^2 = 12.3$) |

[a] SRLS_rh represents the calculation carried out with the fitting scheme allowing for rhombic potentials and arbitrary $N = R_\parallel^L/R_\perp^L$ values, with the $j_{KK'}(\omega)$ functions calculated on the fly. The combined $^{15}N$ relaxation data of residue 124 of RNase H acquired at 11.7, 14.1 and 18.8 T, 300 K, were used. $\tau_m = 9.28$ ns was used. $R^C$ is the same as $\tau_\perp^L/\tau_m$, and $N = R_\parallel^L/R_\perp^L$. $S_{xx}$, $S_{yy}$ and $S_{zz}$ are the components of the Cartesian ordering tensor.

The magnetic tensors have arbitrary symmetry and orientation. Starting with the original MF limit, where the magnetic tensors are collinear, their frame is the same as the local ordering frame, and the global and local diffusion tensors are isotropic, one can then systematically lower symmetries until the complexity of the model matches the integrity of the data. In this case reliable fitting, which extracts properly the dynamic information inherent in the experimental data, can be accomplished. Table 17 illustrates the last part of such a process, where SRLS spectral densities are upgraded to include more detailed features in a stepwise fashion.

The example considered is residue 124 of RNase-H, which pertains to the flexible loop $\alpha_D/\beta_5$. The $^{15}N$ relaxation data acquired at 11.7 T, 300 K, were fit previously with MF model 5.[12] The global motion correlation time of RNase H was determined to be $\tau_m = 9.28$ ns at 300 K, and it has been ascertained that the protein is spherical within a good approximation. We subjected the combined 11.7, 14.1 and 18.8, 300 K, data of this residue (kindly provided by Prof. A. G. Palmer III of Columbia University), to SRLS analysis.

The first row of Table 17 shows the best-fit parameters obtained with SRLS combination 5 (SRLS_5), which is formally analogous with MF model 5. In this scenario the local ordering is axially symmetric and $N = R_\parallel^L/R_\perp^L \gg 1$. The potential is small ($c_0^2 = 3.2$), the corresponding squared order parameter is small ($(S_0^2)^2 = 0.47$), the D-to-M tilt is small ($\beta_{MD} = 16.1°$), and there is only a modest time scale separation between the

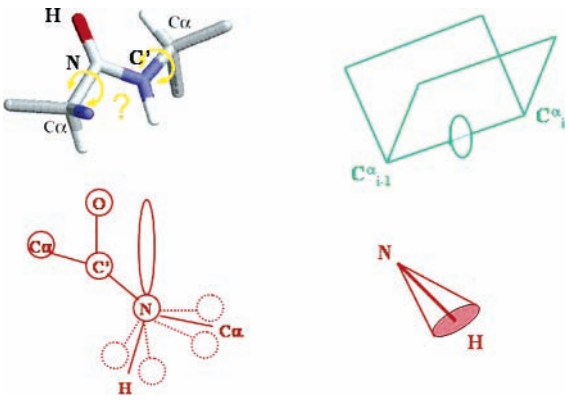


**Figure 30.** Various local motion modes including the anti-correlated $\Phi_i$ and $\Psi_{i-1}$ crankshaft motion (upper left), peptide-plane motion about $C^{\alpha}_{i-1}-C^{\alpha}_{i}$ (upper right), nitrogen pyramidalization (lower left) and fast small-amplitude fluctuations (lower right).

global and perpendicular component, $R^{L}_{\perp}$ (i.e., $R^{C} = 0.44$ in units of $R^{L}_{\perp}$). Similar values were obtained previously for the flexible residues of a large number of proteins and can be considered typical. A modest time scale separation between the global and local motion ($R^{C}$) is expected. Quite unexpectedly, the local potential is weak ($c_0^2 = 3.2$) for the tightly packed globular proteins; i.e., the local ordering is low ($(S_0^2)^2 = 0.40$). Also, the diffusion tilt is on the order of 16° instead of being on the order of 90°, corresponding to preferred ordering around $C^{\alpha}_{i-1}-C^{\alpha}_{i}$ or $N_i-C^{\alpha}_{i}$. No improvement was achieved by allowing $N$ to vary (SRLS_6), indicating that $N \gg 1$ is not the main reason for these difficult-to-reconcile results. On the other hand, significant improvement was achieved by allowing the potential to be rhombic, in addition to allowing $N$ to vary, as shown by the last row of Table 17.

Let us compare the results obtained for axial (SRLS_6) and rhombic (SRLS_rh) potentials. The value of $N = 40$ corresponds to $\tau^{L}_{||} = 53$ ps whereas $N = 916$ corresponding to $\tau^{L}_{||} \sim 0$. The ordering is high in the rhombic case, as implied by $c_2^2 = 10.1$, and low in the axial case. The ratio $c_2^2/c_0^2$ obtained with SRLS_rh corresponds to "nearly planar $Y_M-X_M$ ordering", as expected. This is borne out clearly by the values of the components of the Cartesian ordering tensor shown in Table 17. The diffusion tilt is $\beta_{MD} \sim 90°$ in the rhombic case, compatible with crankshaft fluctuations[38] or peptide-plane reorientation about the $C^{\alpha}_{i-1}-C^{\alpha}_{i}$ axis or the $N_i-C_i$ bond, respresented by $\tau^{L}_{\perp}$, as well as small-amplitude N−H wobbling motion and/or nitrogen pyramidalization,[39] represented by $\tau^{L}_{||}$ (Figure 30). The rate $R^{L}_{\perp} = 0.23 \times 9.28 = 2.1$ ns shows that, as expected, loops move on the same time scale as the entire molecule. Unlike the axial scenario the rhombic scenario is consistent and physically appropriate.

Data fitting with rhombic potentials was also carried out for residues 46 and 47 of adenylate kinase from *E. coli* (AKeco), which are representative of the mobile domain AMPbd of AKeco. The results are shown in Table 18. The symmetry of the rhombic potential is of the same type as found for residue 124 of RNase H, and the angle $\beta_{MD}$ is also close to 90°. However, $R^{C}$ is on the order of 0.8 for the AKeco residues 46 and 47 as compared to 0.2 for residue 124 of RNase-H, and $\tau^{L}_{||} \sim 1.5$ ns for the AKeco residues 45 and 47 as compared to $\tau^{L}_{||} = 75$ ps for residue 124 of RNase-H. This indicates significantly stronger dynamical coupling and smaller local diffusion anisotropy for mobile domains (AKeco) than for flexible loops.

The SRLS version that allows for rhombic potentials and axial local diffusion clearly yields a consistent physical picture. It appears that this is as much as one can extract from $^{15}N$ relaxation data in proteins. Note that nine data points, acquired at three magnetic fields were successfully used in the RNase calculations. The rhombic potential coefficient, $c_2^2$, is the only extra parameter in the SRLS analysis as compared with the extended the MF analysis. On the other hand, for flexible residues that are typically of biological interest, the SRLS model features a single local motion whereas the MF approach features two local motions (fast and slow), so the MF concept is actually a more compounded one.

**TABLE 18: Best-Fit Parameters Obtained with the SRLS Combination 6 Featuring Rhombic Potentials Using Adenylate Kinase Data Acquired at 14.1 and 18.8 T, 303 K[19] [a]**

| res | $c_0^2$ | $c_2^2$ | $R^{C}$ | $S_{xx}$ | $S_{yy}$ | $S_{zz}$ | $\beta_{MD}$, deg | $N$ |
|---|---|---|---|---|---|---|---|---|
| 46 | 5.7 | 10.5 | 0.82 | −0.465 | 0.827 | −0.361 | 101.4 | 9.6 |
| 47 | 4.3 | 10.3 | 0.73 | −0.470 | 0.761 | −0.291 | 100.7 | 6.3 |

[a] $\tau_m = 15.1$ ns was used. $R^{C} = \tau^{L}_{\perp}/\tau_m$. $S_{xx}$, $S_{yy}$ and $S_{zz}$ are the components of the Cartesian ordering tensor.

*6a. Meaning of Mixed Modes.* Let us consider a cylinder diffusing freely in an isotropic medium. The diffusion rates are $R^{L}_{||}$ and $R^{L}_{\perp}$, with $N = R^{L}_{||}/R^{L}_{\perp}$ determined by its shape. The solution of the diffusion equation yields eigenvalues $\tau_K^{-1} = 6R^{L}_{\perp} + K^2(R^{L}_{||} - R^{L}_{\perp})$, with $K = 0, 1, 2$. Let us now consider the same cylinder diffusing in the presence of a locally orienting potential. This is a reasonable model for an N−H bond attached physically to the protein, with the local potential representing the restrictions imposed on its motion by the immediate protein environment. The protein itself is reorienting at a slower rate with respect to a fixed lab frame. When the local and global motions do not occur on a greatly separated time scale, and the local potential is neither very low nor very high, the potential couples or mixes the motions of the N−H bond and the protein. The local ordering can be expressed (as usually done for restricted motions in liquids) in terms of an ordering tensor with principal values defined in terms of the orienting potential.

This is the two-body problem solved by the SRLS model. A Smoluchowski equation of the form of eq 1 is solved where the SRLS diffusion operator $\hat{\Gamma}$ can be written in either of the two equivalent forms given by eq 2 or eq 3. In eq 2 the orientation of each body is referred to the lab (inertial) frame, but with a potential coupling them, which depends on their relative orientations. Simple products of basis functions of the two rotators (N−H body and protein), corresponding to their free diffusion (i.e., zero potential coupling them), are utilized to provide a matrix representation of $\hat{\Gamma}$. This is a convenient basis set when the potential is relatively small, i.e., weak coupling. In eq 3 only the global motion of the protein is referred to the lab frame, whereas the local motion of the N−H bond is referred to the local director frame fixed in the protein. This latter scenario thus describes the local motion in relative coordinates. Then product basis functions for the overall motion and the relative motion are used to provide the matrix representation of $\hat{\Gamma}$. This is a more natural choice when the coupling potential is large. Because these two approaches are mathematically equivalent, one may use either choice. In our past work we have utilized eq 2, whereas in the newer work we have reported in this paper we utilized eq 3.

The eq 2 perspective on mixed modes means that as a coupling potential is added, the new eigenmodes of $\hat{\Gamma}$ become linear combinations of the product functions of the two free rotors. This is a point of view where there are two sources of "mixed-modes": the first results from the coupling between the

**TABLE 19: Dominant Eigenvalues and Respective Weights (in Parentheses) in the $C_0(t)$ Correlation Function for Two Isotropic Rotators, $R^C$ and $R^L = 1$, Mixed by an Axial Potential of Strength $0 \le c_0^2 \le 4$, and Time Scale Separation Given by $R^C = 1.0$, 0.1 and 0.01[a]**

| | | $R^C$ | | |
|---|---|---|---|---|
| $c_0^2$ | $(S_0^2)^2$ | 1.0 | 0.1 | 0.01 |
| 0 | 0 | 6.00 (1.00) | 6.00 (1.00) | 6.00 (1.00) |
| 1 | 0.049 | 4.79 (0.60) | 0.59 (0.06) | 0.06 (0.05) |
| | | 7.57 (0.39) | 5.94 (0.65) | 5.57 (0.32) |
| | | | 7.33 (0.15) | 6.04 (0.27) |
| 2 | 0.193 | 3.90 (0.71) | 0.58 (0.23) | 0.06(0.19) |
| | | 10.0 (0.27) | 6.55 (0.57) | 6.04 (0.26) |
| | | | 8.10 (0.11) | 6.68 (0.36) |
| 3 | 0.366 | 3.41 (0.79) | 0.56 (0.41) | 0.06 (0.37) |
| | | 13.43 (0.17) | 7.95 (0.37) | 7.20 (0.15) |
| | | | 9.47 (0.12) | 8.02 (0.33) |
| 4 | 0.506 | 3.19 (0.85) | 0.55 (0.56) | 0.06 (0.51) |
| | | | 10.06 (0.22) | 10.0 (0.30) |
| | | | 11.54 (0.14) | |

[a] The $(S_0^2)^2$ values corresponding to the $c_0^2$ values are also presented.

two rotors, so that the motion of the internal rotor becomes more that of its motion relative to the protein. This is a feature that exists even when there is time-scale separation, i.e., $R^C/R^L \ll 1$. The second arises when $R^C/R^L \sim 1$, so there is no longer a significant time-scale separation. In that case the diffusive reorientation of the internal rotor becomes a mixture of the global and local motions. That is, an observer that detects just the $^{15}N$ label on a particular N−H bond can no longer distinguish between a local and a global mode of motion. Thus, these modes become mixed. In the case wherein eq 3 and its convenient basis set are used, the intuitive picture changes somewhat, but the final analysis must remain equivalent. In simple mathematical terms this means that the eigenvalues of $\hat{\Gamma}$ are unchanged, but the eigenmodes are represented in (or referred to) the different basis sets, and appear different, although (again) they must be equivalent. Here, for very high ordering and $R^C/R^L \ll 1$, the eigenmodes can be represented by the overall motion and by the relative internal motion with eigenvalues given (for axial potentials) by eq 18, and eigenfunctions given elsewhere (refs 29 and 48), yielding simple limiting correlation functions. As the coupling potential is reduced (but $R^C/R^L \ll 1$), the correlation functions for the relative motion (i.e., for the $D^2_{MK}(\Omega_{CM})$) become more complex, involving several eigenmodes of this motion. Again, as $R^C/R^L_\perp \rightarrow 1$, there must be "mixed modes" of the two coupled dynamic processes.

We illustrate some of these concepts with a relevant computational study presented by Polimeno and Freed.[23] This was performed using the basis set appropriate for eq 2; i.e., the global and internal rotors both referred to the lab frame. Table 19 shows the eigenvalues (in units of $R^L$) and corresponding weights of the two isotropic rotors coupled by an axial potential whose strength is given by $c_0^2$. Values of $R^C/R^L$ of 1.0, 0.1 and 0.01 are considered, and $c_0^2$ ranges from 0 to 4. When $c_0^2 = 0$, the motions are uncoupled, so only the motion of the local rotor relative to the lab frame is relevant. It corresponds to eigenvalue 6 (or more precisely $6R^L$) with weight 1.00, independent of $R^C/R^L$. For the case of $R^C/R^L = 0.01$ there is good time-scale separation of the motions. Thus, as $c_0^2$ is increased the global motion retains the eigenvalue 0.06, but its relative weight in the correlation function $C_0(t)$ increases roughly according to $(S_0^2)^2$. The local motion is represented by several eigenvalues with the (typically two) major ones given in Table 19. The results for $R^C/R^L = 0.1$ are qualitatively similar. For $R^C/R^L = 1$ the results are quite different. As $c_0^2$ is increased from 0, two main mixed modes appear, one of which decreases from the value of 6.00, while the other increases from this value, and the former becomes relatively more important in $C_0(t)$. We can intuitively suggest that the former represents a mixed mode, wherein as the protein reorients in one sense (e.g., clockwise), the internal rotor is attempting to reorient in the opposite (e.g., counterclockwise) sense; the latter mixed mode would correspond to more additive reorientational diffusion (i.e., both are in the same sense).

**TABLE 20: Dominant Eigenvalues and Respective Weights (in Parentheses) of the $C_{KK'}(t)$ Components That Contribute to the Measurable Spectral Density[a]**

| $c_2^2$ | $S_0^2$ | $S_2^2$ | eigenvalue (weight) | $K$ | $K'$ | $(d^2_{00})^2$ or $2(d^2_{KK'})^2$ [b] |
|---|---|---|---|---|---|---|
| 0.0 | 0.439 | 0.0 | 6.58 (0.415) | 0 | 0 | 1.0 |
| | | | 0.006 (0.193) | | | |
| | | | 5.95 (0.193) | | | |
| | | | 8.52 (0.161) | | | |
| 3.0 | 0.088 | 0.572 | 5.40 (0.349) | 0 | 0 | 0.25 |
| | | | 4.44 (0.237) | | | |
| | | | 4.36 (0.232) | | | |
| | | | 8.31 (0.114) | | | |
| | | | 0.006 (0.008) | | | |
| | | | 4.36 (0.214) | 2 | 2 | 0.75 |
| | | | 1.85 (0.209) | | | |
| | | | 5.70 (0.184) | | | |
| | | | 0.006 (0.098) | | | |
| | | | 4.36 (0.428) | 2 | −2 | 0.75 |
| | | | 0.006 (0.163) | | | |
| | | | 14.40 (0.125) | | | |
| | | | 5.40 (0.120) | | | |
| | | | 4.44 (0.08) | | | |

[a] For the axial case we utilized $R^C = 0.001$, $c_0^2 = 2$, $c_2^2 = 0$ and $\beta_{MD} = 0°$, and for the rhombic case we utilized $R^C = 0.001$, $c_0^2 = 2$, $c_0^2 = 3$ and $\beta_{MD} = 90°$. The respective irreducible ordering tensor components, $S_0^2$ and $S_2^2$, are also presented. [b] Where $K \neq 0$ and $K' \neq 0$.

Finally, a comment on the tensors $\mathbf{R}^C$ and $\mathbf{R}^L$ that constitute input values in a given SRLS calculation, or best-fit parameters in fitting actual experiments, is in order. These quantities may represent more complex local and global rotators, and not just the $\mathbf{R}^C$ and $\mathbf{R}^L$ tensors corresponding to simple rotators. One can suggest tentative interpretations, as was done in a recently published SRLS application to nitroxide-labeled T4 Lysozyme.[37] In that paper $R^L_\parallel$ was interpreted as motion around a specific bond of the nitroxide tether, whereas $R^L_\perp$ was associated with motion around the symmetry axis of the helix comprising the nitroxide-labeled residue. For N−H bond motion we associated at this stage of our studies $R^L_\perp$ with motion around the $C^\alpha_{i-1}-C^\alpha_i$ axis and $R^L_\parallel$ with motion around an axis perpendicular to $C^\alpha_{i-1}-C^\alpha_i$ within the peptide plane.

Table 20 illustrates the high sensitivity of the eigenvalues and weights comprised in the time correlation functions $C_{KK'}(t)$ to the symmetry of the coupling potential. The parameters used include $R^C = 0.001$ and $c_0^2 = 2$, with $c_2^2 = 0$ for axial ordering and $c_2^2 = 3$ for rhombic "nearly planar $Y_M-X_M$ ordering". For axial ordering only $C_0(t)$ is relevant. For the $\beta_{MD} = 90°$ geometry only the correlation functions $C_0(t)$, $C_2(t)$ and $C_{2-2}(t) = C_{-22}(t)$ contribute to the measurable spectral density. The dominant eigenvalues and their eigenmode composition depend to a large extent on the symmetry of the coupling potential. The individual Lorentzians in a given function $j_{KK'}(\omega)$, obtained by Fourier transformation of the corresponding time correlation

function, are multiplied by ($d^2_{00}$) or 2($d^2_{KK'}$), where $K \neq 0$ or $K' \neq 0$, to yield the measurable spectral density. The $d^2_{KK'}$ values are also presented in Table 20. The additional contributions, comprising a large number of eigenvalues with small individual weights, are not shown. It can be seen clearly that potentials of similar magnitudes but different symmetries are associated with a different composition of dynamic modes. Obviously potential symmetry is a very influential component, to which the experimental data are highly sensitive.

As indicated, we have developed recently a fitting scheme for SRLS where the spectral densities $j_K(\omega)$ and $j_{KK'}(\omega)$ are calculated on the fly. This fitting scheme allows for rhombic potentials, and arbitrary axiality of the local and global diffusion tensors. Efforts to improve the computational efficiency of this scheme are underway.

## IV. Conclusions

Model-free is a very simplified approach for analyzing spin relaxation data in proteins, such that the quality of the experimental data and their variations (e.g., with magnetic field) are frequently beyond its capabilities. Small data sets (three data points at a given field in the case of N−H bond dynamics) can usually be force-fitted with good statistics but inaccurate best-fit parameters, which are obtained through parametrization of the experimental spectral densities. When larger data sets acquired at several magnetic fields, temperatures, states of complex formation, etc., are subjected to MF analysis, or when N−H and C′−C$^\alpha$ bond dynamics are analyzed in concert, force-fitting is so pervasive that functional dynamics may be missed, qualitatively erroneous results may be derived, and incorrect phenomena may be detected. Conformational entropy derived from parametrizing entities is inaccurate. Entropy profiles over the protein backbone may even be qualitatively inaccurate.

On the other hand, the experimental data can be analyzed significantly more reliably with SRLS spectral densities, which constitute generalized forms of the MF formulas. The main aspects that greatly improve the analysis include axial local motion, rhombic local ordering, rigorous account of mode-coupling, and proper treatment of general features of local geometry. The dynamic picture emerging, which differs significantly from the MF picture, is physically insightful, consistent and comprehensive. Conformational entropy can be derived with SRLS in a straightforward manner from experimentally determined local potentials of arbitrary symmetry.

**Acknowledgment.** This work was supported by the Israel Science Foundation grant number 279/03 and the Binational Science Foundation 2000399 to E.M., and the Damadian Center for Magnetic Resonance research at Bar-Ilan University, Israel. This work was also supported by NIH/NCRR grant P41-RR016292 (to J.H.F.). A.P. acknowledges the support of the Italian Ministry for Universities and Scientific and Technological Research, projects FIRB and PRIN ex-40%.

## References and Notes

(1) (a) Kay, L. E. *Nat. Struct. Biol.* **1998**, *5*, 513−517. (b) Ishima, R.; Torchia, D. A. *Nat. Struct. Biol.* **2000**, *7*, 740−743. (c) Palmer, A. G., III. *Annu. Rev. Biophys. Biomol. Struct.* **2001**, *30*, 129−155.

(2) (a) Case, D. *Acc. Chem. Res.* **2002**, *35*, 325, 325−33. (b) Bruschweiler, R. *Curr. Opin. Struct. Biol.* **2003**, *13*, 175−183.

(3) Palmer, A. G., III. *Chem Rev.* **2004**, *104*, 3623−3640.

(4) Peng, J. W.; Wagner, G. In *Methods in Enzymology*; James, T. L., Oppenheimer, N. J., Eds.; Academic Press: New York, 1994; Vol. 239, pp 563−595.

(5) Abragam, A. *Principles of Nuclear Magnetism*; Oxford University Press (Clarendon): London, 1961.

(6) Lipari, G.; Szabo, A. *J. Am. Chem. Soc.* **1982**, *104*, 4546−4559.

(7) Lipari, G.; Szabo, A. *J. Am. Chem. Soc.* **1982**, *104*, 4559−4570.

(8) Clore, G. M.; Szabo, A.; Bax, A.; Kay, L. E.; Driscoll, P. C.; Gronenborn, A. M. *J. Am. Chem. Soc.* **1990**, *112*, 4989−4991.

(9) Lee, A. L.; Wand, J. *J. Biomol. NMR* **1999**, *13*, 101−112.

(10) Osborne, M. J.; Wright, P. E. *J. Biomol. NMR* **2001**, *19*, 209−230.

(11) Vugmeyster, L.; Trott, O.; McKnight, C. J.; Raleigh, D. P.; Palmer, A. G., III. *J. Mol. Biol.* **2002**, *320*, 841−854.

(12) Mandel, A. M.; Akke, M.; Palmer, A. G., III. *Biochemistry* **1996**, *35*, 16009−16023.

(13) Wang, T.; Cai, S.; Zuiderweg, E. R. P. *J. Am. Chem. Soc.* **2003**, *125*, 8639−8643.

(14) Zeeb, M.; Jacob, M.; H., Schindler, T.; Balbach, J. *J. Biomol. NMR* **2003**, *27*, 221−234.

(15) Korchuganov, D. S.; Gagnidze, I. E.; Tkach, E. N.; Schulga, A. A.; Kirpichnikov, M. P.; Arseniev, A. S. *J. Biomol. NMR* **2004**, *30*, 431−442.

(16) Chang, S.-L.; Tjandra, N. *J. Magn. Reson.* **2005**, *174*, 43−53.

(17) Zhang, P.; Dayie, K.; Wagner, G. *J. Mol. Biol.* **1997**, *272*, 443−455.

(18) Wang, T.; Frederick, K. K.; Igumeniva, T. I.; Wand, A. J.; Zuiderweg, E. R. P. *J. Am. Chem. Soc.* **2005**, *127*, 828−829.

(19) Tugarinov, V.; Shapiro, Yu. E.; Liang, Z.; Freed, J. H.; Meirovitch, E. *J. Mol. Biol.* **2002**, *315*, 171−186.

(20) Shapiro, Yu. E.; Kahana E.; Tugarinov, V.; Liang, Z.; Freed, J. H.; Meirovitch, E. *Biochemistry* **2002**, *41*, 6271−6281.

(21) Pang, Y.; Buck, M.; Zuiderweg, E. R. P. *Biochemistry* **2002**, *41*, 2655−2666.

(22) Tugarinov, V.; Liang, Z.; Shapiro, Yu. E.; Freed, J. H.; Meirovitch, E. *J. Am. Chem. Soc.* **2001**, *123*, 3055−3063.

(23) Polimeno, A.; Freed, J. H. *Adv. Chem. Phys* **1993**, *83*, 89−210.

(24) Polimeno, A.; Freed, J. H. *J. Phys. Chem.* 1**995**, *99*, 10995−11006.

(25) Liang, Z.; Freed, J. H. 1999 *J. Phys. Chem. B* **1999**, *103*, 6384−6396.

(26) Meirovitch, E.; Shapiro, Yu. E.; Tugarinov, V.; Liang, Z.; Freed, J. H. *J. Phys. Chem. B* **2003**, *107*, 9883−9897.

(27) Meirovitch, E.; Shapiro, Y. E.; Liang, Z.; Freed, J. H. *J. Phys. Chem. B* **2003**, *107*, 9898−9904.

(28) Polimeno, A.; Moro, G. J.; Freed, J. H. *J. Chem. Phys.* **1996**, *104*, 1090−1104.

(29) Polnaszek, C. F.; Freed, J. H. *J. Phys. Chem.* **1975**, *79*, 2283−2306.

(30) Lin, W. J.; Freed, J. H. *J. Phys. Chem.* **1979**, *83*, 379−401.

(31) Millet, O.; Muhandiram, D. R.; Skrynnikov, N. S.; Kay, L. E. *J. Am. Chem. Soc.* **2002**, *124*, 6439−6448.

(32) Choy, W.-Y.; Kay, L. E. *J. Biomol. NMR* **2003**, *25*, 325−333.

(33) Akke, M.; Bruschweiler, R.; Palmer, A. G., III. *J. Am. Chem. Soc.* **1993**, *115*, 9832−9833.

(34) (a) Yang, D.; Kay, L. E. *J. Mol. Biol.* **1996**, *263*, 369−382. (b) Yang, D.; Mok, Yu-K.; Forman-Kay, J. D.; Farrow, N. A.; Kay, L. E. *J. Mol. Biol.* **1997**, *272*, 790−804. (c) Kay, L. E.; Muhandiram, D. R.; Farrow, N. A.; Aubin, Y.; Forman-Kay, J. D. *Biochemistry* **1996**, *35*, 361−368. (d) Yang, D.; Mok, Y.-K.; Forman-Kay, J. D.; Farrow, N. A.; Kay, L. E. *J. Mol. Biol.* **1997**, *272*, 790−804.

(35) (a) Li, Z.; Raychaudhuri, S.; Wand, A. J. *Protein Sci.* **1996**, *5*, 2647−2650. (b) Lee, A. L.; Kinnear, S. A.; Wand, A. J. *Nat. Struct. Biol.* **2000**, *7*, 72−77. (c) Lee, A. L.; Wand, A. J. *Nature* **2001** *411*, 501−504.

(36) Massi, F.; Palmer, A. G., III. *J. Am. Chem. Soc.* **2003**, *125*, 11158−11159.

(37) Liang, Z.; Lou, Y.; Freed, J. H.; Columbus, L.; Hubbell, W. L. *J. Phys. Chem. B* **2004**, *108*, 17649−17659.

(38) Brunne, R. M.; Berndt, K. D.; Guntert, P.; Wuthrich, K.; van Gunsteren, W. F. *Proteins* **1995**, *23*, 49−62.

(39) Palmo, K.; Mannfors, B.; Mirkin, N. G.; Krimm, S. *Biopolymers* **2003**, *68*, 383−394.

(40) Lienin, S. F.; Bremi, T.; Brutscher, B.; Bruschweiler, R.; Ernst, R. R. *J. Am. Chem. Soc.* **1998**, *120*, 9870−9879.

(41) Moro, G.; Freed, J. H. *J. Chem. Phys.* **1981**, *74*, 3757−3773.

(42) Moro, G.; Freed, J. H. In *Large-Scale Eigenvalue Problems*; Cullum, J., Willough, R., Eds.; Math Studies Series; North-Holland: Amsterdam, 1986; Vol. 127, pp 143−160.

(43) Freed, H. J.; Nayeem, A.; Rananavare, S. B. In *The Molecular Dynamics of Liquid Crystals*; Luckhurst, G. R., Veracini, C. A., Eds.; Kluwer Academic Publishers: The Netherlands, 1994; Chapter 12, pp 271−312.

(44) Fushman, D.; Tjandra, N.; Cowburn, D. *J. Am. Chem. Soc.* **1998**, *120*, 10947−10952.

(45) Cornilescu, G.; Bax, A. *J. Am. Chem. Soc.* **2000**, *122*, 10143−10154.

(46) Mandel, A. M.; Akke, M.; Palmer, A. G., III. *J. Mol. Biol.* **1995**, *246*, 144−163.

(47) Fushman, D.; Cahill, S.; Cowburn, D. *J. Mol. Biol.* **1997**, *266*, 173−194.

(48) Freed, J. H. *J. Chem. Phys* **1977**, *66*, 4183−4199.
(49) Polnaszek, C. F.; Bruno, G. V.; Freed, J. H. *J. Chem. Phys.* **1973**, *58*, 3185−3199.
(50) Kinosita, K.; Kawato, S.; Ikegami, A. *Biophys. J.* **1977**, *20*, 289−305.
(51) Lipari, G.; Szabo, A. *Biophys. J.* **1980**, *30*, 489−506.
(52) (a) Vold, R. L. In *The Molecular Dynamics of Liquid Crystals*; Luckhurst, G. R., Veracini, C. A., Eds.; Kluwer Academic Publishers: The Netherlands, 1994. (b) Dingemans, T., Photinos, D. J., Samulski, E. T., Terzis, A. F.; Wutz, C. *J. Chem. Phys.* **2003**, *118*, 7046−7061.
(53) (a) Kay, L. E.; Torchia, D. A.; Bax, A. *Biochemistry* **1989**, *28*, 8972−8979. (b) Pawley, N. H.; Wang, C.; Koide, S.; Nicholson, L. K. *J. Biomol. NMR* **2001**, *20*, 149−165.
(54) Damberg, P.; Jarvet, J.; Graslund, A. *J. Am. Chem. Soc.* **2004**, *127*, 1995−2005.
(55) Peng, J. W.; Wagner, G. *J. Magn. Res.* **1992**, *98*, 308−332.
(56) Farrow, N. A.; Zhang, O.; Szabo, A.; Torchia, D. A.; Kay, L. E. *J. Biomol. NMR* **1995**, *6*, 153−162.
(57) Ishima, R.; Nagayama, K. *J. Magn. Reson. Ser. B* **1995**, *108*, 73−76.
(58) Fushman, D.; Cowburn, D. *J. Am. Chem. Soc.* **1998**, *120*, 7109−7110.
(59) Kroenke, C. D.; Rance, M.; Palmer, A. G., III. *J. Am. Chem. Soc.* **1999**, *121*, 10119−10125.
(60) Lee, A.; Sharp, K. A.; Kranz, J. K.; Song, X.-J.; Wand, A. J. *Biochemistry* **2002**, *41*, 13814−13825.
(61) Babu, Y. S.; Bugg, C. E.; Cook, W. J. *J. Mol. Biol.* **1988**, *204*, 191−204.
(62) Ikura, M.; Barbato, G.; Kay, L. E.; Pastor, R. W.; Bax, A. *Biochemistry* **1992**, *31*, 5269−5278.
(63) Tjandra, N., Kuboniwa, H., Ren, H.; Bax, A. *Eur. J. Biochem.* **1995**, *230*, 1014−1024.
(64) Baber, J. L.; Szabo, A.; Tjandra, N. *J. Am. Chem. Soc.* **2001**, *123*, 3953−3959.
(65) Chang, S.-L.; Szabo, A.; Tjandra, N. *J. Am. Chem. Soc.* **2003**, *125*, 11379−11384.
(66) Lee, L. K.; Rance, M.; Chazin, W. J.; Palmer, A. G., III. *J. Biomol. NMR* **1997**, *9*, 287−298.